SEISMIC TESTING & BEHAVIOUR OF A 1936-DESIGNED REINFORCED-CONCRETE BRIDGE

Transfund New Zealand Research Report No. 78

SEISMIC TESTING & BEHAVIOUR OF A 1936-DESIGNED REINFORCED-CONCRETE BRIDGE

J. MAFFEI
Department of Civil Engineering,
University of Canterbury,
Christchurch, New Zealand

Transfund New Zealand Research Report No. 78

ISBN 0-478-10536-3
ISSN 1174-0574

PO Box 2331, Lambton Quay, Wellington, New Zealand
Telephone (04) 473-0220; Facsimile (04) 499-0733

Maffei, J. 1997. Seismic testing and behaviour of a 1936-designed reinforced concrete bridge. *Transfund New Zealand Research Report No. 78.* 95pp.

Key Words: bond, bridges, capacity design, concrete, earthquakes, New Zealand, plain bars, reinforcing steel, retrofitting, seismic evaluation, seismic testing, structural engineering, time-history analyses

AN IMPORTANT NOTE FOR THE READER

The research detailed in this report was commissioned by Transit New Zealand when it had responsibility for funding roading in New Zealand. This funding is now the responsibility of Transfund New Zealand.

While this report is believed to be correct at the time of publication, Transit New Zealand, Transfund New Zealand, and their employees and agents involved in preparation and publication, cannot accept any contractual, tortious or other liability for its content or for any consequences arising from its use and make no warranties or representations of any kind whatsoever in relation to any of its contents.

The report is only made available on the basis that all users of it, whether direct or indirect, must take appropriate legal or other expert advice in relation to their own circumstances and must rely solely on their own judgement and seek their own legal or other expert advice.

The material contained in this report is the output of research and should not be construed in any way as policy adopted by Transit New Zealand or Transfund New Zealand but may form the basis of future policy.

ACKNOWLEDGMENTS

The organisations which helped fund this research are gratefully acknowledged. They included the United States Fulbright Scholarship Foundation, the New Zealand National Society for Earthquake Engineering, and Transit New Zealand.

Professor Bob Park especially is acknowledged for his supervision, and his support and friendship.

Professor Nigel Priestley, Dr Athol Carr, Howard Chapman, Don Kennedy, Dr Jose Restrapo, and others are thanked for their helpful input to this report, and in particular Ray Zelinski of Caltrans. A very special thanks goes to Professor Emeritus Tom Paulay for his thorough comments on several aspects of this report and for the lively and enlightening discussions we have had on so many different topics.

Gratitude is due to Norrie Hickey, Dominic McCarthy, and Mark Griffin who were the laboratory technicians for the testing of the column to foundation-beam specimen, to Val Grey who skilfully prepared many of the figures, Catherine Price and Billie-Jo for typing, and to Dagny Baltakmens for proofreading. The University of Canterbury and the Department of Civil Engineering are also thanked.

CONTENTS

ACKNOWLEDGMENTS 4
EXECUTIVE SUMMARY 9
ABSTRACT 11

1. INTRODUCTION 13
1.1 Background 13
1.2 Objectives 14
1.3 Organisation of Report 14

2. BACKGROUND & REVIEW OF COLUMN TO CROSSBEAM TESTS 15
2.1 Introduction 15
2.2 Description of the Bridge Structure 15
2.2.1 Structural Integrity 15
2.2.2 Column Details 18
2.3 Initial Seismic Assessment 18
2.3.1 Transverse-direction Earthquake 18
2.3.2 Longitudinal-direction Earthquake 20
2.4 Tests of Original Column to Crossbeam Specimen 20
2.4.1 Test Specimen 20
2.4.2 Test Set-up and Procedure 22
2.4.3 Test Results 22
2.5 Tests of an Anchorage-Retrofit Specimen 24
2.5.1 Anchorage Test Block 24
2.5.2 Retrofit Procedure 26
2.5.3 Test Results 26
2.6 Tests of a Confinement-Retrofit Specimen 27

3. COLUMN TO FOUNDATION-BEAM TEST & OBSERVATIONS 29
3.1 Test Specimen and Materials 29
3.1.1 Reinforcement Details 29
3.1.2 Concrete Placement and Strengths 31
3.1.2.1 Construction joint 31
3.1.2.2 Concrete strength 31
3.1.3 Reinforcing Steel Strengths 33
3.1.4 Strength of Test Specimen versus Prototype Column 34
3.2 Test Set-up and Instrumentation 35
3.2.1 Axial Load 35
3.2.2 Base Reaction 36
3.2.3 Instrumentation 36
3.2.4 Interior versus Exterior Column Effect 36
3.3 Test Procedure and Observations 37
3.3.1 Procedure 37
3.3.2 Specimen Cracking 39
3.3.3 Axial Load and Horizontal Reactions 39
3.3.4 Lateral Load-Displacement Hysteretic Behaviour 40
3.4 Failure and Subsequent Testing of Longitudinal-Bar End Welds 41
3.4.1 Failure of Bar-End Welds 42
3.4.2 Testing of Bar-End Weld 43
3.4.3 Estimate of Tension Force at Weld Failure 43

3. COLUMN TO FOUNDATION-BEAM TEST & OBSERVATIONS (continued)
3.5 Continuation of Column-specimen Testing and Observations 44
3.5.1 Procedure 44
3.5.2 Splitting Failure at Bar Bottom Anchorage 44

4. EVALUATION OF EXPERIMENTAL RESULTS & POSSIBLE RETROFIT SOLUTIONS 46
4.1 Introduction 46
4.2 Effect of Plain-Round Reinforcing Bars and Bond Slip 46
4.2.1 Strain Results at Ductility $\mu = 1$ 46
4.2.2 Strain Results to Ductility $\mu = 3$ 47
4.2.3 Additional Evidence of Bond Slip 49
4.2.4 Effect on Structural Performance 50
4.2.5 Lateral Capacity and Strength Degradation 50
4.2.5.1 Combined capacity of top and bottom hinge regions 51
4.2.5.2 Anchorage-retrofit structure 51
4.3 Effect of the Diagonal Reinforcing, and of Column Shear Capacity 52
4.3.1 Diagonal Bar Contribution to Flexural Strength 52
4.3.2 Diagonal Bar Contribution to Shear Strength 53
4.3.3 Calculations of Shear Capacity 54
4.3.4 Comparison to NZ Standards Concrete Code Provisions 54
4.4 Plastic Hinge Behaviour and Concrete Confinement 56
4.4.1 Background 56
4.4.2 Curvature Ductility 56
4.4.3 Plastic-Hinge Length 57
4.4.4 Column-hinge Lengthening and Degradation 58
4.4.5 Required Transverse Reinforcing Steel Areas 59
4.4.6 Required Column-tie Spacing 59
4.4.6.1 Bar-buckling criteria 59
4.4.6.2 Confinement and shear-resistance criteria 61
4.4.6.3 Proposed requirements for the subject bridge 62
4.5 Overall Assessment 62
4.5.1 Seismic Performance 62
4.5.2 Prediction of Seismic Performance 63
4.5.3 Stiffness Degradation and Hysteretic Response 64
4.5.4 Confinement Retrofit 64
4.5.5 Additional Considerations 65
4.5.5.1 Interior versus exterior column details 65
4.5.5.2 Restraint to bond slip provided by test set-up 66
4.5.5.3 Condition of reinforcing bars 67
4.6 Possible Retrofit Measures 67
4.6.1 Retrofit of Bar Anchorage 67
4.6.2 Infill Concrete Wall 68
4.6.3 Added Braces and Energy-dissipation Devices 68

5. INELASTIC EARTHQUAKE TIME-HISTORY ANALYSES 70
5.1 Modelling of Structure Behaviour 70
5.1.1 General Assumptions 70
5.1.2 Modelled Hysteresis Loops 70
5.2 Earthquake Input 74
5.2.1 Selection of Earthquake Records 74
5.2.2 Response Spectra 75

5. **INELASTIC EARTHQUAKE TIME-HISTORY ANALYSES** (continued)
5.3 Analysis Results 76
5.3.1 Structure Drift 76
5.3.2 Bridge Performance Limit States 81
5.3.3 Responses for Different Earthquake Records 83
5.3.4 Response for Different Hysteresis Models 86
5.3.4.1 Bridgeza and El Centro earthquakes 86
5.3.4.2 Pacoima and Parkfield earthquakes 86
5.4 Final Assessment 87
5.4.1 Performance for Code-implied Earthquake Levels 87
5.4.2 Performance for Severe Earthquake Levels 90

6. **CONCLUSIONS & RECOMMENDATIONS** 91
6.1 Conclusions 91
6.2 Recommendations 93

7. **REFERENCES** 94

LIST OF FIGURES

2.1 Partial elevation of the prototype bridge. 16
2.2 Cross section of the prototype bridge (Chapman 1991). 16
2.3 Reinforcement details of the bridge pier that was investigated (Park et al. 1993). . . . 17
2.4 Details of column to crossbeam test specimen and reinforcing (Park et al. 1993). . . . 21
2.5 Test set-up for column to crossbeam specimen (Park et al. 1993). 23
2.6 Definition of yield displacement. 23
2.7 Lateral-load versus lateral-displacement hysteresis loops for column to crossbeam specimen. 25
2.8 Test specimen for anchorage-retrofit detail using a steel end plate (Park et al. 1993). 27
2.9 Confinement-retrofit specimen with new hoops added at A2, B2 and C2 (Dekker and Park 1992). 28
3.1 Column to foundation-beam test specimen and reinforcing details. 30
3.2 Test of the column to foundation-beam specimen: 32
3.3 Typical stress versus strain behaviour of the reinforcing steel used in the column to foundation-beam specimen. 33
3.4 Test set-up for column to foundation-beam specimen. 35
3.5 Instrumentation of column plastic-hinge region. 37
3.6 Load sequence and test observations. 38
3.7 Maximum crack width (mm) measured during testing. 40
3.8 Lateral-load versus lateral-displacement hysteresis loops, to ductility μ=7, for the column to foundation-beam test. 41
3.9 (a) Fracture, (b) testing and (c) replacement of the longitudinal-bar end welds to the specimen top plate. 42
3.10 Lateral-load versus lateral-displacement hysteresis loops, to ductility $\mu \approx 12$, for the column to foundation-beam test. 45

LIST OF FIGURES (continued)

4.1 Concrete and steel strain profiles in the column plastic-hinge region at ductility μ= +1. 47
4.2 Lateral-load versus strain-hysteresis loops up to and including ductility of μ=3. 48
4.3 Lateral-strength versus displacement envelopes for the as-built bridge and anchorage-retrofit bridge. 52
4.4 Column curvature profile over the plastic-hinge region at displacement ductilities of μ=1, 3, 5, 6, 7. 56
4.5 Measured concrete curvature ductility, versus displacement ductility, indicating an increase in concrete plastic-hinge length, l_p. 57
4.6 Column lengthening during the testing of the column to foundation-beam specimen... 58
4.7 (a) Required transverse reinforcement for the subject bridge column, and
(b) Required maximum allowable spacing of column ties, from the current and revised New Zealand concrete codes (SANZ 1982,1995). 60
4.8 Possible seismic strengthening using a reinforced-concrete infill wall and foundation strengthening. 68
4.9 Possible seismic retrofitting using added steel braces with energy-dissipation devices.69
5.1 Hysteresis loops obtained from time-history analyses to model structural behaviour.. 72
5.2 Lateral strength envelopes for hysteresis models. 73
5.3 Response spectra (a) to (f) for the earthquake records used as input to the *Ruaumoko* analysis. 77-79
5.4 Peak structure drift results from the inelastic time-history analyses. 80
5.5 Structure drift time-history results for the Bridgeza earthquake record. 84
5.6 Lateral-force versus lateral-displacement hysteretic response for the Bridgeza earthquake record. 85
5.7 Structure drift time-history results for the Pacoima earthquake record. 88
5.8 Lateral-force versus lateral-displacement hysteretic response for the Pacoima earthquake record. 89

LIST OF TABLES

3.1 Concrete strengths of bridge foundation and column before and at test. 33
3.2 Strengths after testing of reinforcing steel used in the bridge. 34
4.1 Comparison of average concrete strain, including cracking, with steel strains at longitudinal bars. 49
4.2 Calculated shear demands and capacities for the bridge column. 55
5.1 Structural modelling parameters used for time-history analyses. 71
5.2 Values used for *Ruaumoko* input and time-history analyses. 71
5.3 Earthquake records used for the inelastic time-history analysis. 74
5.4 Additional data on earthquake records, taken from Naeim and Anderson (1993) 75
5.5 Maximum structure drift results from the inelastic time-history analyses of the subject bridge. 80
5.6 Estimated relationship of bridge drift level to performance limit states. 82

EXECUTIVE SUMMARY

Summary
This report describes the laboratory testing and inelastic computer analysis of a 1936-designed bridge which is typical of many of the older, reinforced-concrete, multi-span bridges in New Zealand. The structure has plain-round (undeformed) reinforcing bars and anchorage details, shear strength, and column-transverse reinforcement that are potentially deficient. Despite the suspected seismic deficiencies, the testing and analysis of the bridge show that its seismic performance will be good.

An initial seismic assessment of the bridge and tests of a full-scale specimen representing the column to crossbeam region of the bridge are reviewed. The testing of a second critical area of the bridge, the column to foundation-beam region, is described in detail, as is an inelastic computer time-history analysis of the structure.

Conclusions
The studies of the 1936-designed New Zealand bridge lead to several conclusions regarding the seismic assessment of existing reinforced-concrete structures. The conclusions are outlined as follows:

- Compared to deformed reinforcement, plain-round reinforcement offers much poorer bond-resistance and undergoes a more rapid degradation of bond under cyclic earthquake actions.
- Structures with plain-round reinforcement suffer stiffness degradation and a pinching of lateral-force versus displacement hysteretic response which could compromise their earthquake performance.
- Despite the pinched hysteretic response, the subject bridge has high lateral strength and displacement capacity which result in excellent seismic performance.
- If the bridge is retrofitted by welding anchorage end-plates to the tops of the column longitudinal bars the seismic performance would improve, but not dramatically.
- The supplementary diagonal reinforcing bars at the top and bottom end-flares of the bridge column contribute significantly to both flexural and shear strength.
- For the subject bridge the 1982 concrete code (NZS 3101:1982) over-estimates the required amount of transverse steel by a factor of 3.
- For columns with low axial load, good shear capacity, and large-diameter longitudinal reinforcing, the column-tie spacing requirements of the 1982 and 1995 concrete codes (NZS 3101:1982, 1995) may be conservative.
- Conflicting predictions of seismic performance show that assumptions used for the evaluation of existing structures often need to be more accurate than those used for the design of new structures.

- The subject bridge is not vulnerable to earthquake damage related to insufficient transverse reinforcement or shear capacity.
- Concrete structures with plain-round longitudinal bars may require less transverse reinforcement than similar structures with deformed longitudinal bars. Further research is needed in this area.
- Inelastic time-history analyses of the subject bridge show that bridge response depends greatly on the earthquake input.

Recommendations

The research findings raise several important questions which should be investigated further. Additional research on the seismic performance of concrete bridges with plain-round reinforcement is recommended. Specific topics for study should include:

- Determining the required amount of transverse reinforcement to confine concrete and prevent longitudinal-bar buckling in the plastic-hinge regions of structural members.
- Determining the dominant mechanisms of shear resistance and the required shear reinforcement.
- Analysing and modelling the effect of bond slip on structural response.
- Evaluating additional sample bridges with different structural characteristics.

Because structures with plain-round reinforcement are much more prevalent in New Zealand than in California or other areas where seismic structural research is carried out, New Zealand cannot rely entirely on overseas research on this topic.

The response of bridges under earthquakes with strong pulses should also be studied further. As shown in this report, records show that some earthquakes have a much higher potential to cause damage than the earthquake levels that have typically been assumed in bridge design and retrofitting.

ABSTRACT

The laboratory testing and inelastic computer analysis are described for a 1936-designed bridge which is typical of many of the older, reinforced-concrete, multi-span bridges in New Zealand. The structure has plain-round (undeformed) reinforcing bars and anchorage details, shear strength, and column-transverse reinforcement that are potentially deficient. Despite the suspected seismic deficiencies, the testing and analysis of the bridge show that its seismic performance will be good.

The results indicate that (a) seismic retrofitting for the subject bridge is not warranted, (b) code criteria applicable to the design of new structures, with deformed reinforcing, can be overly conservative when used for the assessment of existing structures, and (c) plain-round reinforcing bars under cyclic seismic forces suffer extensive bond deterioration resulting in pinched hysteretic response which, for earthquakes with strong pulses, can lead to greater seismic damage. Also records show that some earthquakes have a much higher potential to cause damage than the earthquake levels that have typically been assumed in bridge design and retrofitting.

1. INTRODUCTION

This report describes the detailed experimental and analytical study of a sample bridge structure: i.e. a 1936-designed, monolithic, reinforced-concrete, multi-column-pier bridge. The bridge is typical of many of the long, multi-span bridges in New Zealand which were built to cross the country's wide, shallow rivers and flood plains. The 1.1 km long bridge has a T-beam superstructure supported on about 90 piers, each of which has four reinforced-concrete columns. The structure has plain-round (undeformed) reinforcing bars and anchorage details, shear strength, and column-transverse reinforcement that are potentially deficient.

The widespread use of plain-round reinforcing bars seems to be a particular characteristic of the New Zealand bridge stock. Deformed reinforcing bars were not commonly used in New Zealand concrete construction until the middle 1960s (T. Paulay, pers.comm. 1993). In California, by contrast, deformed bars have been used since the 1889, and it is thought that few if any bridges use plain-round bars (J. Snyder, Caltrans, pers.comm. 1996).

1.1 Background

As a pilot study on the seismic assessment of bridges, Works Consultancy Services (WCS) conducted seismic evaluations of five structures selected to be representative of common New Zealand bridge types (Chapman 1991). One of these five bridges was the subject structure of this report. This initial assessment identified the critical areas of the subject bridge to be the top and bottom end regions of the columns. The amount of transverse column reinforcment is well below that required by the 1982 New Zealand concrete code (NZS 3101:1982, SANZ), and the top bar-anchorage detail was suspect. The seismic assessment, based on current design codes and practice, concluded that ... *the pier-columns are unlikely to tolerate cyclic displacements much exceeding yield* ...

To determine the severity of the presumed seismic deficiencies and the likely effectiveness of possible retrofit measures, experimental testing was carried out at the University of Canterbury, New Zealand. A full-scale specimen representing the top half of the column and a portion of the crossbeam and deck slab was constructed following the original structural drawings for the bridge. The specimen was tested by Rodriguez and Park in 1990 (Park et al. 1993). Two retrofits of the specimen were subsequently tested by Dekker and Park (1992).

In addition to the column plastic-hinge region near the crossbeam, the bottom column plastic hinge is a second critical area of the bridge. The present author carried out the testing of this column/foundation-beam portion of the structure in March of 1993, using another full-scale laboratory specimen. Based on the results of this and the previous tests, the author conducted detailed analyses of the seismic performance of the bridge, including inelastic time-history analyses.

1.2 Objectives

The objectives of this report are to:

1. Summarise the previous investigations of the subject bridge in light of the findings of the subsequent studies, and tie together all the research findings.
2. Describe the testing of the column to foundation beam specimen and the test results.
3. Evaluate in detail the expected seismic performance of the bridge, based on the test results and inelastic analyses.
4. Assess the effects on seismic response of the plain-round reinforcing bars and other design features of the bridge.
5. Consider the applicability of current design codes and practices for the evaluation of the subject bridge.
6. Identify any areas where further research is needed.

1.3 Organisation of Report

The body of this report is divided into four chapters. Chapter 2 reviews previous studies of the bridge, which include an initial seismic assessment and tests of the column to crossbeam region of the structure.

Chapters 3 and 4 discuss the laboratory testing of the column to foundation-beam region.

Chapter 5 presents inelastic, dynamic time-history analyses of the bridge which complement the experimental studies.

Chapter 6 presents the conclusions and recommendations for the study.

2. BACKGROUND & REVIEW OF COLUMN TO CROSSBEAM TESTS

2.1 Introduction

This chapter describes the structural features of the subject bridge and reviews previous seismic investigations and laboratory testing. The previous studies include an initial seismic assessment by WCS (Chapman 1991), testing of the column to crossbeam portion of the bridge by Rodriguez and Park (Park et al. 1993), and testing of two retrofit measures for the column to crossbeam specimen by Dekker and Park (1992).

Although this chapter covers only work done by others, the discussions of the work presented here are influenced somewhat by the subsequent findings of the present author. The testing of the column to foundation-beam specimen and the inelastic analysis of the bridge offer some new insights into the results of the previous studies.

2.2 Description of the Bridge Structure

The subject bridge is illustrated in Figures 2.1 and 2.2. It is typical of many of the long, multi-span bridges in New Zealand which have been built to cross the country's wide shallow rivers and flood plains. The overall length of the bridge is 1100 m (3600 ft)[1] consisting of ninety 12.2 m (40.0 ft) spans. The bridge has a reinforced concrete T-beam superstructure supported on four-column piers[2]. The four columns are in turn supported on a foundation beam with five octagonal reinforced concrete piles. The piles extend 8.2 m (27 ft) below the bottom of the foundation beams.

Figure 2.3 shows the reinforcing details of the four-column piers. Plain-round (undeformed) reinforcing bars were used throughout the structure. Deformed reinforcing was not commonly used in New Zealand concrete construction until the middle 1960s.

2.2.1 Structural Integrity

At the time the bridge was designed, structural integrity was emphasised as an important seismic design consideration. A New Zealand Public Works Department design instruction from 1933 required that ... *wherever possible the structure should be made monolithic, and where this is not possible the structure shall be well tied together...* This sound design philosophy was a result of the magnitude 7.8 Napier earthquake in 1931, New Zealand's most destructive earthquake to date (Chapman 1991).

---

1 Imperial units were used in the original plans drawn in 1936.
Metric units were used in the testing carried out in 1996. Both are provided in this report.

2 The term 'pier', rather than 'bent', is used in New Zealand.

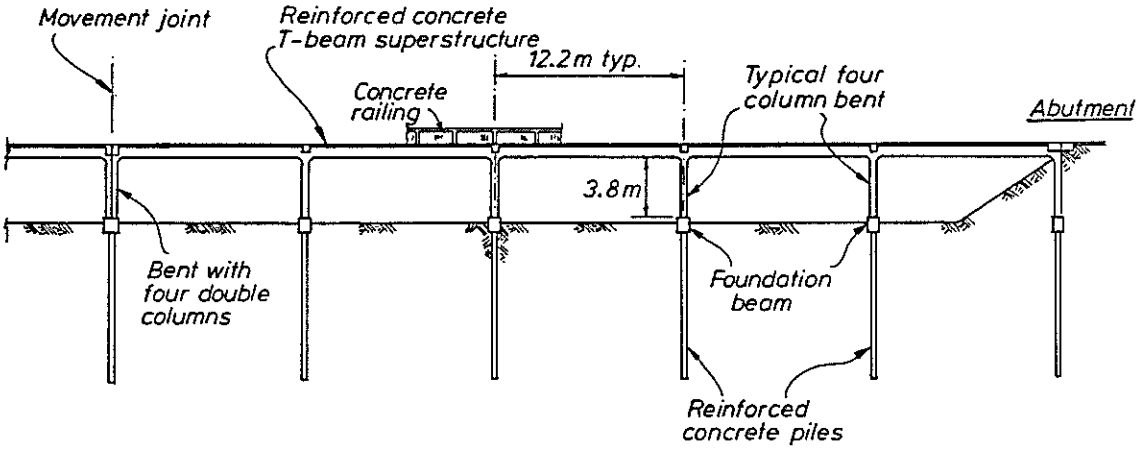

Figure 2.1 Partial elevation of the prototype bridge.

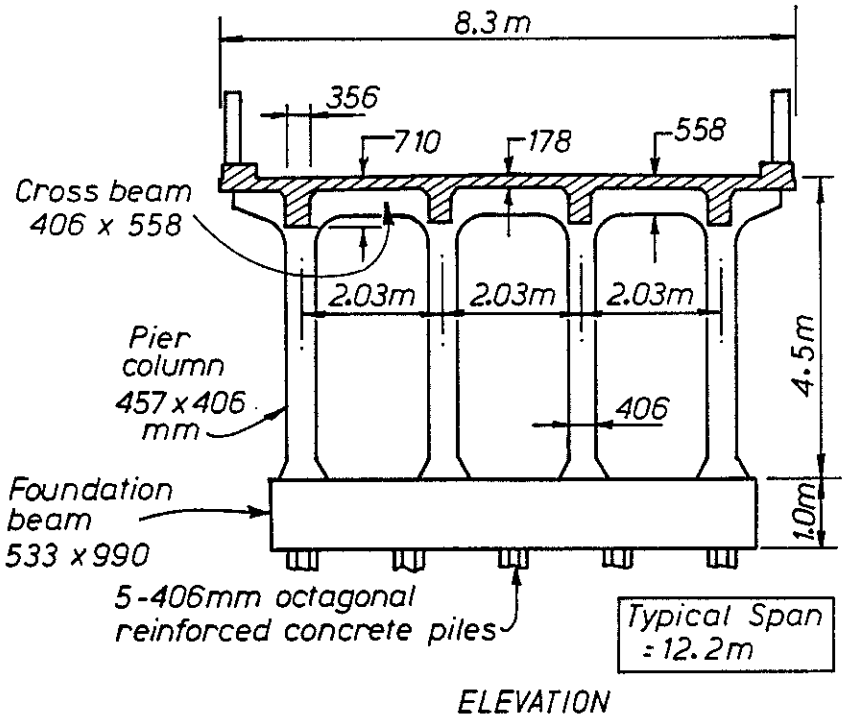

Figure 2.2 Cross section of the prototype bridge (Chapman 1991).

Although long structures need movement joints, the design of the subject bridge incorporates the movement joints without sacrificing the monolithic integrity of the structure. The bridge contains 17 movement joints, one at every fifth span. At each movement joint, double columns are used so that separate columns support the spans on each side of the joint as shown in Figure 2.1. The double columns share a common pile foundation. Additional control joints are placed between every span, down the centre of the transverse crossbeam (pier or bent-beam) as shown in Figure 2.3, Section D-D. The girder top reinforcing is not continuous through this joint so that, despite the continuous appearance of the bridge, each span of the superstructure is in fact simply supported.

Figure 2.3 Reinforcement details of the bridge pier that was investigated (Park et al. 1993).

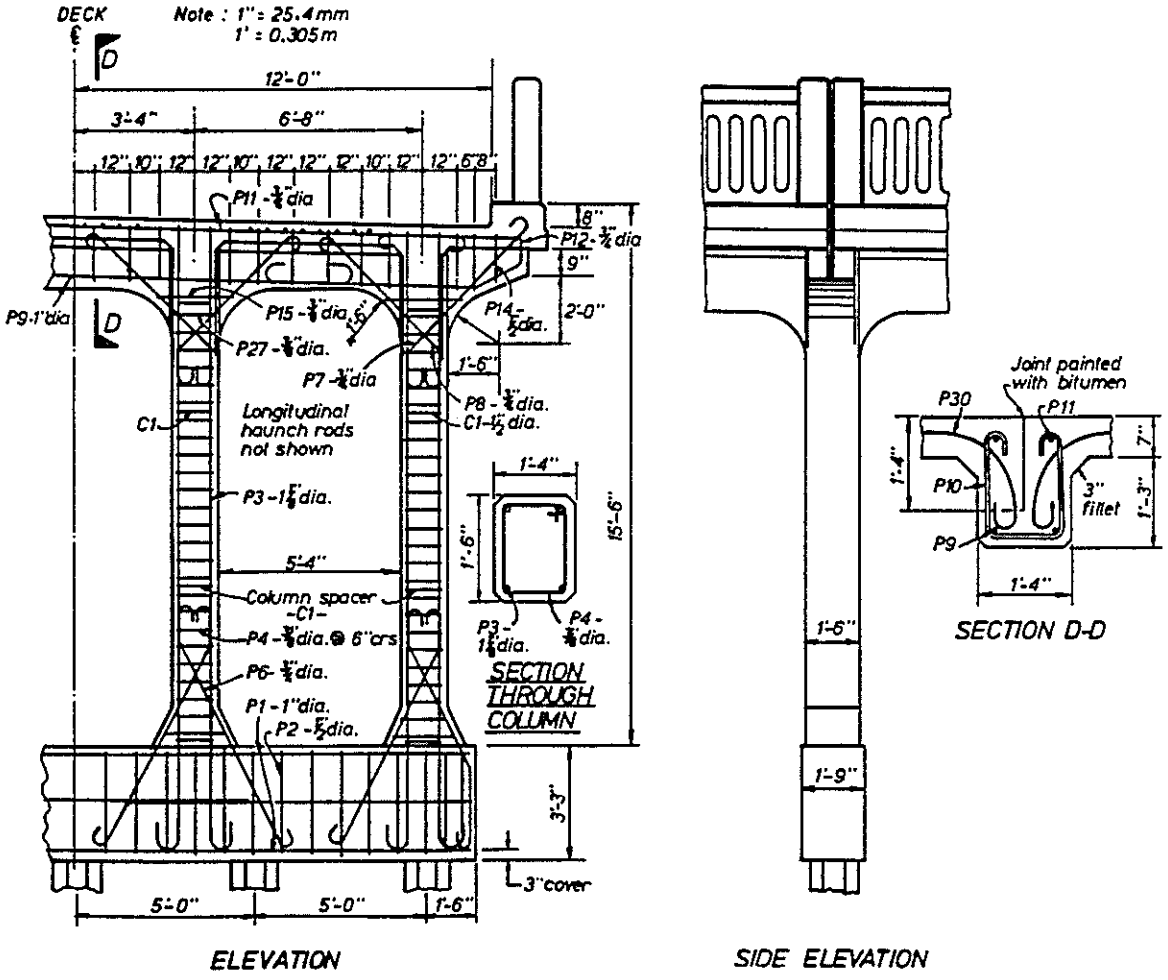

2.2.2 Column Details

As shown in Figure 2.3, the columns of the typical pier are each 457 mm wide by 406 mm deep (18 by 16 inches). The longitudinal reinforcement in each column consists of four 28.6 mm (1-inch) diameter bars. Transverse reinforcement steel consists of 9.5 mm (⅜-inch) diameter rectangular hoops at a 152 mm (6-inch) spacing. Four 19.0 mm (¾-inch) diameter diagonal bars are used at the flared bottom end of the column, at a slope of 2 vertical to 1 horizontal. The top end of each column is flared both longitudinally and transversely, and eight 19.0 mm (¾-inch) diagonal bars – two pairs of bars in each direction – are used at a slope of 1 to 1. The column longitudinal bars have 180° end hooks at the bottom and a straight anchorage length at the top. The diagonal bars and transverse hoops all have 180° hooks at both ends (NZPW 1936).

2.3 Initial Seismic Assessment

As a pilot study on the seismic assessment of bridges, WCS conducted seismic evaluations of five structures selected to be representative of common New Zealand bridge types (Chapman 1991). One of these five bridges was the subject structure. The pilot study indicated that the bridge columns were likely to be the weakest link in the seismic resistance of the structure. The crossbeam and foundation beam, each of which the columns frame into, have greater moment capacity than the column section itself. Thus a weak-column–strong-beam plastic mechanism is expected to develop under lateral seismic forces in the plane of the pier (i.e. forces are transverse with respect to the bridge axis). Although this is an undesirable mechanism in multi-storey buildings, it is an acceptable mechanism for single-level structures such as bridges. In fact, the weak-column–strong-beam plastic mechanism may be preferable for bridges because damage to columns is easier to inspect and repair than damage to pier-beams or foundation beams. The critical areas of the subject structure, then, are the potential plastic-hinge regions at the top and bottom of each column.

For the subject bridge, the pile foundations are typically well contained by the surface soil, thus the foundation was judged not to be a critical link in the seismic capacity of the bridge. This may not be the case for other New Zealand bridges of similar construction which have foundation piles in river beds subject to erosion and scour.

2.3.1 Transverse-direction Earthquake

The brief seismic assessment of the bridge made in the pilot study came to the following conclusions (Chapman 1991). For transverse seismic forces ... :

(1) Assuming the probable, rather than the specified, minimum yield strength of the reinforcing steel, the pier columns would yield at a seismic loading of 0.3 g, provided that the piles do not yield first and that the column reinforcement anchorages do not fail (see below).

(2) With the above structure yield strength, an available structure displacement ductility of four is necessary to meet current design requirements for the most important bridges in the most active seismic areas.

(3) The pier-columns are unlikely to tolerate cyclic displacements much exceeding yield because:

(a) the rectangular hoops are widely spaced so that the column core concrete is poorly confined and the main reinforcement would be poorly restrained against buckling,

(b) the capacity of the upper part of the column to resist shear forces necessary to develop a plastic mechanism is marginal, and,

(c) the top anchorage length of the plain round column bars into the cross beam is approximately 50% of the current design code requirements, suggesting that bar anchorage failure would be likely.

(4) The piles are strong enough to resist the shear forces from the column hinging, but would themselves hinge first in flexure if they are standing as columns with a free height of more than approximately 1.5 to 2 metres (such as in a river bed). ...

The subsequent experimental and analytical studies of the bridge at the University of Canterbury have provided additional information on the above conclusions. The details of the further studies are presented in Chapter 5 in this report, but a preview of the results directly relating to the above conclusions from the pilot study is as follows:

- *For conclusion 1:* The test results and calculations by the present author indicate a lateral strength of 0.45 times the seismic weight. The calculations consider (a) the contribution of the diagonal bars and axial load to flexural strength, (b) the shorter clear span between column plastic hinges related to the end flares and diagonal bars, (c) the 24% strength reduction at the top bar anchorages, and (d) probable material strengths and seismic weights.

- *For conclusion 3(a):* The transverse ties meet current code requirements for bar-buckling restraint, and bar buckling did not occur in the tests even at very high ductility. The confinement of concrete was also shown by the tests to be adequate. The conservative confinement requirements of the former New Zealand concrete code (NZS 3101:1982, SANZ) have recently been relaxed for columns with low axial load levels (NZS 3101:1995, SANZ).

- *For conclusion 3(b):* Calculations based on the New Zealand concrete code (NZS 3101:1982) indicate inadequate shear strength at the plastic hinges (90 kN capacity to 102 kN demand) if the diagonal bars are ignored. However, the diagonal bars increase the shear capacity significantly. Also, the code assumption that the concrete mechanism carries no shear ($V_c = 0$) is a conservative one.

- *For conclusion 3(c):* Bar-anchorage failure does indeed control the moment capacity at the top of the column. Test results (Dekker and Park 1992) indicate that the moment capacity is diminished by 24% compared with an anchorage-retrofit specimen.

2.3.2 Longitudinal-direction Earthquake

For seismic forces in longitudinal direction, the pilot study (Chapman 1991) concluded that: ... *the bridge is likely to be supported by the abutment approach fills and by interaction between sections of its length. Longitudinal behaviour is unlikely to be critical on firm ground as each span is monolithic with its supporting piers. On soft or sandy silts where soil liquefaction could occur pier/pile damage could result from individual longitudinal movements of the piles relative to the superstructure.* ...

2.4 Tests of Original Column to Crossbeam Specimen

The initial assessment identified the critical areas of the subject bridge to be the top and bottom end regions of the columns. The amount of transverse column reinforcing was well below that required by the 1982 New Zealand concrete code (NZS 3101:1982), and the top bar-anchorage detail was suspect. Experimental testing of specimens representing the column-hinge regions of the bridge was carried out at the University of Canterbury to determine the severity of the presumed seismic deficiencies and the likely effectiveness of possible retrofit measures.

2.4.1 Test Specimen

A full-scale specimen representing the top half of the column and a portion of the crossbeam and deck slab was constructed, following the original structural drawings for the bridge. The specimen was tested upside-down with the crossbeam bolted to the laboratory floor. Figure 2.4 shows the column to crossbeam-test specimen and reinforcing details.

The rectangular column section is 457 mm by 406 mm (18.0 by 16.0 inches) and is reinforced by four plain (undeformed) longitudinal bars 28 mm in diameter. The concrete was placed with the formwork in the upright position (with the crossbeam on top) as it would have been in the construction of the actual bridge. The specimen was cast with one batch of concrete. Before testing, the specimen was inverted.

The compressive strength of the concrete for the specimen, obtained by testing 200 mm high x 100 mm diameter (7.9 x 3.9 inch) cylinders at 28 days, was f'_c = 19 MPa (2800 psi). The measured yield strengths of the plain-round steel reinforcement were f_y = 308 MPa (44 700 psi) for the R28 (1.10 inch diameter) longitudinal reinforcement and f_{yh} = 350 MPa (50 800 psi) for the R10 (0.39 inch diameter) hoops.

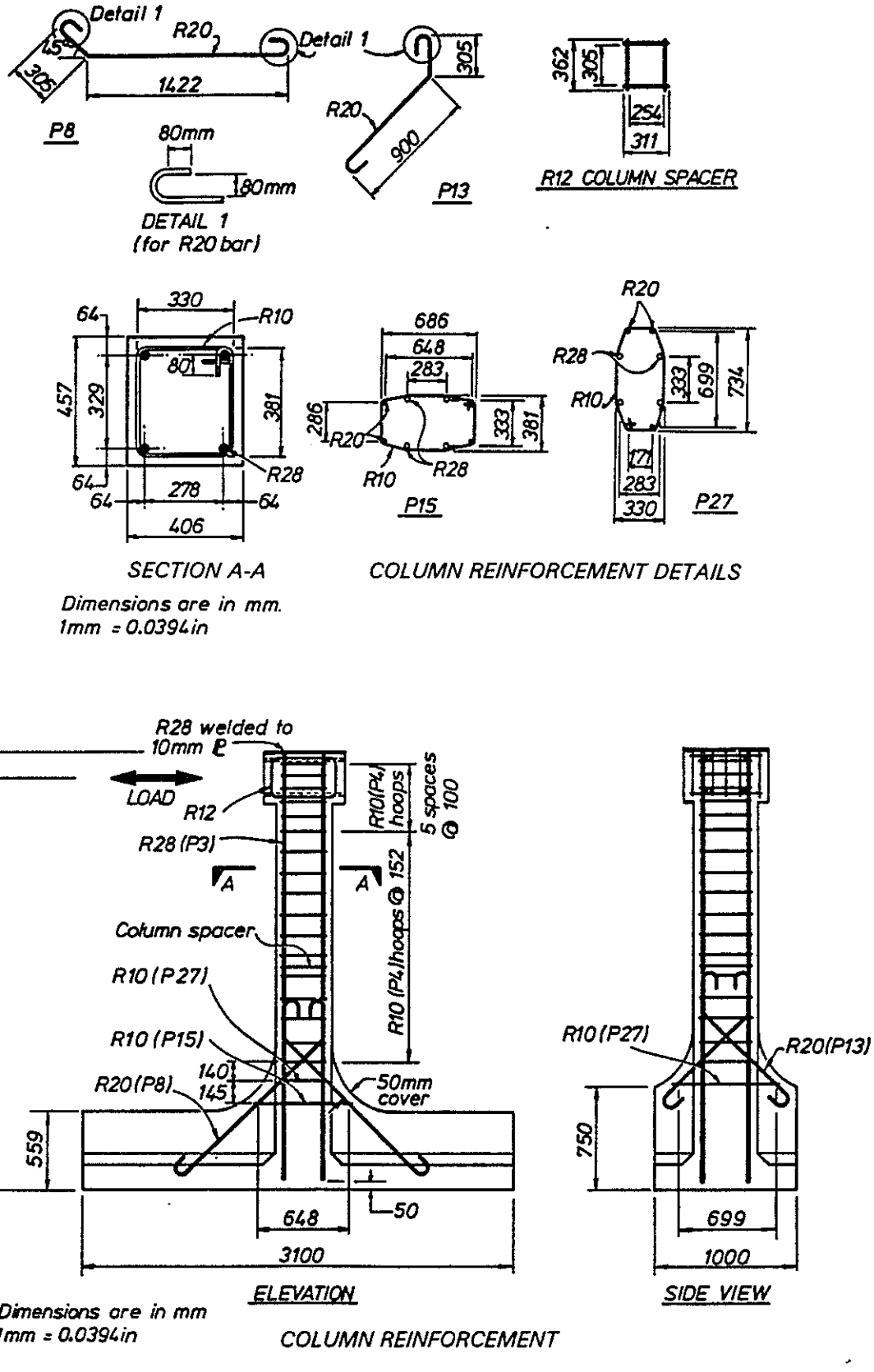

Figure 2.4 Details of column to crossbeam test specimen and reinforcing (Park et al. 1993).

The longitudinal and transverse column reinforcement was from Grade 275 steel, as was the crossbeam and slab reinforcement. The prototype bridge would have been constructed using steel with a specified yield strength of 240 MPa (34 800 psi).

However, Chapman (1991) reports that site sampling in New Zealand has shown that, in structures built during the period 1930 to 1970, 95% of the samples of steel reinforcement possessed a yield strength which was at least 15 to 20% greater than the specified value. That is, the 5 percentile value was 276 to 288 MPa (40 000 to 41 800 psi).

2.4.2 Test Set-up and Procedure

Figure 2.5 shows the test set-up for the column to crossbeam specimen. A 100-tonne hydraulic jack was used to apply the cyclic, static lateral loading at the top of the specimen. The axial compressive load was applied to the column by steel rods on each side of the specimen, tensioned by hydraulic jacks.

The axial load ratio was maintained at $P_u/A_g f'_c = 0.085$ throughout the testing. Linear potentiometers were used for measuring the lateral displacements of the top of the unit and the longitudinal deformations in the potential plastic-hinge region of the column. Electrical-resistance strain gauges were attached to the column longitudinal reinforcement and to the hoops in the expected plastic-hinge region.

As shown in Figure 2.6, the experimental yield displacement, Δ_y, was calculated by extrapolating a straight line from the origin of the measured lateral-load versus lateral-displacement curve through the point on the curve at 0.75 V_i, up to V_i, where V_i is the theoretical ultimate lateral capacity. V_i was calculated from the column flexural strength using the code approach of a rectangular compressive stress block, an ultimate concrete stain of 0.003, the measured values of the concrete compressive strength and steel yield strength, and assuming a strength reduction factor $\phi = 1$.

Having defined Δ_y, the subsequent cycles of loading were displacement-controlled to increasing levels of displacement ductility ratio, $\mu = \Delta/\Delta_y$.

The specimens were tested with (typically) two cycles of lateral load at each ductility level up to a displacement ductility, μ, of 7. Figure 2.7(a) shows the measured lateral-load versus lateral-displacement hysteresis loops for the specimens. The dashed lines in the figure indicate the theoretical ultimate lateral load V_i including the reduction due to the P-Δ effect.

2.4.3 Test Results

The first flexural cracks in the unit commenced at about 50% of the theoretical ultimate lateral load. Starting from low levels of ductility, one main flexural crack developed at the critical section of the column. At $\mu = 6$ this crack opened to a width of about 10 mm. As the testing progressed, the measured lateral-load versus lateral-displacement hysteresis loops became pinched and there was a significant loss of stiffness in the column.

Figure 2.5 Test set-up for column to crossbeam specimen (Park et al. 1993).

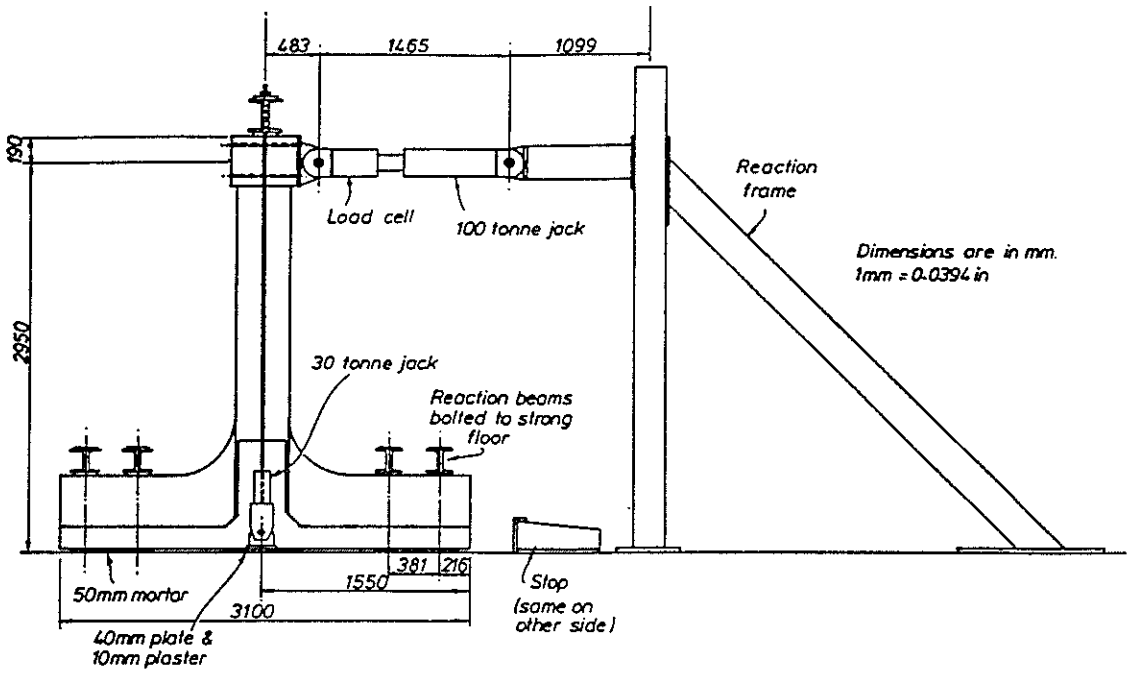

Figure 2.6 Definition of yield displacement.

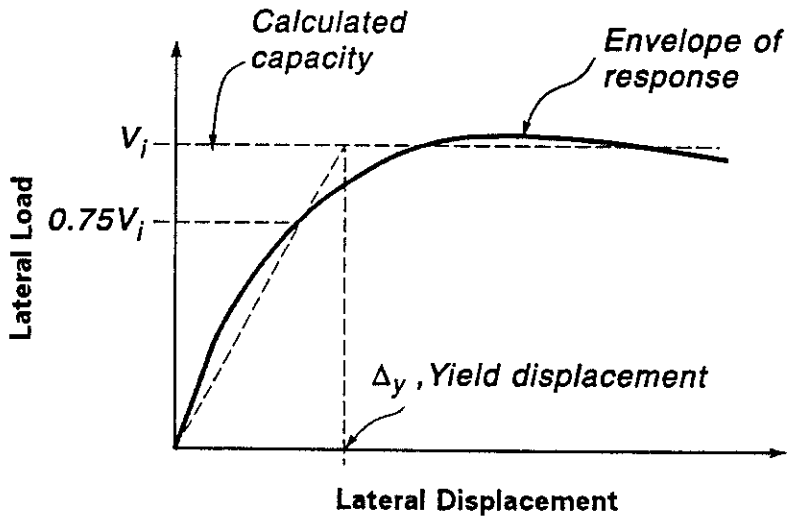

The maximum measured lateral load was about 70% of the theoretical lateral capacity, V_i, calculated assuming adequate anchorage of longitudinal reinforcement. The flexural strength was calculated at the critical section of the column and included the contributions from both the longitudinal column bars and the inclined column bars at that section. The test confirmed the poor anchorage of the straight, undeformed, longitudinal column bars. The poor anchorage led to reduced lateral capacity and to an increasingly flexible structure as the test progressed.

The test was terminated after the load cycle to a displacement ductility of $\mu = \pm 7$. At this level of lateral load there was some concrete crushing and the longitudinal and transverse reinforcement were exposed in one corner of the column. The critical section in the column, where the major crack formed, was about where the diagonal bars crossed the longitudinal bars in the column.

The strain measurements confirm that, as the test progressed, the anchorage of the longitudinal bars deteriorated, resulting in slip of the bars. The longitudinal concrete strain at the critical region of the column, measured by the linear potentiometers attached to the column, is much higher than the strain measured on the longitudinal bars in that region by strain gauges. The difference in measured strains indicates that significant slip of the plain round bars occurred from the onset of inelastic behaviour of the sub-assemblage. The pinching of the lateral-load versus lateral-displacement hysteresis loops shown in Figure 2.7(a) also reflects the bond deterioration of the plain-round reinforcing bars.

The strain gauges on the column hoops recorded strains below yield. Hence the concrete mechanisms of transferring shear were making a significant contribution to the shear strength of the column (Park et al. 1993).

2.5 Tests of an Anchorage-Retrofit Specimen

The first repair and upgrade of the original specimen was designed to improve the anchorage of the column longitudinal bars. This was achieved by breaking into the deck-slab concrete, welding steel plates onto the exposed ends of the column longitudinal bars, and reinstating the removed concrete.

2.5.1 Anchorage Test Block

First a trial of the procedure was conducted by casting a concrete block with a 28 mm (1.10 inch) diameter plain round Grade 275 bar in it, as shown in Figure 2.8. When the concrete had gained strength a hole was chipped in the end of the block to expose the end of the bar, so that a steel plate with a centrally drilled hole could be fitted over the bar and welded in place from above. The remaining cavity was then filled with a cement-based mortar. The 28-day compressive strength of the concrete was 24 MPa (3500 psi); the 28-day strength of the mortar was 30 MPa (4400 psi).

Figure 2.7 Lateral-load versus lateral-displacement hysteresis loops for column to crossbeam specimen.

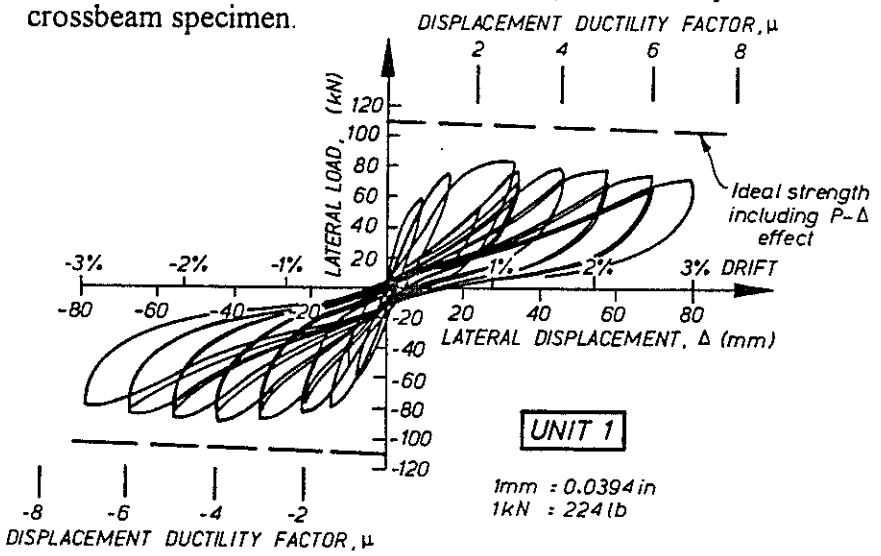

(a) As-built specimen

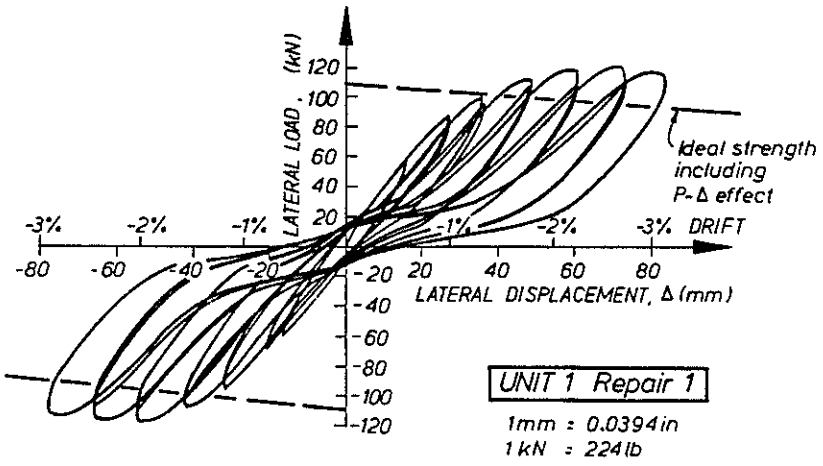

(b) Anchorage-retrofit specimen

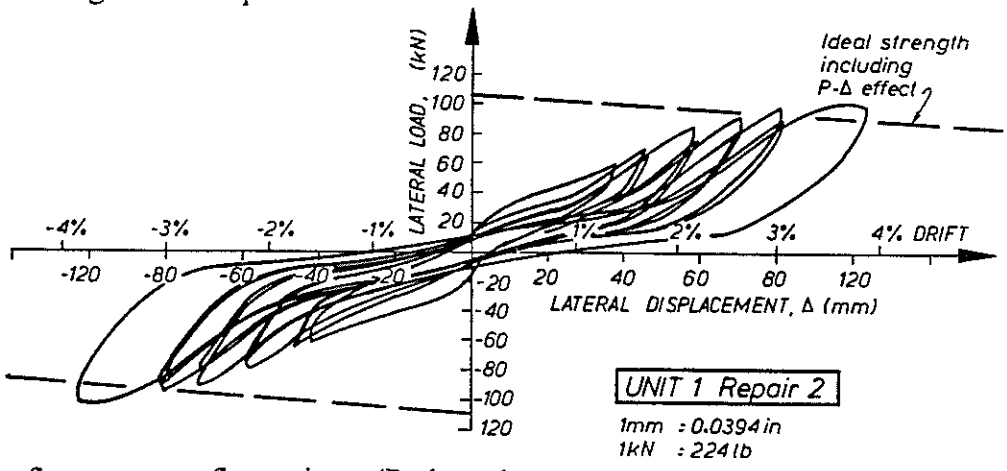

(c) Confinement retrofit specimen (Park et al. 1993).

The protruding end of the bar at the other end of the block was loaded in tension in a testing machine, with the block held to provide the reactive load. The test revealed that the steel plate provided sufficient anchorage to allow the bar to develop its yield strength in tension. The anchorage block was then tested with the reinforcing bar in compression. At a force of 64% of the steel yield strength the specimen failed with a cracking around the concrete-mortar interface.

2.5.2 Retrofit Procedure

The procedure was then used to retrofit the anchorage of the longitudinal bars in the column to crossbeam specimen. After chipping out the deck concrete to expose the ends of the longitudinal bars, it was discovered that the deck reinforcement running in both directions directly adjacent to the column bars prevented the square steel plates from sliding over the column bars far enough for adequate welding. To get around this problem, the plates were trimmed to fit past the slab bars, and were welded to the slab bars as well as to the end of the longitudinal columns bars. In practice, construction adjustments of this type resulting from "on-site discoveries" are common in the seismic retrofitting of structures. The excavated concrete around the ends of the bars was replaced with cement mortar as for the test block, shown in Figure 2.8. The repair of the specimen was completed by injecting epoxy resin into the flexural cracks of the specimen which had formed in the previous lateral load test.

2.5.3 Test Results

The anchorage-retrofitted specimen was then tested under the same set-up and loading as were previously used for the original specimen. For this test, it was again found that cracking tended to concentrate in one or two large cracks. Figure 2.7(b) shows the measured lateral-load versus lateral-displacement hysteresis loops. The test demonstrated that the addition of the end-plate anchorages permitted the column to reach its full theoretical flexural strength, although the lateral-load versus lateral-displacement hysteresis loops again showed a marked pinching and loss of stiffness at low lateral-load levels. It was evident that significant elongation of the column bars was occurring over their unbonded length, between the critical section for flexure in the column and the anchor plates at the bar ends. Hence the degradation of bond strength that had occurred along the column bars during the first test had not been restored by the epoxy-resin injection. Some crushing of column concrete was observed at the end of the test, particularly at the column corners in the plastic hinge region (Park et al. 1993).

2.6 Tests of a Confinement-Retrofit Specimen

The second repair and retrofit of the column to crossbeam specimen involved chipping off the cover concrete of the column in the vicinity of the plastic hinge region and placing additional transverse hoops. The three new hoops, shown as A2, B2, and C2 in Figure 2.9, were each placed as two C-shaped halves, lapped, and fillet welded in place. The cover concrete that had been removed was then reinstated. The installation of the new hoops reduced the hoop spacing from 152 mm in the original specimen to 76 mm in the confinement-retrofit specimen.

The confinement-retrofit specimen was then tested under the same set-up and loading as were used previously. It was found that the lateral-load versus lateral-displacement behaviour of the sub-assemblage was again dominated by the earlier bond failure along the end regions of the longitudinal column bars (Figure 2.7(c)). The column deformations resulted mainly from the elongation of the unbonded lengths of longitudinal bar between the critical section in the column and the anchor plates. Hence large plastic-hinge rotations were not required to occur in the column. The unit achieved its theoretical ultimate strength only at large lateral displacements, because of its very flexible behaviour (Park et al. 1993). The added transverse reinforcing is likely to have had no effect on the response.

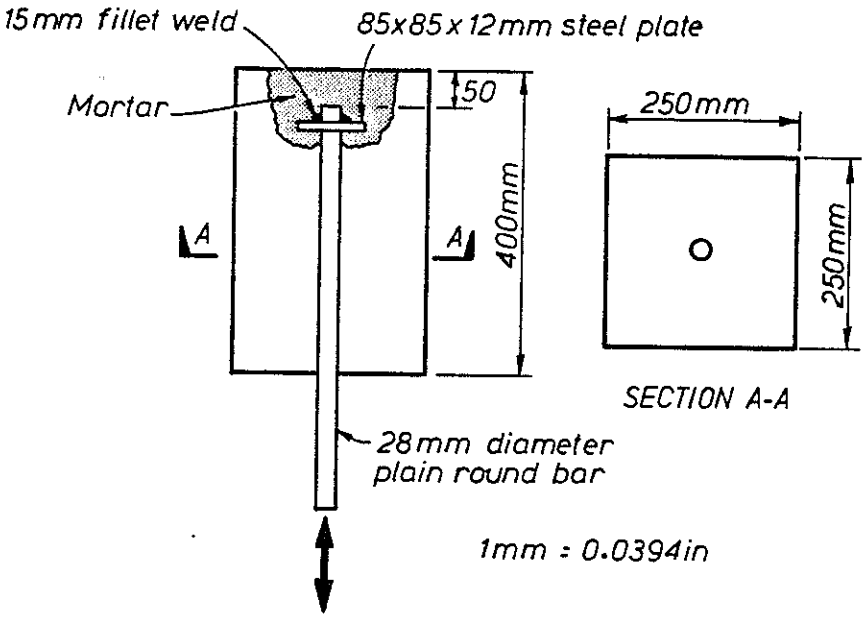

Figure 2.8 Test specimen for anchorage-retrofit detail using a steel end plate (Park et al. 1993).

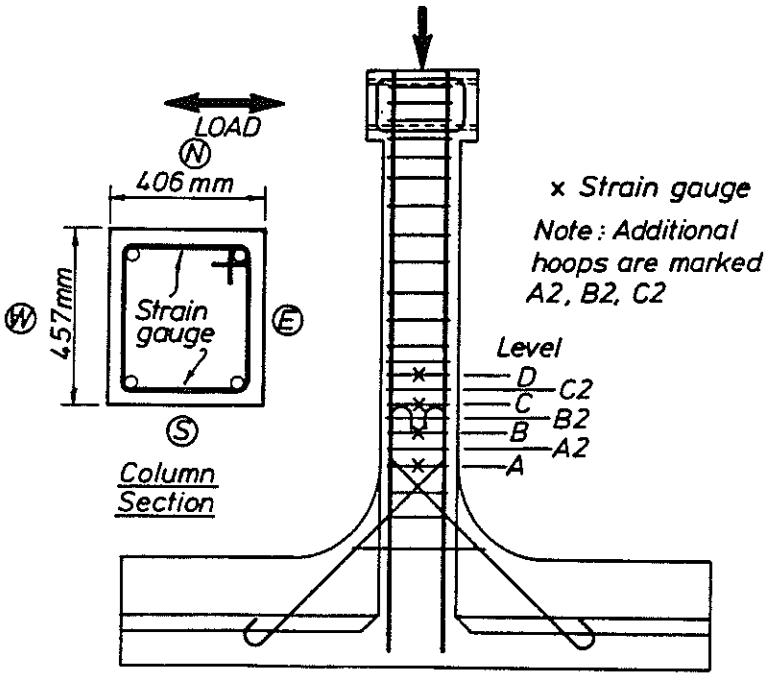

Figure 2.9 Confinement-retrofit specimen with new hoops added at A2, B2 and C2 (Dekker and Park 1992).

3. COLUMN TO FOUNDATION-BEAM TEST & OBSERVATIONS

After the testing of the as-built and retrofitted column-top plastic-hinge detail, by Rodriguez, Dekker and Park (Dekker and Park 1992, Park et al. 1993) described in Chapter 2 of this report, the present author undertook the testing of the second critical area of the bridge, the column-bottom plastic-hinge region. This Chapter 3 describes the column to foundation-beam testing and observations. Originally it was planned to test a confinement-type retrofit of the column to foundation-beam specimen, but the seismic evaluation and initial testing results showed clearly that such a retrofit would have little effect on the seismic response of the structure.

3.1 Test Specimen and Materials

A full-scale specimen representing the bottom half of the column and a portion of the foundation beam was constructed, following the original structural drawings of the bridge. Figure 3.1 shows the column to foundation-beam test specimen and reinforcing details.

3.1.1 Reinforcement Details

As with the previous (column to crossbeam) test specimen, the rectangular column section is 457 mm by 406 mm (18.0 by 16.0 inches). It is reinforced with four plain-round longitudinal bars 28 mm in diameter, approximating the 1-inch (28.6 mm) bars of the actual bridge. The bars are anchored into the foundation beam with a 915-mm embedment length and 180° degree end hooks, as shown in Figure 3.1 (test specimen) and Figure 2.3 (the actual bridge). Diagonal bars 20 mm in diameter approximate the ¾-inch (19.1 mm) diameter diagonal bars of the prototype, and 10 mm hoops are used to represent the ⅜-inch (9.53 mm) diameter hoops of the prototype. The diagonal bars and hoops both have 180° hooks at the ends of the bars. The hook diameters and extensions are representative of the standard used at the time of the bridge's design (NZBRC 1931) and check against the overall bar lengths given in the reinforcement schedule of the original drawings.

At the top of the specimen, the column-longitudinal bars are welded to a 10 mm-thick steel plate. Similarly, at each end of the foundation beam the beam-longitudinal bars are welded to a 10 mm-thick end plate. The reinforcing steel cage for the column to foundation-beam specimen is shown in Figure 3.2(a). All of the reinforcing is undeformed.

Figure 3.1 Column to foundation-beam test specimen and reinforcing details.

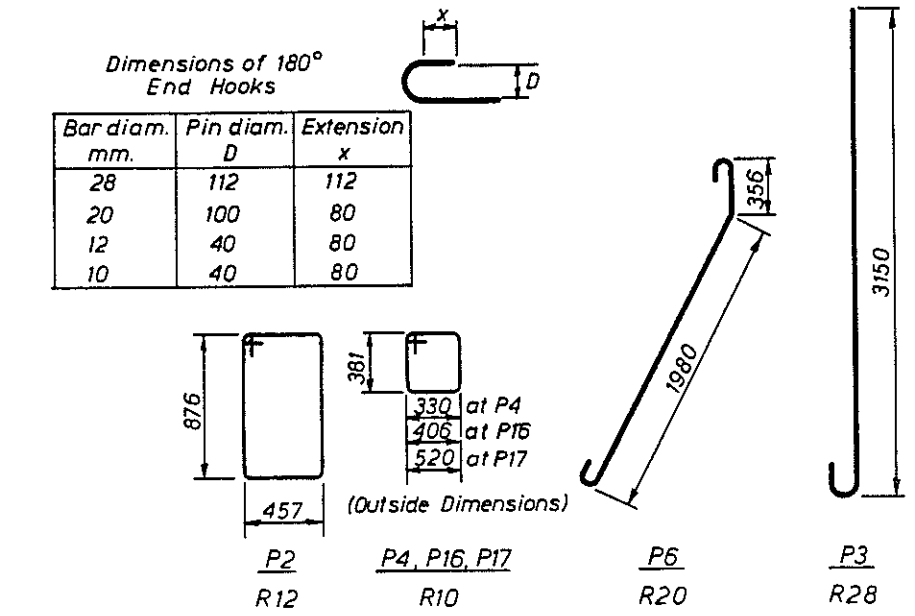

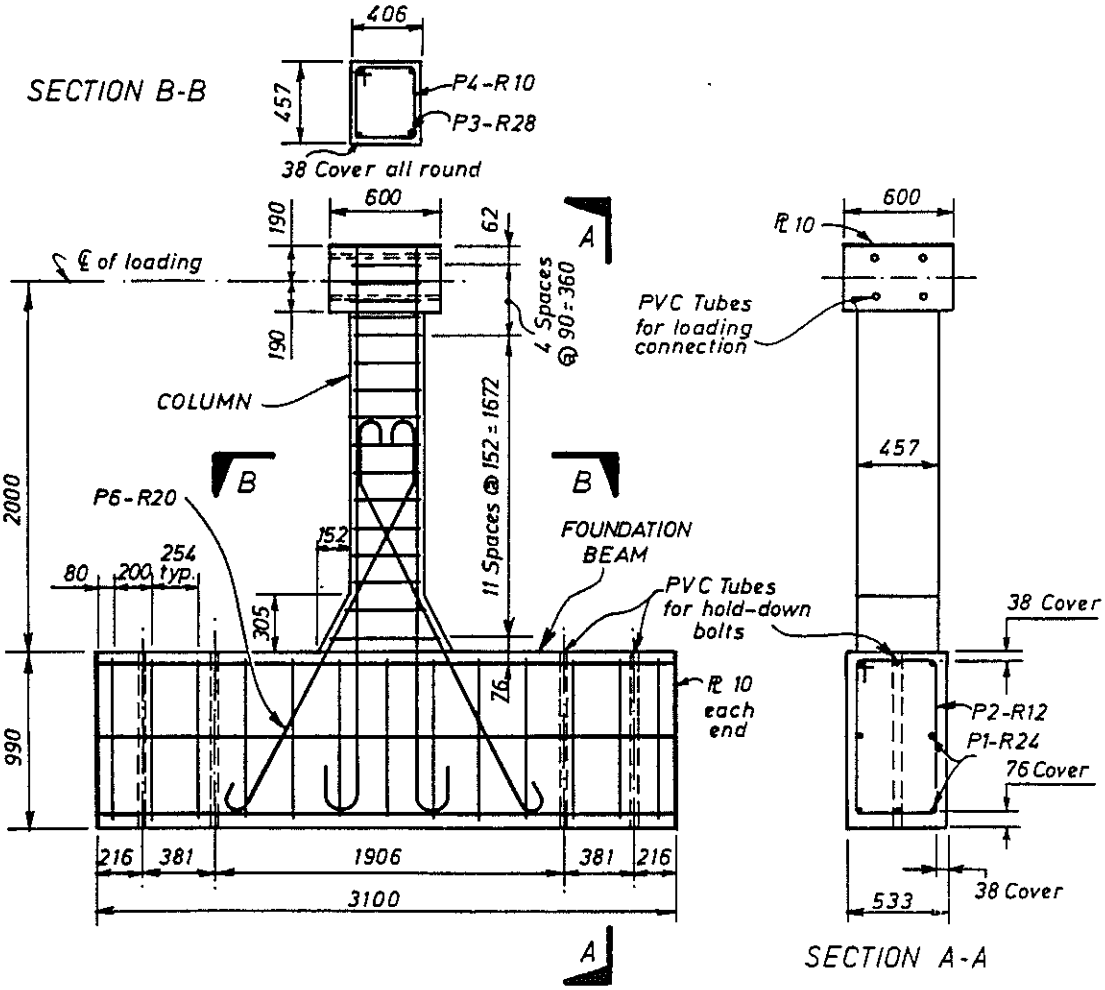

3.1.2 Concrete Placement and Strengths

The specimen was held upright for the placement of the concrete. The concrete was placed in two batches as would have been done for the construction of the actual bridge. The first batch of concrete was used to place the foundation beam. The specified slump of the concrete was 100 mm, but the actual slump of the concrete when delivered to the laboratory was 180 mm. It was decided to accept the concrete despite its non-conformance to the slump specification, because (a) the expected critical plastic-hinge region did not extend into the foundation beam, (b) it was judged that the concrete would still come up to near its specified strength, and (c) material specifications and quality control in 1937, when the bridge was constructed, were probably not strict, particularly for foundation concrete. Thus some of the actual bridge foundations could have been cast with concrete mixes having higher actual slump.

3.1.2.1 Construction joint

The column to foundation-beam specimen is designed to have a construction joint level with the top surface of the foundation beams, between the two pours of concrete. One day after the concrete placement it was intended to roughen the construction joint surface by wire-brushing away the still-pliant mortar paste and exposing a rough surface of coarse aggregate to an amplitude of 6 mm (¼-inch). This was not possible, however, because the high-slump mix allowed segregation of the concrete, and the top few centimetres of the foundation beam contained little coarse aggregate.

To create a sound construction joint, the concrete at the column location was chipped down 70 mm (3 inches) below the top surface of the foundation beam, where a rough surface of projecting coarse aggregate could be exposed. The surface was air-blasted clean before placement of the column concrete. The original structural drawings for the bridge give no details regarding construction joints. In practice the joints may have been prepared with a roughened surface or may have been formed with keys.

3.1.2.2 Concrete strength

The column concrete was placed, from one batch in two lifts, eight days after the placement of the foundation concrete. The slump was 110 mm. Both batches of concrete were specified to have a 20 mm top-size aggregate and 19 MPa compressive strength at 28 days. Table 3.1 shows the results of the compressive strength tests, taken from 200 mm high by 100 mm diameter (7.9 by 3.9 inch) uncapped cylinders. The foundation concrete had a 28-day average strength of 19.3 MPa (2800 psi) and an average strength of 20.1 MPa (2920 psi) at the time (105 days after placement) of the column to foundation-beam test. The column concrete had a 28-day strength of 20.0 MPa (2900 psi) and a strength at test of 23.6 MPa (3430 psi). For the structural calculations, a strength of 23.6 MPa was used for the test specimen, and 20 MPa was assumed for the actual bridge.

Figure 3.2 Test of the column to foundation-beam specimen:

(a) Reinforcing steel cage

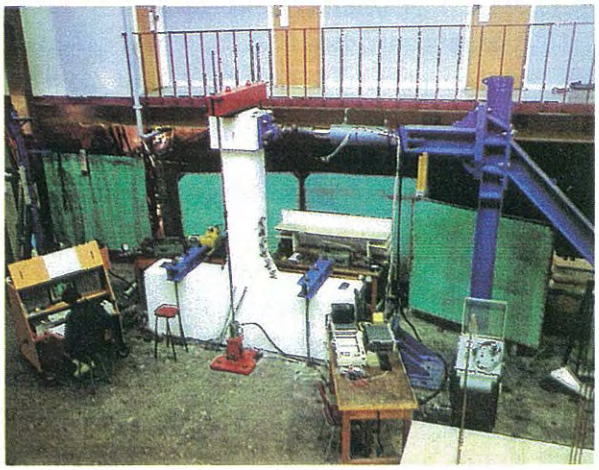

(b) Test set-up

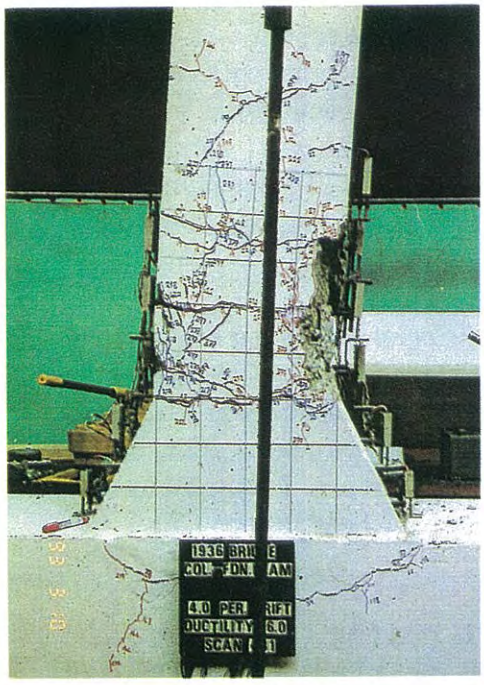

(c) Damage to the plastic-hinge region at ductility μ = 6

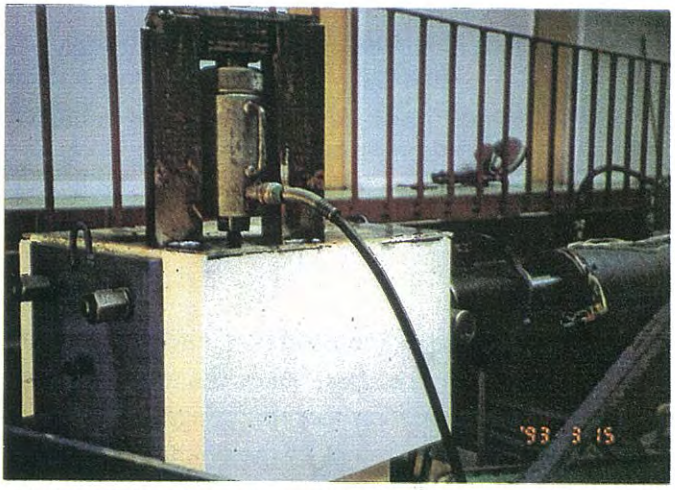

(d) Top plate where three of the longitudinal bar end welds failed; thus testing the capacity of the fourth weld

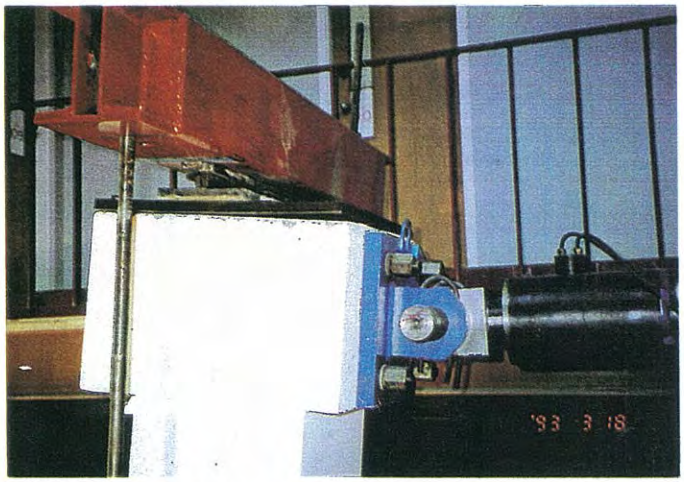

(e) Displacement of the new top plate caused by bond slip

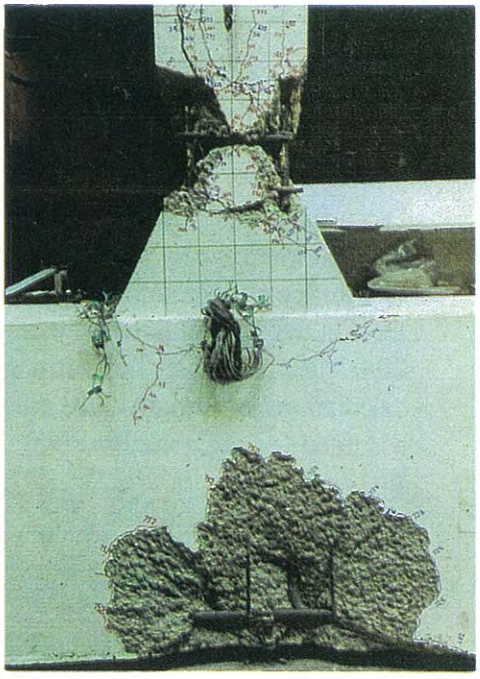

(f) Anchorage splitting failure at bottom ends of longitudinal bars

3.1.3 Reinforcing Steel Strengths

Grade 275 (40 000 psi) reinforcing steel was used in the test specimen. Tension tests on sample lengths of the reinforcing steel showed that actual yield strengths are 15% to 23% greater than the 275 MPa specified minimum. Figure 3.3 shows the stress-strain behaviour of one of the test samples, and all the test samples showed the well-defined yield point and yield plateau as shown in Figure 3.3. The plain-round reinforcing exhibits an upper yield point approximately 10 MPa above the lower yield point and yield plateau. Deformed reinforcing typically does not show such a sharp yield transition or an upper yield point (J.Restrepo pers.comm. 1993). This is because stress concentrations at the deformations cause a slight premature yielding and a rounding of the stress-strain curve for deformed reinforcing.

Table 3.1 Concrete strengths of bridge foundation and column before and at test.

Location (Date Placed)	Slump (mm)	Age at Test (days)	Compressive Strength Results (MPa)	Average Strength (MPa)
Foundation (23 November 1992)	180	1.2	1.8	1.8
		7	12.0, 12.6, 10.2	11.6
		29	17.8, 21.0, 19.0	19.3
		105 (at test)	19.9, 20.2, 20.1	20.1
Column (1 December 1992)	110	7	13.0, 14.8, 14.0	14.3
		28	20.4, 19.9, 19.7	20.0
		97 (at test)	23.2, 23.3, 24.3	23.6

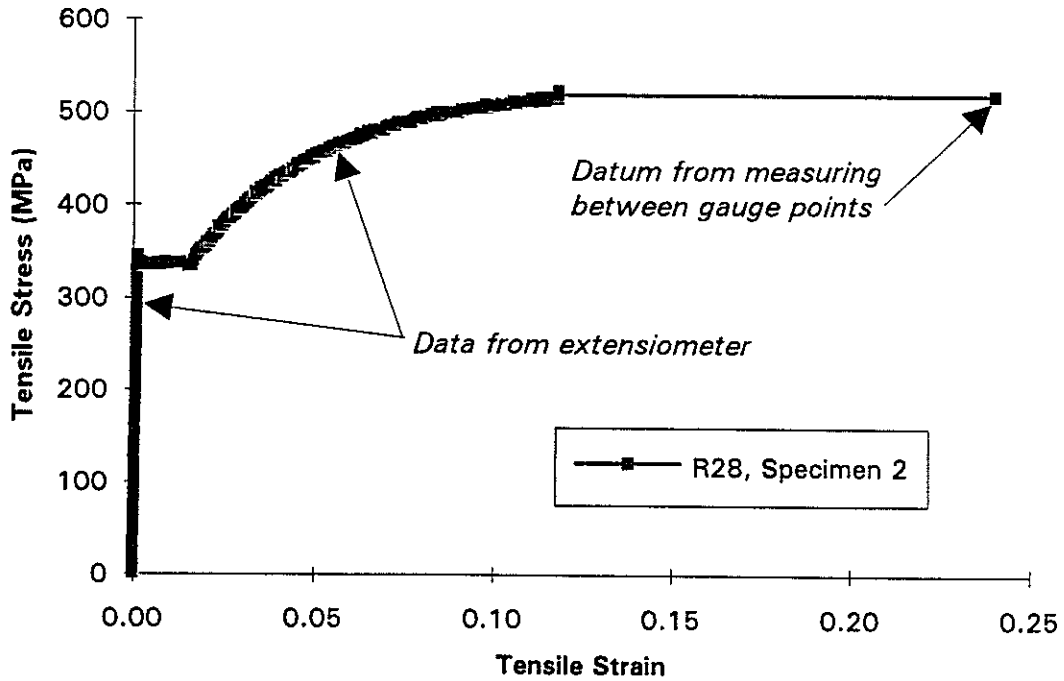

Figure 3.3 Typical stress versus strain behaviour of the reinforcing steel used in the column to foundation-beam specimen.

Table 3.2 shows the results of the reinforcing steel testing. In the structural calculations 337 MPa (48 900 psi), the average for the R28 specimens, is used as the steel yield strength for the test specimen. For the actual bridge, the specified yield strengths would have been 240 MPa (34 800 psi). However, to account for typical overstrengths (Chapman 1991), a strength of 280 MPa (40 600 psi) is used for the prototype bridge in the structural calculations.

Table 3.2 Strengths after testing of reinforcing steel used in the bridge.

Bar Size	Yield Strength Results (MPa)	Average Yield (MPa)	Ultimate Strength Results (MPa)	Average Ultimate (MPa)	Elongated lengths between 60 mm gauge points (mm)	Average % Elongation**
R28	431 331 349	337	519 519 519	519	73-76-85*-74-74 72-74-88*-76-76-74 74-90*-74-75-77-74	24
R24	314 330 312	319	485 487 480	485	74-74-86*-76-74 76-77-88*-74-72 72-76-87*-79-73	23
R20	334 341 339	338	495 495 495	495	70-72-84*-73-73-72 72-85*-74-74-72 71-73-85*-72-73-73	21
R12	319 312 319	317	432 434 437	434	68-68-79*-70-69 68-78*-71-67-68 66-69-71-78*-68	14
R10	335 341 333	336	463 472 463	466	68-81*-70-69 70-67-76*-67-69 78*-72-70-68-68	15

* Indicates gauge segment where necking and fracture occurred.

** Average % elongation is the average for all those gauge segments except those where necking and fracture occurred.

3.1.4 Strength of Test Specimen versus Prototype Column

The strength of the test-specimen column differs from the strength of the prototype column. This is because of:

- the difference in steel yield strengths as indicated above,
- the slight difference in reinforcing bar areas, e.g. a 28.0 mm-diameter bar is used to model the prototype's 1⅛ inch (28.6 mm)-diameter bar, and
- the slight difference in concrete strength.

These differences result in the moment strength of the test column being 16% greater than that of the prototype. The differences in moment strength as well as shear strength have been taken into account in both the calculations and the results, in this and the subsequent chapters of this report.

3.2 Test Set-up and Instrumentation

As shown in Figure 3.4, the test set-up for the column to foundation-beam specimen was similar to that for the column to crossbeam specimen. Cyclic static lateral loading was applied to the top of the specimen, the load point corresponding to the mid-column-height inflection point in the actual structure. The lateral load was applied by a hydraulic jack reacting against a steel frame, and was monitored by a full-bridge load cell on an 8-volt DC power supply. The lateral displacement of the column was recorded by two linear potentiometers, one at the level of the lateral load and one at a level 500 mm below.

3.2.1 Axial Load

An axial compressive load of 300 kN (67 000 lb) was applied to the column at its centreline, by a crosshead and roller assembly over the top of the specimen. The crosshead was pulled down by two steel rods, one on each side of the specimen, tensioned with hydraulic jacks. The tensioned rods were connected to a 40-mm steel plate which passed underneath the specimen and was bolted to the laboratory reaction strong floor. Hydraulic lines connected the two axial-load jacks in parallel to a single hand pump, so that the loads on the jacks were equal. The applied axial load of 300 kN was monitored by calibrating the pressure gauge on the hand pump.

Figure 3.4 Test set-up for column to foundation-beam specimen.

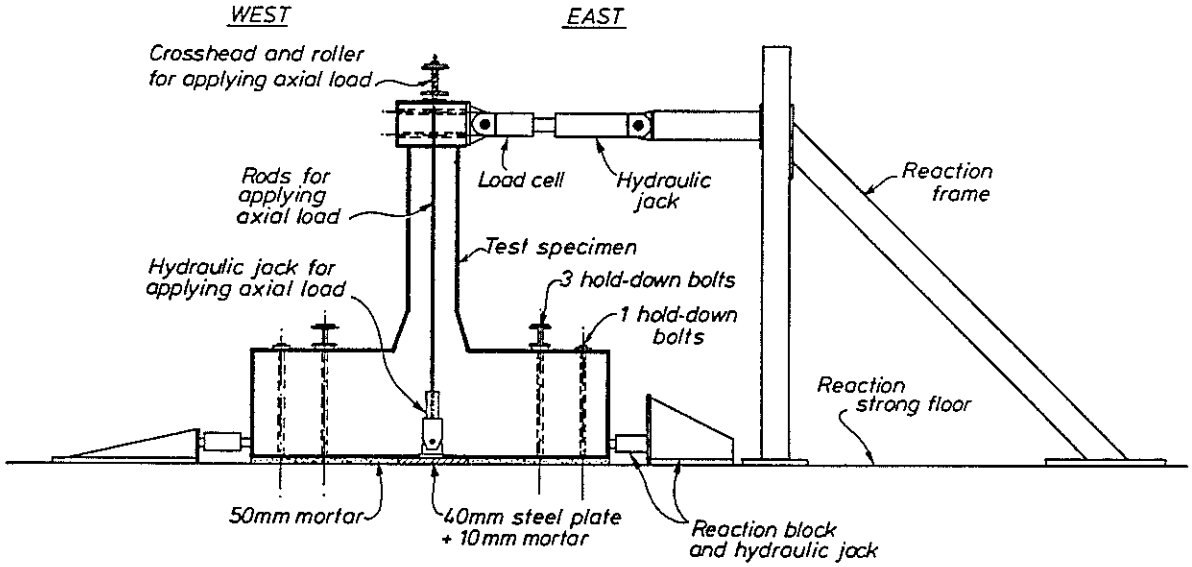

3.2.2 Base Reaction

Hydraulic jacks were also placed between the base of the specimen and reaction blocks at each end to prevent the potential sliding of the specimen. The pressure gauge for each of these jacks was calibrated so that any change in the horizontal reaction force, indicating sliding at the base of the specimen, could be observed. Before testing, a compressive load of 200 kN was applied to each jack to lock the base of the specimen in place. A horizontal dial gauge was set up to record any sliding movement.

Four 38 mm (1½-inch)-diameter bolts held each end of the foundation beam down to the reaction floor. This tie-down reaction was located at points on the foundation beam corresponding to the likely inflection points of the actual bridge foundation beam under lateral forces, i.e. at points half-way between adjacent bridge columns. For compressive base reactions, a 50 mm (2-inch) thick layer of cement mortar was placed underneath the entire specimen. A vertical dial gauge was installed to check if any uplift displacement of the specimen had occurred at the hold-down bolts during testing. The test specimen was painted white so that any development of cracks could be observed more clearly.

3.2.3 Instrumentation

The instrumentation of the column plastic-hinge region is shown in Figure 3.5. Six linear potentiometers were attached to each side of the column to measure the longitudinal deformations of the concrete. Eighty electrical-resistance strain gauges were attached to the reinforcing steel in the column plastic-hinge region. Strain gauges were placed on each of the four longitudinal bars at five levels, on each of the four diagonal bars at three levels, and on both legs of four of the transverse hoops. At each strain gauge location, two gauges were used on opposite sides of the bar. so that bar-bending strains could be accounted for.

The load-cell, linear potentiometers, and strain gauges were all connected to a data-acquisition unit. Half-bridge circuits were used for the potentiometers and quarter-bridge circuits were used for each of the strain gauges. Excitation for the potentiometers and strain gauges was 4 volts DC. The data-acquisition unit was controlled by a micro-computer and the custom-designed *PC Lab* software. In addition to the digital data acquisition, an analog x-y plotter was used to record lateral-load versus lateral-displacement, and a strain indicator was used to check the load cell output. Figure 3.2(b) shows the test set-up just before testing.

3.2.4 Interior versus Exterior Column Effect

The test models one of the interior columns of the typical four-column bridge pier shown in Figures 2.2 and 2.3. The details at the base of the exterior column are somewhat different than those at the interior column as shown in Figure 2.3. The significance of the different detailing the exterior columns is discussed in Section 4.4.

Figure 3.5 Instrumentation of column plastic-hinge region.

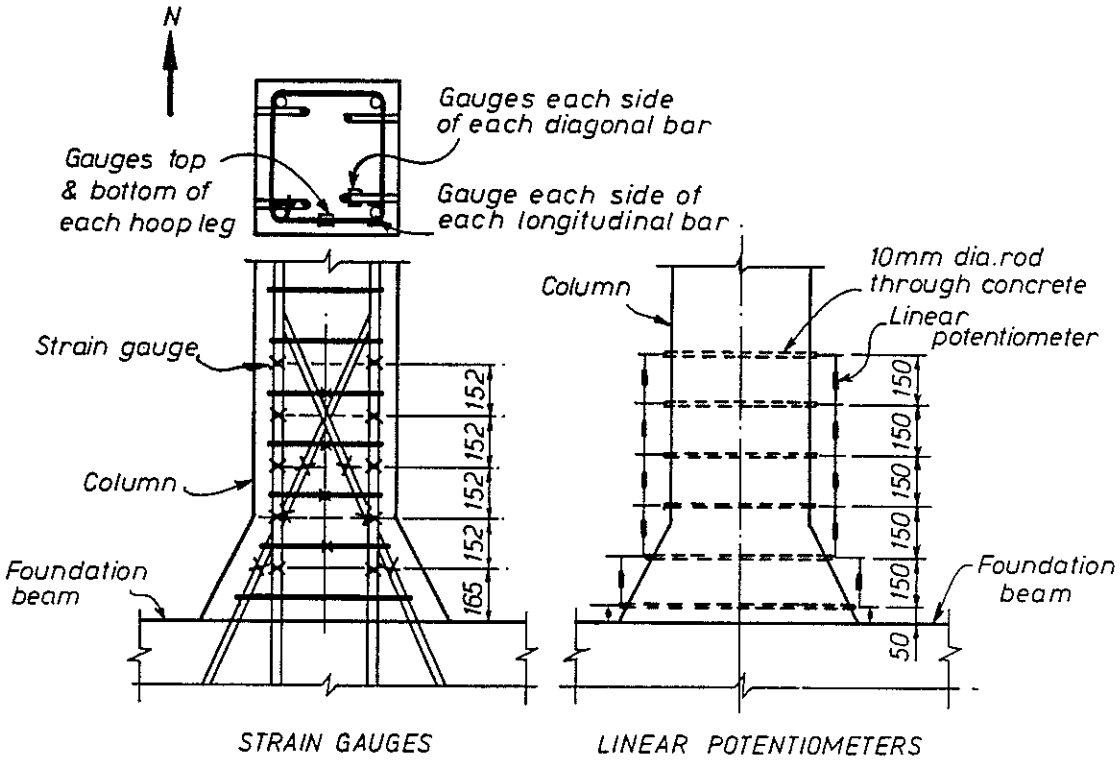

3.3 Test Procedure and Observations

3.3.1 Procedure

Figure 3.6 shows the loading sequence for the column to foundation-beam specimen. Lateral loading and displacements to the east (i.e. tension in the load cell) were defined as positive. The first two cycles in each direction were load-controlled to 0.75 times the calculated ideal capacity of the specimen, V_i. Following the method illustrated in Figure 2.6, the experimental yield displacement, Δ_y, was calculated as 1.33 times the deflection recorded at 0.75 V_i. The yield displacement Δ_y for the specimen was 16.0 mm (0.67% structure drift). Because of an error in calibrating the load-cell, the first cycle was actually taken to a load of only 0.68 V_i. However, the calibration error was detected by comparing the strain indicator readings to those of the data acquisition system, the load cell was re-calibrated, and the readings from the first cycle were corrected.

After the first four cycles of load, remaining cycles were displacement controlled. The specimen was displaced two cycles in each direction to the yield displacement, 16.0 mm, then two cycles in each direction to μ=2 (Δ = 32.0 mm), then to μ=3 (Δ = 48.0 mm), and so on up to μ=7, with two cycles in each direction at each increment of ductility, μ. At each of the ductility levels μ= 8, 9, and 10, one cycle of displacement in each direction was applied. Although it is not shown in Figure 3.6, three additional cycles in each direction to the maximum displacement stroke of the

hydraulic jack (approximately μ=12) were applied before finishing the test. The cycles of testing to the larger ductilities were conducted because they could potentially provide further useful information about the structural behaviour. However, for the actual bridge such large ductility demands would not be expected.

Figure 3.6 Load sequence and test observations.

Test Observations:

A Flexural-tension cracks on west face first observed at V (capacity) = 35 kN.
B Remove and recalibrate load cell.
C Flexural-tension cracks on east face first observed at V = –26 kN.
D Cracking caused by compression crushing on east face (ductility μ = +2.0).
E Minor cracking caused to compression crushing on west face.
F More extensive cracking caused to compression crushing on west face (μ = –3.0).
G Spalling on east face (μ = +5.0).
H Fracture of top-plate weld for first east longitudinal bar.
I Fracture of top-plate weld for second east longitudinal bar.
J Fracture of top-plate weld for one west longitudinal bar.
K Test remaining top-plate weld and repair top plate.
L Spalling on west face (μ = –6.0).
M Anchorage splitting cracks occur at the base of the foundation beam.

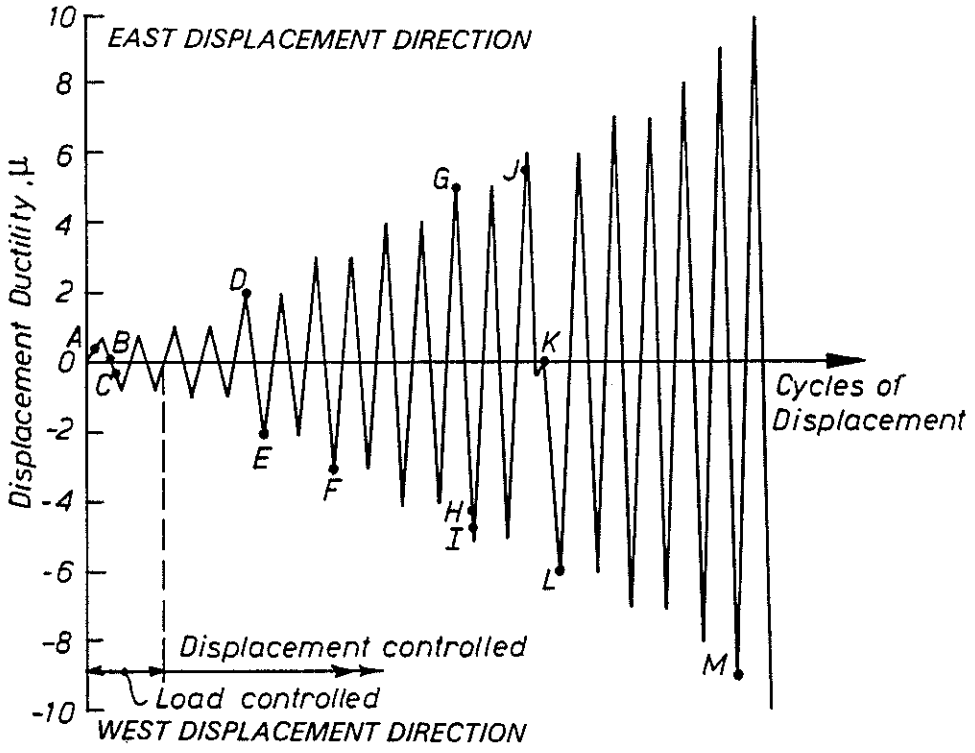

3.3.2 Specimen Cracking

The first flexural cracking of the specimen in each direction was observed during the first cycles at a lateral load of approximately 30 kN, 23% of the flexural capacity of the section. Cracks in the specimen occurring under eastward displacement cycles were marked with a red pen; cracks occurring under westward displacement cycles were marked with a blue pen. The number of the data scan at the time of cracking was also marked on the specimen alongside each crack as shown in Figure 3.2(c).

The first cracking of concrete caused by compression occurred, on the eastern face of the column, at ductility μ=2. Only minor cracking caused by compression on the opposite, western face occurred during cycles to $\mu = -2$ in the opposite direction. It was not until $\mu = -3$ that a similar level of cracking related to compression occurred on the western column face.

Likewise, spalling of the compression concrete occurred one ductility level sooner for the eastern column face than for the western column face. Spalling at the eastern face occurred at μ=5; spalling at the western face occurred at μ=6.

Figure 3.2(c) shows the column plastic-hinge region of the specimen at μ=6. Throughout testing, the flexural cracks which developed in the specimen were spaced relatively far apart, as would be expected in concrete members with plain-round reinforcing bars. The spacing between adjacent cracks over the height of the column was typically 150 to 300 mm (6 to 12 inches). For each direction of loading, the first crack in the specimen occurred just at the top of the flared column base, 300 mm (12 inches) above the foundation beam. The column diagonal bars cross the longitudinal bars at approximately this location. Up to ductility μ=5, the horizontal crack in this location was the widest of the flexural cracks. Figure 3.7 shows that the maximum width of this crack was 6.0 mm (0.24 inches) at μ=3 and 10.5 mm (0.41 inches) at μ=5.

The locations of this crack, and the two horizontal cracks 200 mm and 350 mm above it, coincide with the location where most of the crack opening and closing took place. Beyond ductility μ=5, the upper two of the three cracks began opening wider, indicating that the plastic-hinge region was lengthening. As shown in Figure 3.2(c), diagonal shear cracking occurred in the upper part of the column but did not occur in the region where the diagonal bars are present.

3.3.3 Axial Load and Horizontal Reactions

During the testing, the force in the axial load jacks fluctuated as the column was displaced laterally. The tendency is for the axial load to increase with lateral displacement and as testing progresses, because the axial loading system restrains the lengthening of the column. For the actual bridge under earthquake movement, column lengthening is not restrained and the axial load would not increase in this way.

Therefore, during testing, the pressure in the axial load jacks was periodically adjusted so that the applied axial load would remain roughly constant at 300 kN. Typically the axial load was adjusted two or three data scans before the peak lateral displacement

was reached. At the peak lateral displacement of each cycle, recordings of axial load varied from 283 kN to 326 kN. Between the peak lateral displacements in each direction the axial load tended to drop slightly. The minimum recorded axial load was 254 kN.

Readings taken from the dial gauges and reaction rams at the base of the specimen indicate that there was no sliding of the specimen and that the foundation beam remained fixed at its hold-down locations throughout the test, as intended. Periodic readings of the excitation voltage to the load cell, displacement potentiometers, and strain gauges indicate that the voltage remained constant.

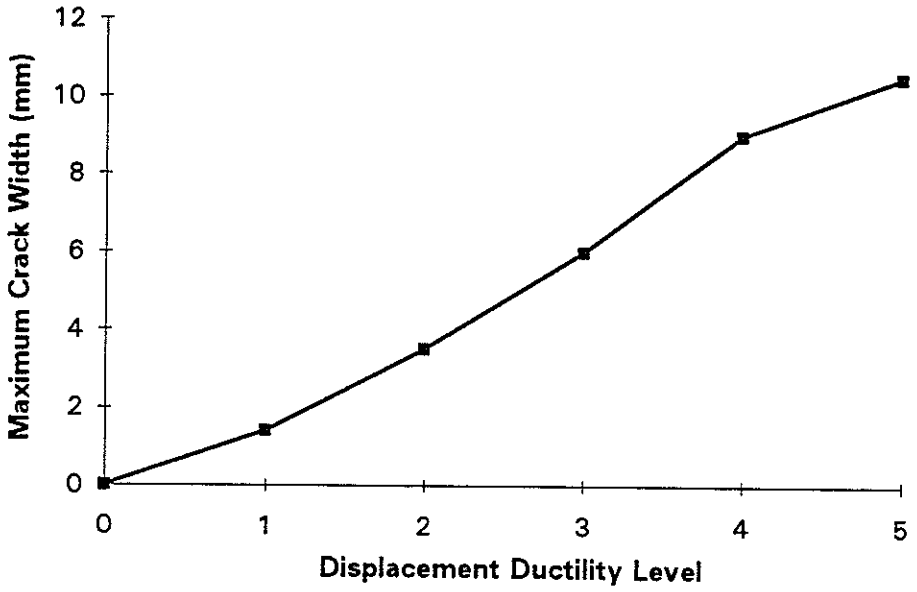

Figure 3.7 Maximum crack width (mm) measured during testing.

3.3.4 Lateral Load-Displacement Hysteretic Behaviour

The lateral-load versus lateral-displacement hysteresis loops of the column to foundation beam test up to ductility μ=7 are shown in Figure 3.8. The decreasing slope of the loops during the first four cycles in each direction (μ=0.75 and μ=1.0) indicates some stiffness degradation of the specimen occurring prior to the yielding of the tension reinforcing steel. This yielding occurred at ductility μ=2 in each direction, at which time the specimen reached its theoretical capacity, as shown by the hysteresis loops of Figure 3.8. Slight pinching of the hysteresis loops can be observed at μ=1.0. The pinching becomes pronounced by μ=3. The stiffness degradation and pinching of hysteresis loops indicates bond-slip of the flexural reinforcing.

The theoretical lateral-force capacity of the specimen, calculated using
(a) the (approximate) actual material strengths, f_y = 337 MPa and f = 22 MPa,
(b) the contributions of the diagonal bars, and
(c) an ultimate concrete strain of 0.005,
was 135 kN (30.3 kips).

The maximum capacity measured during testing was 138 kN in the eastward direction and 144 kN in the westward direction. Both maximum capacities were reached at the first cycle to ductility μ=2 in each direction.

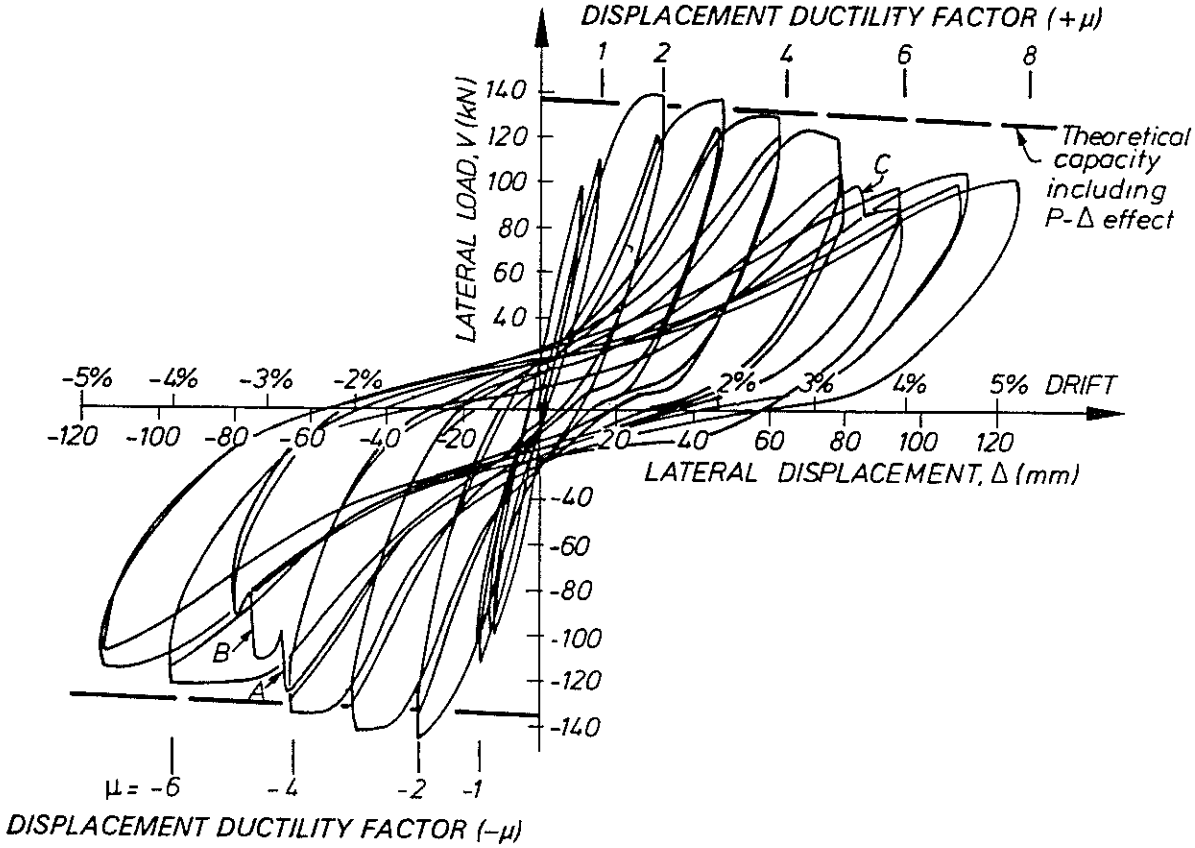

Figure 3.8 Lateral-load versus lateral-displacement hysteresis loops, to ductility μ=7, for the column to foundation-beam test.

3.4 Failure and Subsequent Testing of Longitudinal-Bar End Welds

On the first cycle of displacement to ductility μ= –5, nearing the peak displacement at a lateral load of 124 kN (27.9 kips), two loud bangs were heard indicating that something had broken. At each of these loud noises the lateral-load capacity suddenly dropped by approximately 20 kN (4.5 kips) as shown at points A and B in Figure 3.8.

3.4.1 Failure of Bar-End Welds

On inspecting the specimen it was discovered that the welds had fractured at the connection of the two longitudinal bars on the east side of the column to the steel plate at the top of the specimen. As shown in Figure 3.9(a), the longitudinal bars slipped approximately 5 mm with respect to the top plate as a result of the weld fracture.

Figure 3.9 (a) Fracture, (b) testing and (c) replacement of the longitudinal-bar end welds to the specimen top plate.

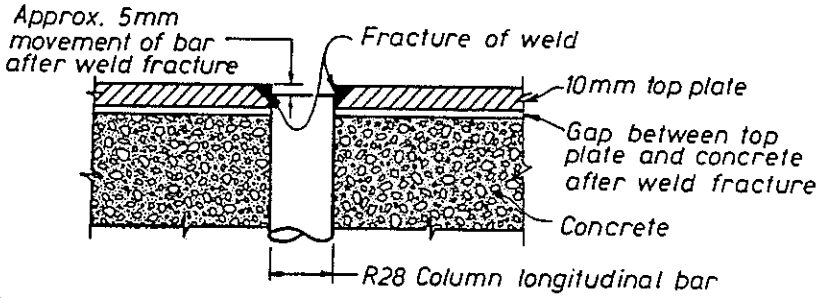

(a) Fracture of welds at NE, SE, NW longitudinal bars

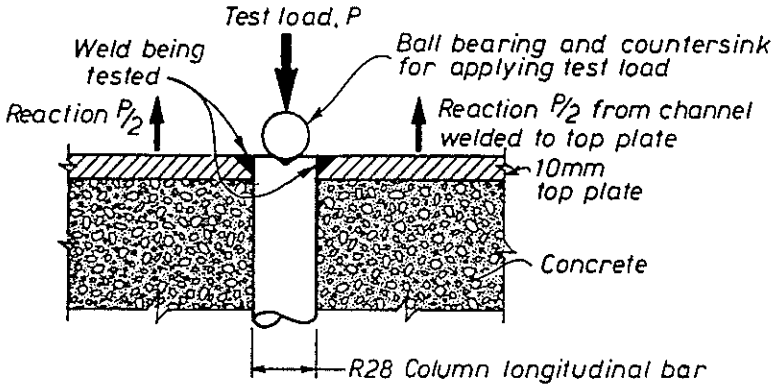

(b) Testing of weld at SW longitudinal bar

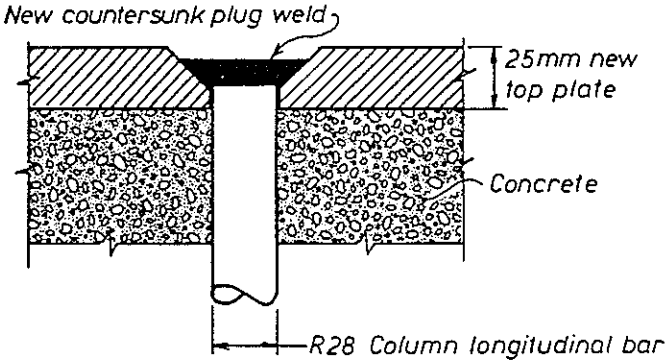

(c) Replacement of top plate and welds

Testing was continued. On the next cycle in the other direction, to μ= +5, capacity was diminished 13% compared with the previous cycle to μ= +5 (i.e. 103 kN compared with 119 kN previously). But the welds of the two tension bars on the west side of the column did not fracture as had the welds on the east bars. The slightly diminished capacity in this direction, at μ= +5, probably resulted from the loss of anchorage of the two compression bars, whose end welds had failed.

The second cycle to ductility μ= –5, showed a 30% drop in capacity (87 kN compared with 125 kN just before the weld fracture). This loss of capacity clearly resulted from the loss of end anchorage at the top of the column, of the two tension bars. The slip of these bars with respect to the top plate was again approximately 5 mm.

On the first cycle to μ= +6, at a displacement corresponding to μ= +5.3, one of the westward longitudinal-bar end welds failed with a loud bang. At this failure, the lateral-load capacity immediately dropped 15 kN as shown at point C of Figure 3.8. Testing was continued and the peak displacement at μ= +6 was reached without failure occurring in the last remaining longitudinal-bar end weld.

The failure of these end welds was not anticipated. The end welds are located 190 mm (7.5 inches) above the column inflection point and 1.9 m (6.2 ft) above the critical section of the column. It had been assumed that over this 1.9 m length, equal to 68 bar diameters, enough bond resistance would be present so that the tension force in the end welds would be small. This assumption was shown, by the fracture of the welds, to be incorrect.

3.4.2 Testing of Bar-End Weld

Because no instrumentation was in place to measure bar strains away from the plastic-hinge region, the tension force present at the ends of the R28 bars, which caused the welds to fail, was not known. To gain this important piece of data, it was decided to test the capacity of the remaining intact weld. This was accomplished by setting up a hydraulic jack which pushed down on the end of the bar and reacted against the steel top plate.

The testing of the weld is shown in Figures 3.2(d) and 3.9(b). As shown in Figure 3.9(b), the top end of the R28 bar was countersunk so that a concentric point load could be applied to it through a ball bearing. The reaction to this load was carried into the steel top plate through a small crosshead frame around the hydraulic jack as shown in Figure 3.2(d). The crosshead frame was made up of 150 mm-deep steel channel sections, and was welded to the top plate. The hydraulic jack and its pressure gauge were calibrated before the weld test.

3.4.3 Estimate of Tension Force at Weld Failure

The weld failed under a test load of 95 kN (22 kips). This equals 46% of the yield strength of the R28 bar. How representative this test result is of the capacity of the three other welds which failed previously, during the testing of the column to foundation-beam specimen, must be considered. On the one hand, the capacity of the fourth weld should be somewhat greater than the capacity of the first three welds,

because it did not fail under the column testing to μ=6. On the other hand, a small amount of grinding on top of the top plate at the weld was necessary to locate the bar before testing the weld. This grinding may have slightly reduced the capacity of the weld.

The capacity of the first three welds which failed can also be estimated, based on the drop in lateral load at fracture during the column test. Assuming a moment arm between internal tension and compression forces that stays constant at 300 mm at the critical section, the lateral-load drop of 20 kN (for the first two bars) corresponds to a drop in bar tension of 110 kN at the critical section. The lateral-load drop of 15 kN for the third bar corresponds to a bar-tension drop of 85 kN. However, the drop in bar-tension at the critical section is not necessarily equal to the loss of capacity at the end weld. The change in the amount of bond-resistance along the 1.9 m length between the critical section and the end weld may have been caused by the sudden increase in bar-slip upon the fracturing of the end welds.

Considering the above factors and test data, the tension in the ends of the longitudinal bars, at a column displacement ductility μ of 5, was estimated to be between 35 and 55% of the yield force (72 kN to 114 kN).

3.5 Continuation of Column-specimen Testing and Observations

3.5.1 Procedure

After testing the weld, the top plate of the specimen was removed and replaced with a new 25 mm-thick top plate. The new top plate was attached to the four longitudinal bars using countersunk plug welds as shown in Figure 3.9(c). Testing of the column to foundation-beam specimen was then continued.

Slip of the bars at the top of the specimen was still occurring. On loading in each direction, the two longitudinal bars which were in compression pushed the new top plate away from the specimen. At a ductility of μ=10, the slip at the compression bars caused a gap of as much as 10 mm between the top plate and the concrete as shown in Figure 3.2(e).

Because the stiffness and strength degradation characteristics of the specimen seemed to result mainly from the poor bond characteristics of the plain-round reinforcing bars, it was judged that testing a confinement retrofit or jacketing of the column would have little purpose. Thus the original specimen was tested instead to extreme ductility levels. Figure 3.10 shows the lateral-load versus lateral-displacement hysteresis loops through to the end of testing, to approximately μ=12.

3.5.2 Splitting Failure at Bar Bottom Anchorage

At displacement ductility factor μ=9, splitting failure cracks were observed in the bar-anchorage region of the foundation beam. At μ=10 the foundation beam concrete was spalling as a result of the splitting failure at the bar anchorage. Figure 3.2(f) shows,

at the conclusion of testing, the splitting failure at the bottom end-hooks of the column longitudinal bars. The splitting failure occurred at both sides of the foundation beam.

After the conclusion of testing the specimen was laid on its side, and the longitudinal splitting cracks were seen to have propagated to the bottom surface of the beam. On removing the loose concrete, the end hooks of the longitudinal bars were seen to have slipped approximately 4 mm, and the concrete above and below the hooks was pulverised because of anchorage-bearing stresses.

Figure 3.2(f) also shows the spalling of the column plastic-hinge zone at the conclusion of the test. Close inspection of the plastic-hinge region showed a gap of approximately 1 mm between the longitudinal bars and the surrounding concrete. This gap was probably caused by the dilation of the crushed concrete rather than to the diameter reduction of the reinforcing caused by Poisson's effect. Measurement between the longitudinal-bar strain gauge locations, originally 152 mm apart, showed almost no residual elongation in the reinforcing. This confirms that, because of the poor bond, the yielding of the steel was distributed over a substantial length of the longitudinal bar, and that large steel strains were not concentrated in the plastic-hinge region. The longitudinal bars did not buckle during the testing.

Figure 3.10 Lateral-load versus lateral-displacement hysteresis loops, to ductility $\mu \approx 12$, for the column to foundation-beam test.

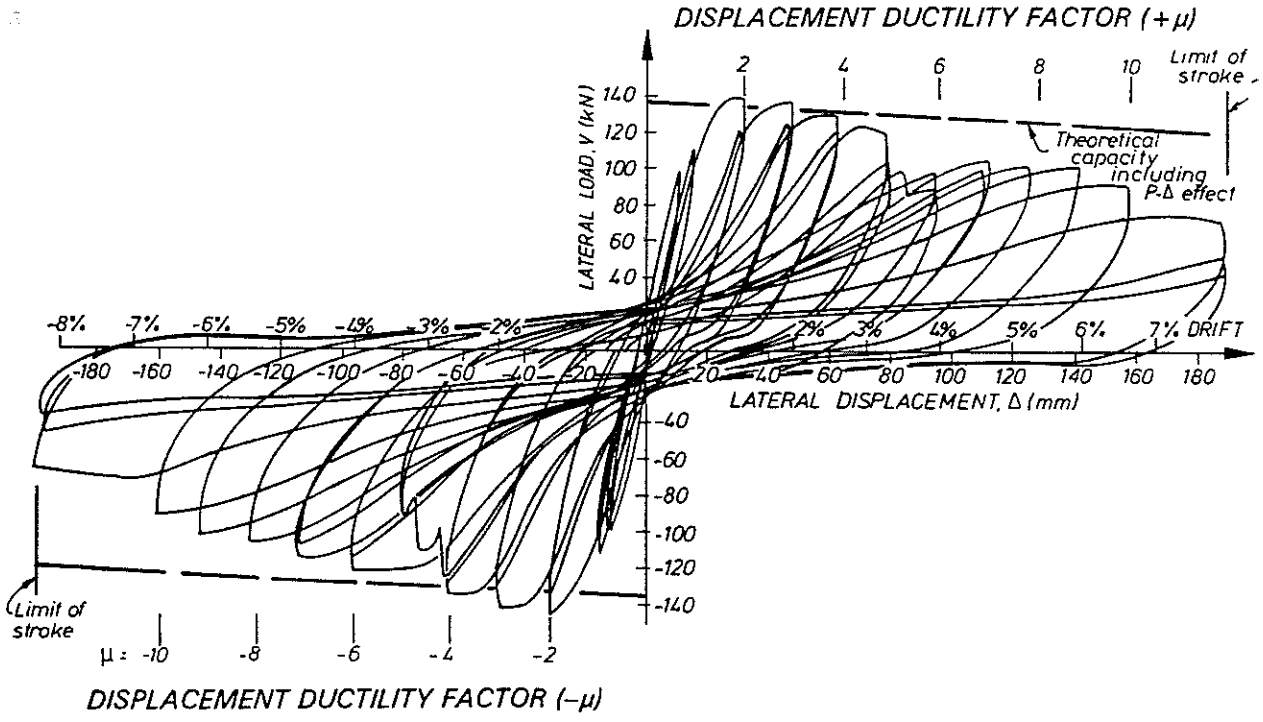

4. EVALUATION OF EXPERIMENTAL RESULTS & POSSIBLE RETROFIT SOLUTIONS

4.1 Introduction

The analysis of the column to foundation-beam test results presented in this chapter is organised around three topics:
(a) the effect of the plain-round reinforcing bars and the consequent bond slip and stiffness degradation,
(b) the effect of the supplementary diagonal bars and the column shear capacity – these two topics are related because the diagonal bars contribute to shear capacity, and
(c) the plastic-hinge behaviour related to concrete confinement and bar-buckling restraint.

The experimental results are compared with the seismic performance which would be predicted by a typical engineering assessment, using structural design codes or similar provisions.

4.2 Effect of Plain-Round Reinforcing Bars and Bond Slip

As mentioned in Chapter 3 of this report, the slope of the load versus displacement-hysteresis curves for the column to foundation-beam specimen decreased during the first four cycles in each direction (μ=0.75 and μ=1.0, Figure 3.8). This stiffness degradation, before yielding of the reinforcing steel, suggests that bond slip in the specimen began in the very early stages of testing. The steel and concrete strain measurements confirm that bond slip occurred in the specimen even in the first "elastic" cycles of testing.

4.2.1 Strain Results at Ductility $\mu = 1$

Figure 4.1 shows readings of steel and concrete strains in the column plastic-hinge region at the peak westward displacement of the first cycle to ductility factor μ= +1. The steel strains are taken at five heights on each of the four longitudinal bars, and at three heights on each of the four diagonal bars as shown in Figure 4.1. The concrete strains include crack-opening displacements and are averaged over the first 200 mm above the foundation beam where one flexural crack was present, and over the next 600 mm of the plastic-hinge height where the three main flexural cracks of the column were present. The concrete strain readings are measured by the linear potentiometers attached to the tension and compression faces of the column, and are translated to strains at the depths of the longitudinal bar centrelines. Thus the difference between concrete and steel strain readings in Figure 4.1 indicates the bond slip between the two materials, at the longitudinal bars.

At ductility μ=1, the longitudinal tension reinforcement had reached a maximum strain equal to 87% of yield. The average concrete strain (including crack opening) over the same region is almost 2 times the steel yield strain and 2.2 times the maximum steel strain. Thus, bond slip at the tension reinforcement is evident.

Some bond slip also occurs at the compression reinforcement. At μ=1, the maximum strain in the compression-longitudinal bars is 46% of yield strain. The average compression strain in the concrete at the same location is 60% of the steel yield strain, and 1.3 times the maximum steel strain.

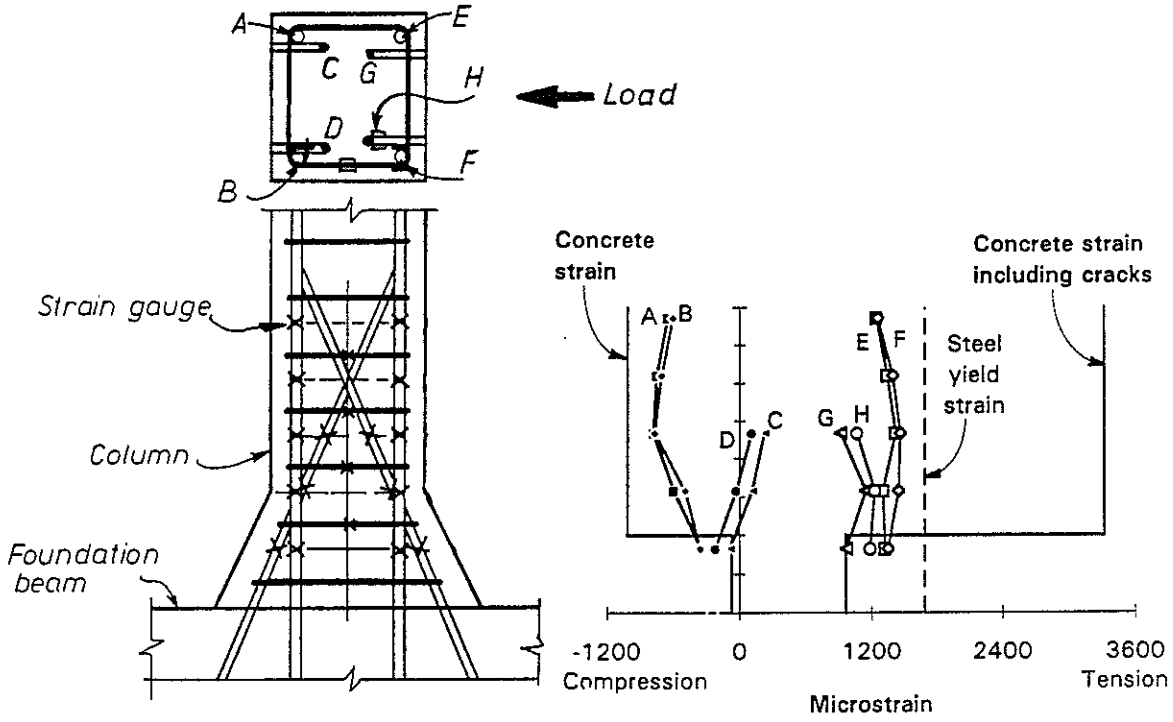

Figure 4.1 Concrete and steel strain profiles in the column plastic-hinge region at ductility μ= +1.

4.2.2 Strain Results to Ductility μ = 3

The amount of bond slip between the reinforcing steel and the surrounding concrete increases with testing to higher ductility levels. Figure 4.2 shows lateral-load versus strain-hysteresis loops for steel strain and average concrete strain in the plastic-hinge region of the column specimen. The steel strain is taken at a point on one of the longitudinal bars near the centre of the plastic-hinge region. The concrete strain includes crack displacements and is taken at the location of the longitudinal bars, on a 600 mm gauge length over the plastic-hinge region. Again, the difference between concrete and steel strains indicates the amount of bond slip taking place.

Figure 4.2 indicates that at ductility μ=3 the tensile strain in the longitudinal reinforcing steel is 1.4 times yield. The concrete tensile strain at the same location is 8.3 times the steel yield strain and 5.9 times the strain in the longitudinal steel. The

large difference between concrete and steel strains shows that extensive bond slip occurs, and confirms that bond slip is the cause of the pinching of the lateral-load versus displacement-hysteresis loops.

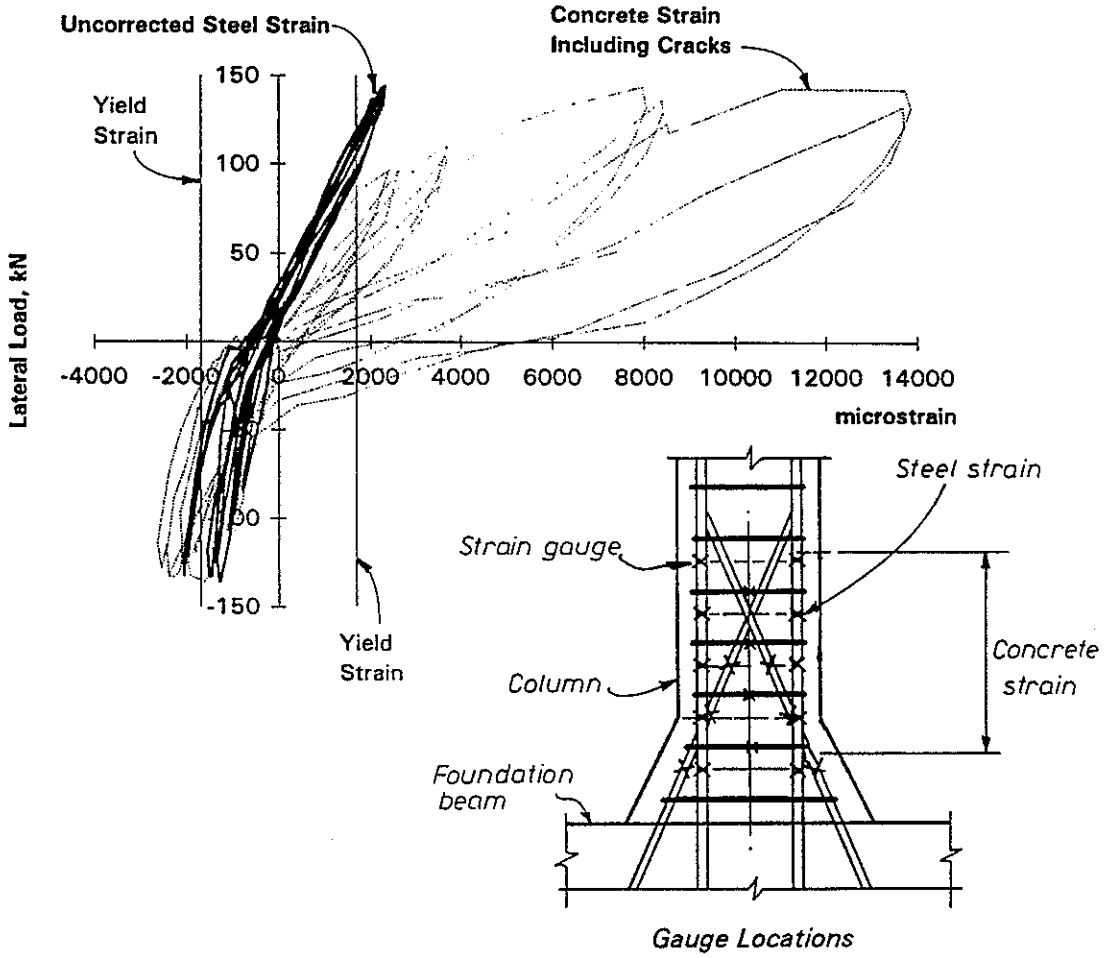

Figure 4.2 Lateral-load versus strain-hysteresis loops up to and including ductility of μ=3.

Figure 4.2 also shows that bond slip increases with testing to increased ductility levels. Table 4.1 indicates that the longitudinal reinforcing reaches a strain of 1.4 times yield at ductility μ=2. Then, at increasing column displacements to ductility μ=3, the steel strain does not increase beyond the previous maximum value of 1.4 times yield. Thus the column is accommodating increasing lateral displacements without increasing steel strain, but instead is accommodating them with an increasing zone of yielding, i.e. an increasing length of the longitudinal reinforcement yields with each cycle to increasing displacement. Thus the zone of yielding of the reinforcement becomes much longer than the typical plastic-hinge lengths found in columns with well-bonded deformed reinforcing.

Figure 4.2 and Table 4.1 show that the ratio of concrete strain to steel strain in the plastic-hinge region steadily increases with increasing column-displacement ductility.

The ratio is 2.2 at ductility μ=1, 3.6 at ductility μ=2, and 5.9 at ductility μ=3. These results indicate that substantial bond slip occurs even at low to moderate ductility levels.

Table 4.1 Comparison of average concrete strain, including cracking, with steel strains at longitudinal bars.

Displacement Ductility Factor	*Steel Tensile Strain / Yield Strain*	*Concrete Strain / Steel Yield Strain*	*Concrete Strain / Steel Strain*
1	0.87	2.0	2.2
2	1.4	5.0	3.6
3	1.4	8.3	5.9

4.2.3 Additional Evidence of Bond Slip

Unfortunately the strain gauges on the longitudinal bars debonded above ductility μ=3, and no steel strain data were obtained for the testing to higher ductilities. However, other data confirmed that the bond of the flexural reinforcing steadily deteriorated as testing continued. The severe deterioration of bond is evident in the following observations:

1. The pinching of the lateral-load versus lateral-displacement hysteresis loops, shown in Figure 3.8, begins at μ=1 and becomes more pronounced with cycles to increasing displacement. This directly reflects the progressive degradation of bond along the length of the longitudinal reinforcing. The lateral-load versus displacement-hysteresis loops for the previous test, of the column to crossbeam specimen (Figure 2.7), show similar pinching and progressive stiffness degradation.

2. The failure of the longitudinal bar-end welds at the top of the column to foundation-beam specimen, occurring at μ=5, indicates that a tremendous amount of bond deterioration had taken place. As discussed in Section 3.4, the end welds were located 1.9 m above the critical section of the column and failed under a tensile load of approximately 45% of the bar yield force. This means that over the 1.9 m length, equal to 68 bar-diameters, only 55% of the bar yield force could be taken out in bond resistance. If a uniform bond stress is assumed over the surface area of the bar for the 1.9 m length, a very low bond stress is calculated:

$$\text{Bond stress} = \frac{0.55\ f_y\ A_s}{\pi\ d_b\ l}$$

$$= \frac{0.55\ (337\,\text{MPa})\ (616\,\text{mm}^2)}{\pi\ (28\ \text{mm})\ (1900\,\text{mm})}$$

$$= 0.69\ \text{MPa} = 0.14\sqrt{f_c'}\left(100\,\text{psi} = 1.7\ \sqrt{f_c'}\right)$$

3. The anchorage-splitting failure of the concrete at the column bar-end hooks in the foundation beam indicates very low bond resistance in the straight embedment length above the end hooks. The splitting failure, described in Section 3.5, initiated at the end hooks at a displacement ductility of μ=9, when the bond-resistance along the length of the longitudinal bar was well degraded. The longitudinal bars are embedded 1.2 m below the critical column section into the column haunch and foundation beam where they are terminated with 180° hooks. For the anchorage-splitting failure to occur, almost all of the tensile force in the longitudinal bars must have been transferred to the end hooks, meaning that there was almost no bond resistance along the 1.2 m of anchorage length above the hooks.

4.2.4 Effect on Structural Performance

Compared with deformed reinforcing, the plain-round reinforcing bars offer poor bond-resistance and undergo a more rapid deterioration of bond strength under cyclic earthquake actions. The New Zealand concrete code NZS 3101:1982 (SANZ 1982) specifies that the embedment length of plain-round reinforcing should be twice that required of deformed reinforcing. This factor of 2 may be unconservative for plain-round reinforcing subjected to cyclic earthquake forces, particularly at higher ductility levels. The pending 1995 revision of the NZS3101 code prohibits the use of plain-round bars for main longitudinal reinforcing. In other circumstances where plain-round bars may be used, straight-bar anchorages or lap splices are prohibited. Bar anchorages must have hooks, and both bars of lap splices must have hooks (SANZ 1995, D.Bull, pers.comm. 1995)).

Structures with plain-round reinforcing suffer greater stiffness degradation under earthquake actions than structures with deformed reinforcing. This stiffness degradation, and a pronounced pinching of lateral-load versus displacement-hysteresis loops, are related to the bond slip at the reinforcing bars. Further insight into the behaviour of structures with plain-round reinforcing could be gained by mechanically modelling structures which undergo bond slip.

The pinched hysteresis loops indicate a reduced ability of the structure to dissipate earthquake energy, compared with a structure with deformed reinforcing steel. The stiffness degradation and pinched loop shape could compromise the earthquake performance of structures in which plain-round reinforcing steel is used. However, the extent to which earthquake performance is affected is unknown and requires further study.

4.2.5 Lateral Capacity and Strength Degradation

Relatively little strength degradation occurs in the response of the column to foundation-beam specimen. The reduction of lateral capacity which is evident results from the spalling of the concrete in the plastic-hinge region and to the P-Δ effect. At a structure drift of 2.7%, the lateral capacity of the column to foundation-beam specimen had diminished by 8%. The 8% reduction is calculated by comparing, from the hysteresis loops of Figure 3.8, the lateral capacity of 130 kN at 2.7% drift with the 141 kN maximum capacity at 1.2% drift.

The column to crossbeam test specimen, with its straight-bar anchorages, showed a more rapid degradation of strength. From the hysteresis hoops of Figure 2.7(a), the lateral strength at 2.7% structure drift (equal to 3.0% test-specimen drift) is 74 kN. The peak lateral strength is 88 kN, indicating a strength degradation of 16%. The column to crossbeam specimen suffers strength degradation because of the end-anchorage deterioration of the straight-column bars. This causes a capacity reduction in addition to that caused by concrete spalling and the P-Δ effect.

4.2.5.1 Combined capacity of top and bottom hinge regions

The lateral-load versus displacement characteristics of the two tests can be combined to estimate the earthquake response of the whole bridge structure. The column to foundation-beam test describes the behaviour of the bottom plastic-hinge region, while the column to crossbeam test describes the behaviour of the top plastic-hinge region. These two sets of test results are adjusted from the steel-yield strengths of the test specimens (308 MPa for the column to crossbeam and 337 MPa for the column to foundation-beam) to the estimated steel-yield strength of the actual structure, 280 MPa. Structure drift for these tests is defined as equal to the structure's lateral displacement divided by the height of 4.80 m from the centreline of the foundation-beam to the centreline of the crossbeam. The lateral-capacity versus displacement-envelopes of the two plastic-hinge regions are easily combined to give a lateral-capacity envelope for the entire structure.

Figure 4.3 shows the estimated lateral-capacity versus displacement envelope of the bridge structure under transverse earthquake loads. For the as-built (i.e. unretrofitted) structure, the peak lateral capacity is 0.45 times the seismic weight. At a structure drift of 2.7% this capacity is diminished by 12%. The 12% reduction reflects the combination of the 8% reduction which occurs in the column-bottom plastic hinge and the 16% reduction which occurs in the column-top plastic hinge.

4.2.5.2 Anchorage-retrofit structure

If end plates are added to the tops of the column-longitudinal bars to retrofit the bar-anchorage condition, the maximum lateral capacity is increased and the rate of degradation of strength is reduced.

The dashed line on Figure 4.3 shows the estimated lateral-capacity versus displacement-envelope of the anchorage-retrofit structure. The lateral capacity is increased to 0.53 times the seismic weight, because of the improved moment strength at the top of the column. The reduction of lateral capacity at 2.7% structure drift is 8%.

The upgraded capacity and strength-degradation characteristics of the anchorage-retrofit structure will improve its earthquake performance. The extent of the improvement is unknown however, and would depend on the particular earthquake characteristics. Having defined the strength-envelopes, stiffness-degradation, and hysteresis-loop-pinching characteristics of the earthquake response, accurate analytical studies of the bridge using different earthquake records can now be conducted. Inelastic time-history structural analyses can be carried out to compare the earthquake

performance of the as-built bridge structure with that of the proposed anchorage-retrofit structure. Such analyses are presented in Chapter 5.

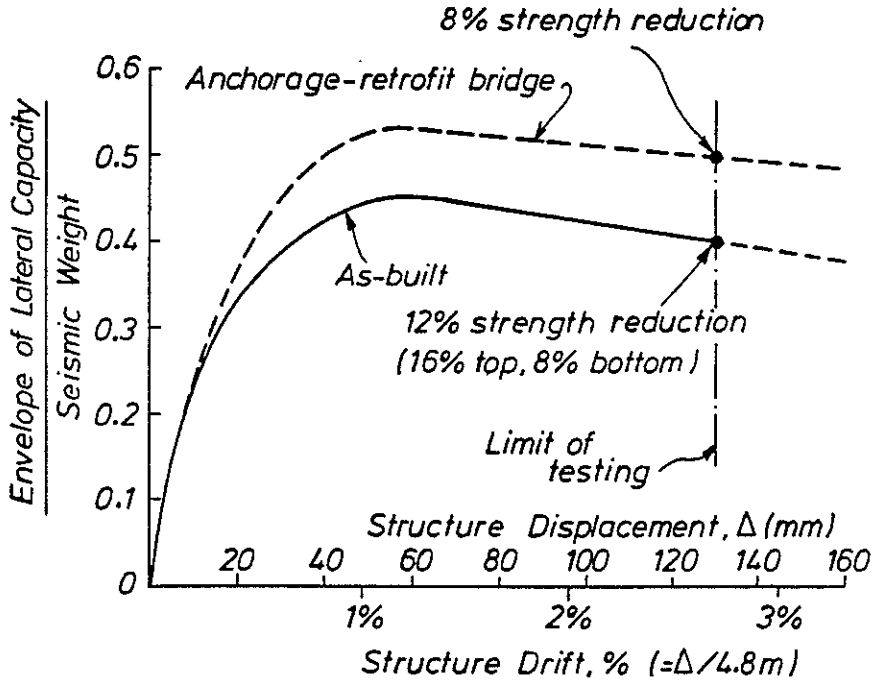

Figure 4.3 Lateral-strength versus displacement envelopes for the as-built bridge and anchorage-retrofit bridge.

4.3 Effect of the Diagonal Reinforcing, and of Column Shear Capacity

The supplementary diagonal bars at the column haunch contribute to both the shear and flexural strength of the column.

4.3.1 Diagonal Bar Contribution to Flexural Strength

Figure 4.1 shows the diagonal-bar and longitudinal-bar strains in the column plastic-hinge region at ductility, μ=1. The two diagonal bars which extend past the tension face of the column haunch, bars G and H, carry significant tension because of column flexure, with strains similar to those of the main flexural reinforcement, the longitudinal bars E and F. Thus the diagonal bars make a substantial contribution to the flexural strength of the column, and hence to the lateral capacity of the structure.

The above conclusion is confirmed by the measured strength of the column to foundation-beam specimen. The peak lateral capacity was recorded, at ductility factor μ=2, to be 138 kN (31.0 kips) in the east direction and 144 kN (32.4 kips) in the west direction. These measured capacities correspond closely to the calculated nominal

flexural strength of 135 kN (30.3 kips). The assumption used in calculating the nominal strength, that the two tension-diagonal bars reach yield and fully contribute to the flexural strength, is thus verified.

For the column to crossbeam test specimen, Figure 2.4, diagonal bars are present in both plan directions, anchored into the longitudinal girders and the transverse crossbeam. Thus there are eight diagonal bars at the top of each column. All of these diagonal bars contribute to the flexural strength of the column under earthquake actions. The nominal moment strength of the critical section at the top of the column is calculated as 244 kNm (180 kip-ft). This corresponds closely to the measured maximum moment strength of 236 kNm (174 kip-ft) from the anchorage-retrofit specimen. Thus the assumption used in the calculations, that the diagonal bars in each direction contribute to the column flexural strength, is verified for the top end of the column as well as for the bottom.

4.3.2 Diagonal Bar Contribution to Shear Strength

The diagonal bars also contribute to the shear strength of the column. As shown in Figure 4.1, under lateral forces two of the diagonal bars are subjected to significant tensile strains while the other two bars carry little strain. The two diagonal bars G and H, which extend past the tension face of the column haunch, yield in tension when the column reaches its flexural strength. The horizontal component of the yield force in these two bars provides a substantial portion of the column's shear resistance at the plastic hinge. Meanwhile, the opposite two diagonal bars, bars C and D in Figure 4.1, tend to carry a small compression or tension force which does not significantly increase or decrease the column-shear resistance. It is thus considered accurate to assume that two of the diagonal bars contribute to the shear strength while the contribution of the other two bars can be ignored.

The contribution of the diagonal bars to shear strength is also evident in the crack development of the column to foundation-beam specimen. Unlike the column stirrups which do not contribute to shear strength until diagonal cracking develops, the two tension diagonal bars resist a portion of the column shear even before diagonal cracking. The tension in the diagonal bars reduces the shear stress in the concrete and reduces the amount of diagonal shear cracking.

This effect is evident in the photo of Figure 3.2(c), taken at ductility factor μ=6 for the column specimen. At the top of the photo is the portion of the column just above the diagonal bars. In this location, flexural cracks in each direction have extended into diagonal shear cracks. Below these two crossing diagonal cracks, are the three main flexural cracks in the plastic-hinge region which have extended horizontally across the column and joined up without turning into diagonal shear cracks. Thus the presence of the diagonal bars in this region has reduced the amount of diagonal shear cracking. The reduced diagonal cracking does not affect the overall seismic performance of the bridge, but it re-confirms the assumption that the diagonal bars contribute to the column-shear strength.

4.3.3 Calculations of Shear Capacity

Calculations of the shear capacity of the column specimen have been made by this author. Results of the calculations are shown in Table 4.2. According to the NZS 3101 concrete code provisions (SANZ 1982, 1995), if the diagonal bars are not considered, the shear capacity of the column plastic-hinge region is deficient. The code assumes $V_C = 0$ and $V_S = 90$ kN to give a shear capacity of only 89% of the shear demand, which is 102 kN. However, if the diagonal-bar contribution is included, the shear capacity is calculated as 161 kN, or 158% of the shear demand.

Furthermore, the code assumption that $V_C = 0$ is a conservative one. The less conservative expression proposed by Paulay and Priestley (1992, p.127), $V_C = 4V_b \sqrt{P_t/A_g f'_c}$, results in $V_C = 58$ kN. Thus a more realistic estimate of the column-shear strength at the plastic-hinge regions would be

$$V_C + V_S + V_{SDIAG} = 58 + 90 + 71 = 218 \text{ kN}.$$

This strength is comfortably above the earthquake shear demand of 102 kN. As observed in the tests, column shear failure did not occur. The less conservative calculation for V_C indicates that even without the diagonal bars shear strength will be adequate,

$$V_C + V_S = 58 + 90 = 148 \text{ kN}.$$

4.3.4 Comparison to NZ Standards Concrete Code Provisions

The foregoing comparison of possible calculation assumptions shows that if the shear strength of the subject bridge column is assessed by the NZS 3101 concrete code (SANZ 1982, 1995), and if an assumption is made to neglect the diagonal bar contribution, then the conclusion is that the column-shear capacity is deficient. Such assumptions might be considered conservative, but would not be unreasonable in engineering practice. In fact the pilot-study assessment of the bridge (Chapman 1991) concluded that the shear capacity is marginal. A more detailed evaluation of the column shear capacity, allowing $V_C > 0$ or some contribution to shear capacity from the diagonal bars, shows however that the column shear capacity is adequate.

This example illustrates the point that the assumptions used for the seismic evaluation of existing structures often need to be more accurate than those used for designing new structures. For new bridges conservative design assumptions would only slightly increase construction costs. But for an existing bridge, an overly conservative assessment of column-shear capacity could require expensive retrofitting, whereas a more detailed and accurate assessment of shear capacity could eliminate the need to retrofit.

Paulay (pers.comm. 1994) has postulated that for members with plain-round bars which undergo significant bond slip, the *...entire shear mechanism changes..*, compared with that for structures with deformed bars. *...The reason is that the traditional truss mechanism, relying on perfect bond, cannot develop. Typical 45°*

struts in the concrete will not develop. An arch mechanism must be mobilised ... instead. Consequently, *...the shear provisions of NZS 3101, or ACI 318 for that matter, are entirely irrelevant...* for structures with plain-round reinforcing bars.

However, Kordina et al. (1989) have tested (monotonically) the shear strength of prestressed concrete beams with unbonded tendons. They conclude that *...even for prestress without bond, shear stress can be predicted best on the basis of a truss analogy... a tied-arch model seems less suitable for the determination of the shear-carrying capacity.*

Also, engineers evaluating concrete structures with plain-round reinforcement have little choice but to use the shear-strength provisions from design codes or research results, which were developed for structures with deformed reinforcement. Special shear-strength evaluation provisions for concrete structures with plain-round reinforcing have not been developed. Further research in this area would be useful.

Table 4.2 Calculated shear demands and capacities for the bridge column.

	Test Specimen	**Actual Structure**
Shear Demand	**135 kN**	**102 kN**
Data needed to calculate shear strength		
f_y	337 MPa	280 MPa
f'_c	22 MPa	20 MPa
Governing axial load condition	$P_u = P_{test}$ = 300 kN	P_u = 0.8 DL – EQ = 46 kN
$P_u/A_g f'_c$	0.074	0.012
Steel contribution to shear strength		
V_S, stirrups	120 kN	90 kN
V_{SD}, 2 diagonal bars	94 kN	71 kN
Concrete contribution to shear strength		
- by **NZS 3101 (1982, 1995)**:		
V_C at plastic hinge	0 kN	0 kN
V_C outside plastic hinge	$0.226\sqrt{f'_c}$ = 166 kN	$0.192\sqrt{f'_c}$ = 134 kN
- by **Paulay & Priestley (1992)**:		
V_C at plastic hinge	$0.201\sqrt{f'_c}$ = 147 kN	$0.081\sqrt{f'_c}$ = 58 kN
V_C outside plastic hinge	$0.226\sqrt{f'_c}$ = 166 kN	$0.192\sqrt{f'_c}$ = 134 kN

4.4 Plastic Hinge Behaviour and Concrete Confinement

4.4.1 Background

Based on the strain readings of the linear potentiometers, the curvature profiles of the plastic-hinge concrete section have been calculated for the column to foundation-beam test. Figure 4.4 shows the column curvature measured over segments of the plastic-hinge region at ductility factors of μ=1, 3, 5, 6 and 7. As shown in Figure 4.4, up to a ductility factor of 5, the curvature was concentrated in one of the 150 mm gauge lengths, which is where the main flexural crack was located, approximately 300 mm above the foundation beam. As shown in Figure 3.7 this crack opened to a maximum width of 10.5 mm at ductility factor of 5.

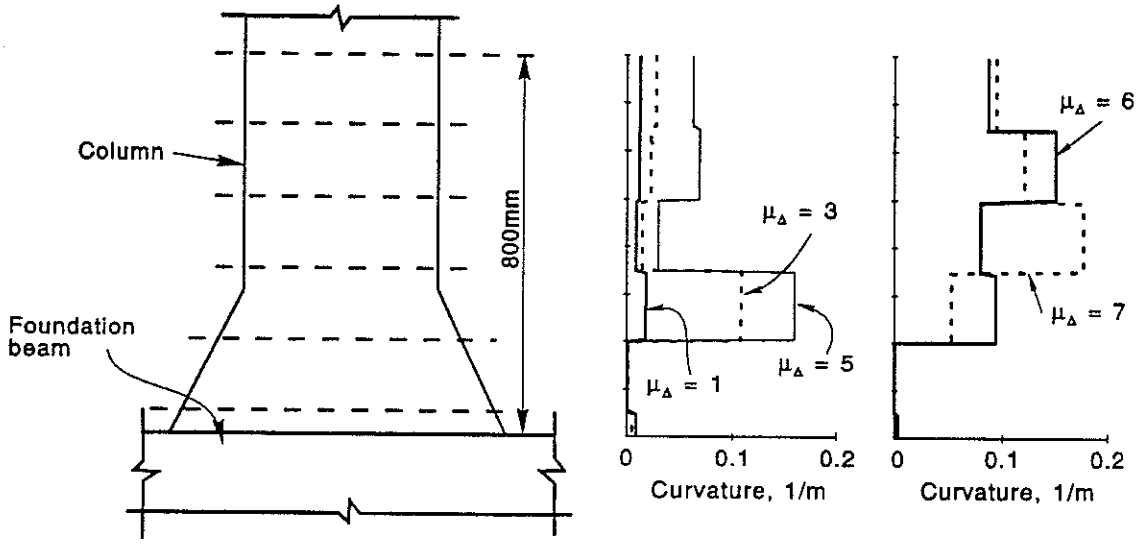

Figure 4.4 Column curvature profile over the plastic-hinge region at displacement ductilities of μ=1, 3, 5, 6, 7.

Beyond ductility μ=5, the maximum opening widths of the other two flexural cracks began to increase, indicating an increase in curvature further up the column. The curvature began to develop over a greater length of the column at ductilities 6 and 7 (Figure 4.4).

4.4.2 Curvature Ductility

Based on the curvature measurements, the average curvature ductilities can be calculated. The curvature ductility is taken as the maximum measured column curvature, over a 150 mm gauge length, divided by the plastic-hinge curvature measured over the 150 mm gauge length of the main flexural crack during testing to ductility factor μ=1. Figure 4.5 shows the measured concrete curvature ductilities during testing to increasing displacement ductilities.

In general, curvature ductilities will increase in step with displacement ductilities. If the plastic-hinge length remains constant, curvature ductility will increase linearly with displacement ductility. However, the column can also accommodate increased displacement ductilities without increased curvature ductilities, if the plastic-hinge length increases.

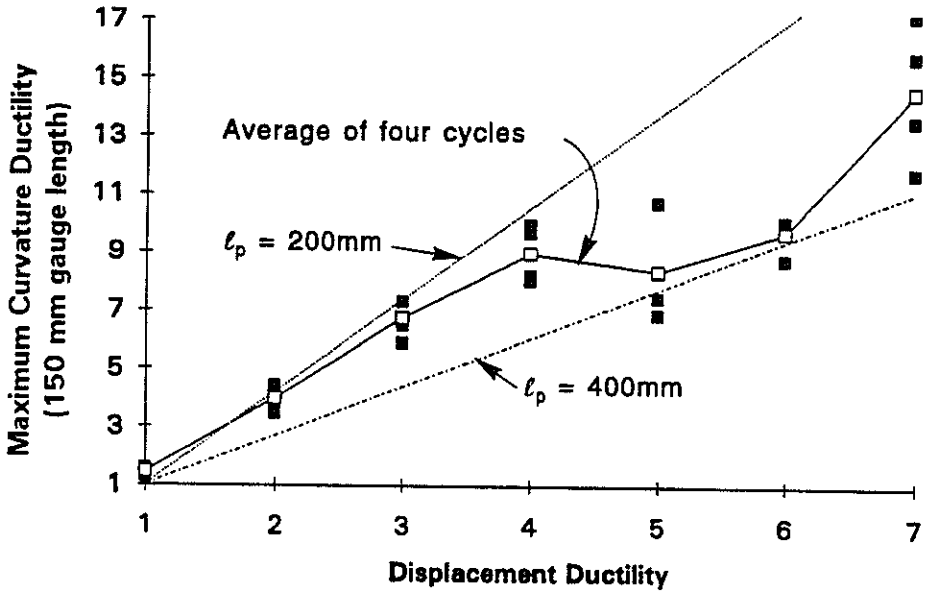

Figure 4.5 Measured concrete curvature ductility, versus displacement ductility, indicating an increase in concrete plastic-hinge length, l_p.

4.4.3 Plastic-Hinge Length

Figure 4.5 shows that initially the column plastic-hinge length, l_p, is about 200 mm, 0.5 times the overall section depth. As the column is tested to cycles of increasing displacement however, the curvature profile over the column length becomes less peaked. At the displacement ductilities μ=4, 5, and 6, the curvature profile is more even because the plastic-hinge length, l_p, has increased to about 400 mm, 1.0 times the overall section depth. The relationship between plastic-hinge length, curvature ductility, and displacement ductility is given in Park and Paulay (1975, p.553):

$$\mu_\phi = 1 + \frac{(\mu_\Delta - 1)}{3(\ell_p/\ell)\left[1 - 0.5\,(\ell_p/\ell)\right]}$$

The significance of the concrete-section curvature and plastic-hinge length results for the column is diminished by the extensive bond slip resulting from the use of plain-round reinforcing bars. The bond slip at the reinforcing bars means that the column section behaviour violates the typical assumption of structural mechanics that *plane sections remain plane*, and the typical relationship between curvature and material strains is no longer relevant. Because of the bond slip, the length of yielding of the reinforcing bars is much greater than the plastic-hinge length based on concrete-

section curvature. Thus the concrete-curvature ductility at the plastic hinge does not give an indication of the maximum reinforcing steel strain, as it would do for well-bonded reinforcement. This point is reflected in Figure 4.2 where, under the same column displacement demands, the concrete-strain ductility demand is shown to be several times greater than the steel-strain ductility demand.

4.4.4 Column-hinge Lengthening and Degradation

The linear-potentiometer readings were also used to record the axial lengthening of the column specimen during the testing to increased levels of lateral displacement. Figure 4.6 shows the progressive lengthening of the column during testing. The lengthening is substantially restrained by the constant axial load on the column, so that the residual column lengthening, after testing to displacement ductility μ=7, is only 4.5 mm. Another reason for the small amount of plastic-hinge lengthening is that the inelastic strains which develop in the plain-round column bars are substantially less than those which would develop in deformed column bars.

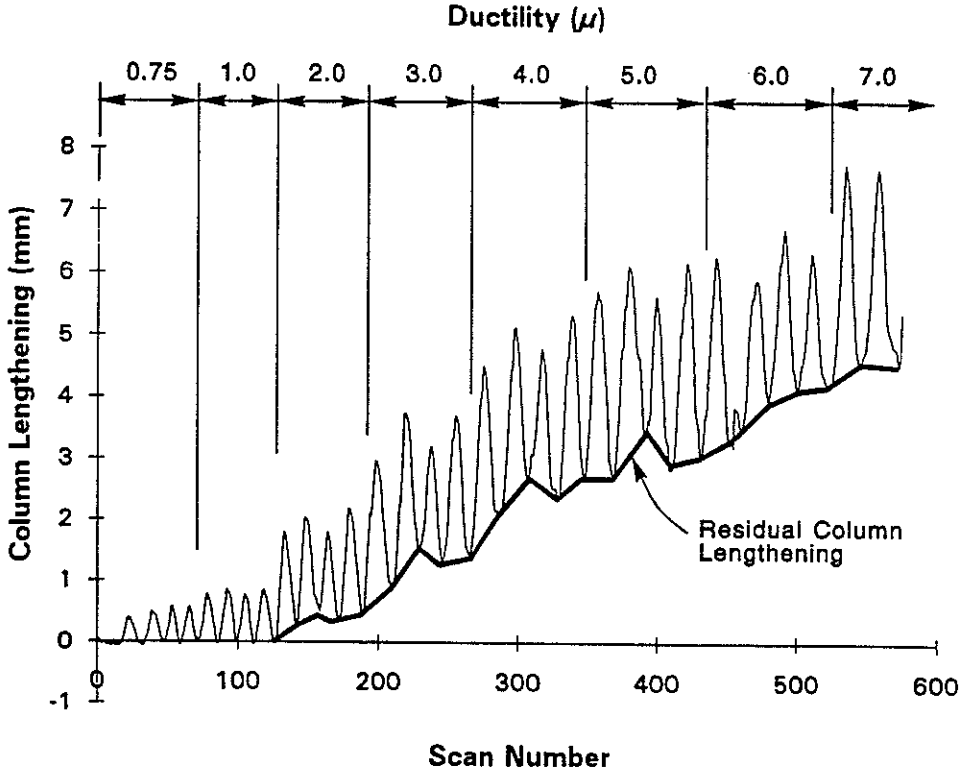

Figure 4.6 Column lengthening during the testing of the column to foundation-beam specimen.

Although the cover concrete of the column specimen began to crack on the compression face at displacement ductilities of μ=2 to 3, and major spalling began at ductility μ=5, the strength degradation of the specimen was not pronounced. At a displacement ductility of μ=5 the column strength had degraded to 88% of its maximum strength, measured at ductility μ=2. This 12% degradation of strength results from the loss of cover concrete. The amount of strength degradation was small because the core concrete remained intact and was adequately confined by the transverse reinforcing. Figure 3.2(c) shows that the column core was intact at a displacement ductility of μ=6. Figure 3.2(f) shows a degraded column core, but the degradation occurred only after several cycles to extreme displacements (μ=12).

4.4.5 Required Transverse Reinforcing Steel Areas

The pilot-study assessment of the bridge had indicated that the column-core concrete is poorly confined. This assessment was made based on the requirements for transverse reinforcement in the NZS 3101:1982 concrete code (SANZ 1982). For the subject bridge column, the 1982 code requires an area of transverse reinforcing 3.15 times that which is provided by the 9.5 mm (3/8 inch) ties at 152 mm (6-inch) spacing.

Research results over the last ten years have shown, however, that the 1982 concrete confinement requirements are unduly conservative for columns with low to moderate axial loads (Watson et al. 1994). For the subject column with its low axial load level, the revised version of the concrete code (SANZ 1995) requires no transverse reinforcement for concrete confinement. Transverse reinforcement is required to stabilise the longitudinal bars against buckling but not for confinement. The area of transverse reinforcement provided in the subject bridge column is adequate, equal to 1.17 times that required for bar-buckling prevention. Bar buckling did not occur in the tests even after testing to extreme ductility levels.

These points are illustrated in Figure 4.7. Figure 4.7(a) shows a comparison of the transverse reinforcement requirements of the 1982 and 1995 versions of the New Zealand concrete code. It also shows the required transverse steel area for the subject bridge column as a function of axial-load level. The actual axial-load level and transverse steel area of the subject bridge column are shown on the plot as well. By the 1982 criteria the subject column is seen to be deficient in transverse reinforcement by a factor of 3, but by the 1995 criteria the provided amount of transverse reinforcement is adequate.

4.4.6 Required Column-tie Spacing

Figure 4.7(b) shows the maximum allowable spacing of column ties according to the previous and current versions of the New Zealand concrete code (SANZ 1982, 1995).

4.4.6.1 Bar-buckling criteria

To stabilise the longitudinal reinforcing against buckling, ties are required at a spacing no greater than $6d_b$, where d_b is the diameter of the longitudinal bars. For the subject bridge this maximum spacing is 6 x 28.6 = 171 mm. Thus the actual tie spacing of 152 mm meets the criteria to prevent longitudinal bar buckling.

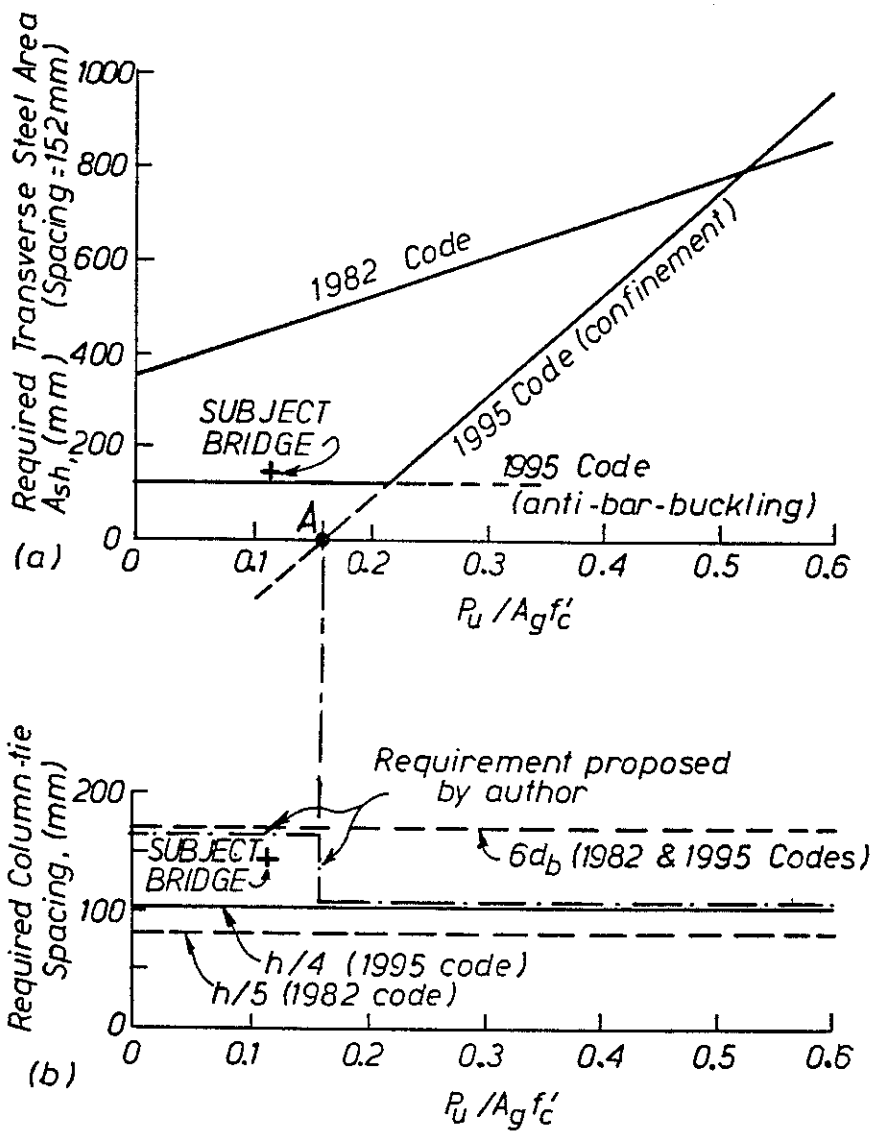

Figure 4.7 (a) Required transverse reinforcement for the subject bridge column, and (b) Required maximum allowable spacing of column ties, from the current and revised New Zealand concrete codes (SANZ 1982,1995).

Plain-round bars may be less susceptible to buckling under earthquake actions than deformed bars. For the subject test Paulay has pointed out that ...*inelastic strains in the plain bars were much smaller (than they would be for deformed bars) because of the breakdown of bond.* For the columns similar to those of the subject bridge Paulay (1994) estimates that...*at μ=8 deformed bars would probably have buckled because much larger reversive inelastic strains would have been sustained*...in the steel.

This estimate of ductility capacity (μ=8), and the compliance with the 1995 NZS concrete code criteria for transverse steel area and the $6d_b$ maximum tie spacing,

indicate that even with deformed bars the seismic performance of the column with respect to bar-buckling would have been satisfactory.

Although plain-round bars may be less susceptible to buckling, they are not immune to buckling and still need some transverse ties for anti-buckling stability. Rodriguez and Park (1994) tested columns with plain-round longitudinal bars with ties spaced at $13d_b$. This excessive tie spacing allowed the longitudinal bars to buckle and cause significant strength reductions at a displacement ductility of approximately 3.8 (interstorey drift of 1.8%).

4.4.6.2 Confinement and shear-resistance criteria

The 1995 draft NZS concrete code also requires, for concrete confinement and shear resistance, that column ties are spaced no further apart than h/4, where h is the least dimension of the column section. This requirement is relaxed from the h/5 maximum spacing required by the 1982 NZS code. For the subject bridge, the h/4 criterion equates to a maximum tie spacing of 102 mm. This h/4 criterion governs over the $6d_b$ anti-bar-buckling criterion, and thus the column-tie spacing is deemed inadequate by the 1995 NZS code.

The NZS code requirement for column-tie spacing[3] to be less than h/4 can be conservative for columns with low axial load and shear demand, particularly if diagonal bars are present. The h/4 tie-spacing criteria is appropriate for new construction, because a more detailed criterion would be more complicated and the resulting savings in construction cost would be insignificant. For the seismic evaluation of an existing structure then, a more accurate estimate of required column-tie spacing may be necessary because it could eliminate the need for expensive retrofitting.

For the subject bridge column, the 1995 NZS code requires no transverse reinforcement for confinement, and the shear capacity of the plastic-hinge region is good because of the contribution of the diagonal bars. However, a tie spacing of h/4 is still required. The issue is illustrated in Figure 4.7. At an axial-load level below that indicated by point "A" in Figure 4.7, transverse ties are not needed for concrete confinement, and they are only needed for bar-buckling restraint. At axial-load levels less than point "A", then, it is not necessary for concrete confinement to have ties spaced at h/4 (102 mm). And because the two diagonal bars will cross any potential diagonal shear crack in the plastic-hinge region, the shear capacity of the column does not rely on a close spacing of ties.

Outside the column plastic-hinge region, the NZS concrete code (SANZ 1982 and 1995) specifies a maximum tie spacing, for shear resistance, of d/2. As for the subject column, d/2 equals 170 mm, and thus the tie spacing of 152 mm outside the plastic-hinge region complies with the code.

---

[3] h = overall depth of member
d = depth from extreme compression fibre to centroid of tension reinforcement

4.4.6.3 Proposed requirements for the subject bridge

Because the column ties are not heavily relied on for confinement or shear resistance, the subject column should only need to meet the tie-spacing requirement of $6d_b$ (171 mm) to prevent longitudinal-bar buckling, even if it had deformed longitudinal bars. This proposed requirement is shown in Figure 4.7(b) by the dash-dot line.

The proposed tie-spacing requirement would then indicate that the column-tie spacing of the subject bridge is acceptable, a conclusion which is validated by the test results. The proposed requirement is recommended as a basis for assessing the ductility capacity of existing columns similar to those of the subject bridge, with either deformed or plain-round reinforcement. The requirement gives a better indication of the true column-tie spacing required for the ductile earthquake response of column plastic-hinge regions. Additional study may be needed, however, to determine the maximum allowable tie spacing for shear resistance.

Additional research is also needed on the performance with respect to shear resistance and bar buckling of concrete members having plain-round reinforcement. Transverse ties may not be effective in the shear resistance of such members because an arch mechanism of shear resistance is developed instead of the traditional truss mechanism. Also less transverse reinforcement may be required to prevent bar buckling in such members, compared with members with deformed longitudinal bars.

4.5 Overall Assessment

The testing of the column to foundation-beam specimen and the associated structural analysis have revealed several new insights into the seismic behaviour of the 1936-designed New Zealand bridge. The conclusions drawn from the testing and detailed analysis could not have been deduced from a less detailed assessment which had relied only on the then-current design codes and practice. The detailed investigation of the present study has, in general, shown that the bridge is less vulnerable to earthquake damage than previously thought.

4.5.1 Seismic Performance

The preliminary seismic assessment of the subject bridge (Chapman 1991) concluded that *...the pier-columns are unlikely to tolerate cyclic displacements much exceeding yield...* This conclusion is generally supported by code provisions and other structural design guidelines. However, the laboratory testing of the column to crossbeam and column to foundation-beam specimens presented here has shown that conclusion to be incorrect.

For the subject bridge to survive a severe earthquake, it needs to have adequate strength and lateral displacement capacity in its transverse direction. And the lateral capacity of the bridge is governed by the flexural strengths at the top and bottom of each of the bridge columns. As the tests and calculations indicate that the lateral capacity is 0.45 times the weight of the structure, this bridge has a lateral capacity that is two or three times greater than that required of many new bridges.

Even with a high lateral capacity, the bridge structure needs to accommodate the displacement demands imposed by a strong earthquake. The lateral-displacement capacity of the bridge depends primarily on the inelastic rotation capacity at the plastic-hinge regions at the top and bottom of each of the bridge columns. The lateral-force versus displacement-hysteresis loops for both the column to crossbeam test, Figure 2.7, and the column to foundation-beam test, Figure 3.8, indicate that these regions have a ductile response to earthquake actions. The hysteresis loops show pinching and stiffness degradation, caused by bond deterioration, but show only moderate strength degradation. The column to crossbeam and column to foundation-beam tests indicate that, at a structure drift of 2.7%, the lateral capacity of the bridge will diminish by only 12%.

Thus, the subject bridge has satisfactory lateral strength and inelastic displacement capacity to survive earthquake ground motions. This combination of strength and displacement capacity for the bridge means that it is likely to perform well even in a severe earthquake. By considering the earthquake response spectra of the New Zealand loadings code, NZS 4203:1992 (SANZ 1992), the bridge has adequate strength and ductility capacity to sustain the level of earthquake shaking specified by the code. This indicates that the subject bridge will probably perform in an earthquake just as well as a new bridge designed to the NZS 4203:1992 criteria. The analytical studies of Chapter 5 confirm this conclusion.

4.5.2 Prediction of Seismic Performance

The prediction of satisfactory earthquake performance from the subject bridge is based on the test results. These results show satisfactory lateral strength and displacement capacity. However, using the NZS 3101:1982 concrete code (SANZ 1982) criteria, the opposite conclusion was reached, i.e. poor earthquake performance was predicted for the bridge. But assessing the structure using a detailed seismic evaluation procedure, which does not rely solely on code-implied criteria, verifies both the test results and the conclusion that the bridge's seismic performance will be satisfactory. Essential to such an accurate seismic assessment of the bridge are the following points:

1. For columns with low axial load, the NZS 3101:1982 concrete code (SANZ 1982) is overly conservative in its requirements for concrete confinement. The 1995 draft code (SANZ 1995) has more accurate requirements.

2. The supplementary diagonal bars at the top and bottom end flares of the subject bridge column contribute significantly to both flexural and shear strength. For such columns, the structural engineer must determine the critical section for moment capacity and plastic hinging, which may or may not be in the flared region of the column. For the subject bridge, a seismic evaluation which neglected the contribution of the diagonal bars would be overly conservative.

3. The code assumption (in both SANZ 1982 and 1995) that V_c, the column shear capacity of the concrete section, equals zero may be overly conservative for the

evaluation of existing structures. Paulay and Priestley (1992) and Priestley et al. (1994) offer less conservative criteria.

4. For columns with low axial load, good shear capacity, and large-diameter longitudinal reinforcing, the column-tie spacing requirements of the NZS 3101:1982 and 1995 concrete codes can be conservative. A more accurate requirement, described in Figure 4.7, may be used instead. However, a limit in the maximum tie spacing is still required to ensure that the ties act as efficient shear reinforcement. Currently the code specifies the maximum tie spacing to be h/4.

5. Concrete structures with plain-round longitudinal bars can be less susceptible to bar-buckling, shear failures, and loss of confinement, and thus may require less transverse reinforcement, than similar structures with deformed longitudinal bars. The bond slip at plain-round bars makes bar buckling less likely and promotes an arch mechanism of shear resistance rather than the traditional truss mechanism. Bond slip can lessen curvature demands at plastic hinges and thus reduce the need for concrete confinement.

4.5.3 Stiffness Degradation and Hysteretic Response

Although the hysteretic response of the plastic-hinge regions of the subject bridge column indicate good displacement capacity and little strength degradation, the response also shows pronounced stiffness degradation and pinching. The stiffness degradation and pinching may have an adverse effect on earthquake performance because the energy-dissipation capacity of a structure is reduced. However, the hysteresis-loop shape generally does not have a big effect on seismic response, particularly for structures with longer periods of vibration.

Further insight on expected damage to the bridge for different earthquake scenarios could be gained by conducting inelastic time-history analyses of the structure. Such analyses can be used to check the validity of the code-specified earthquake demands, assess the effect of the pinched hysteretic response, and compare the earthquake performance of the as-built bridge with that of the bridge after seismic retrofitting. Such analyses have been carried out and are discussed in Chapter 5. Mechanically modelling the response of structures which undergo bond slip would also provide insight into the behaviour of structures with plain-round reinforcing.

4.5.4 Confinement Retrofit

The subject bridge is shown by the tests and the detailed evaluation not to be vulnerable to earthquake damage caused by insufficient transverse reinforcing or shear capacity. Thus a confinement-retrofit of the bridge columns, such as adding new column ties or an external column jacket, would give no benefit. Originally the plan had been to test a confinement-retrofit of the column to foundation-beam specimen, but the idea was discarded once it was concluded that the existing column was not in fact deficient in transverse reinforcing or shear capacity.

4.5.5 Additional Considerations

Three additional related considerations concern how representative the testing is of the actual seismic performance of the prototype bridge. Two issues, the different detailing at exterior columns and the restraint provided by the test-specimen top plate, suggest that the actual bridge will suffer slightly higher stiffness and strength degradation than is evident in the response of the test-specimen. The third issue of surface rust on the plain reinforcing bars suggests the opposite effect: i.e. less stiffness degradation for the actual bridge compared to the test specimen.

In summary, these additional issues discussed below are not considered to have a substantial effect on the validity test results reported here. One or more of the issues could instead be studied as part of some future testing of structures with plain-round reinforcing.

4.5.5.1 Interior versus exterior column details

The test has examined the behaviour of one of the interior columns of the typical four-column pier of the prototype bridge. As shown in Figure 2.3, the detailing at the base of the exterior column is different from that of the interior column. The seismic performance at this column would probably not be as good as that at the interior column, because of bond slip of foundation-beam bars and poorer confinement of the column bar-end hooks.

Based on the test observations and results of Chapter 2 and this Chapter 4 of the report, it is possible to estimate the effect of the different detailing at the exterior column. Three observations can be made:

1. The strength of the exterior column base region will initially be the same as that for the interior column. This similarity is because the strength will still be governed by the column-yielding mechanism, since the moment strength of the foundation beam is more than twice that of the column. In fact, the *cracking moment* of the foundation beam is approximately equal to the moment capacity of the column, so that full development of the foundation-beam bars is not necessary to force plastic hinging into the column.

2. Upon repeated cycles of seismic forces at moderate to high ductilities, the cracking moment of the foundation beam may be exceeded, after which bond slip at the foundation-beam bars is likely to take place. Such bond slip would increase the amount of stiffness degradation in the response of the bridge. Conceivably, the bond slip could eventually degrade the capacity of the foundation beam and joint region to a level less than that required to force plastic hinging into the column. In this case, the response of the bridge would exhibit an increased rate of strength degradation.

3. In the testing of the interior-column to foundation-beam specimen at high ductility levels, a splitting failure occurred at the column bar-end hooks, as described in Section 3.5. The splitting cracks were first observed at a displacement ductility factor, μ=9 (structure drift of 6.0%). At μ=10 (structure

4.6.2 Infill Concrete Wall

The second possible retrofit would provide a more dramatic strength increase to the bridge structure. This retrofit, illustrated in Figure 4.8, involves the addition of a new reinforced-concrete infill wall between the centre two columns of the four-column bent. The reinforcing for the infill wall should make use of diagonal bars as is done in the coupling beams of walls for multi-storey buildings. Such a big increase in the strength of the multi-column bent is likely to require the strengthening of the foundations, including the addition of new piles and the jacket-strengthening of the foundation beam. However not all piers of a multi-span bridge would need to be strengthened in this way. For example, strengthening two piers in each 5-span segment of the subject bridge may be adequate.

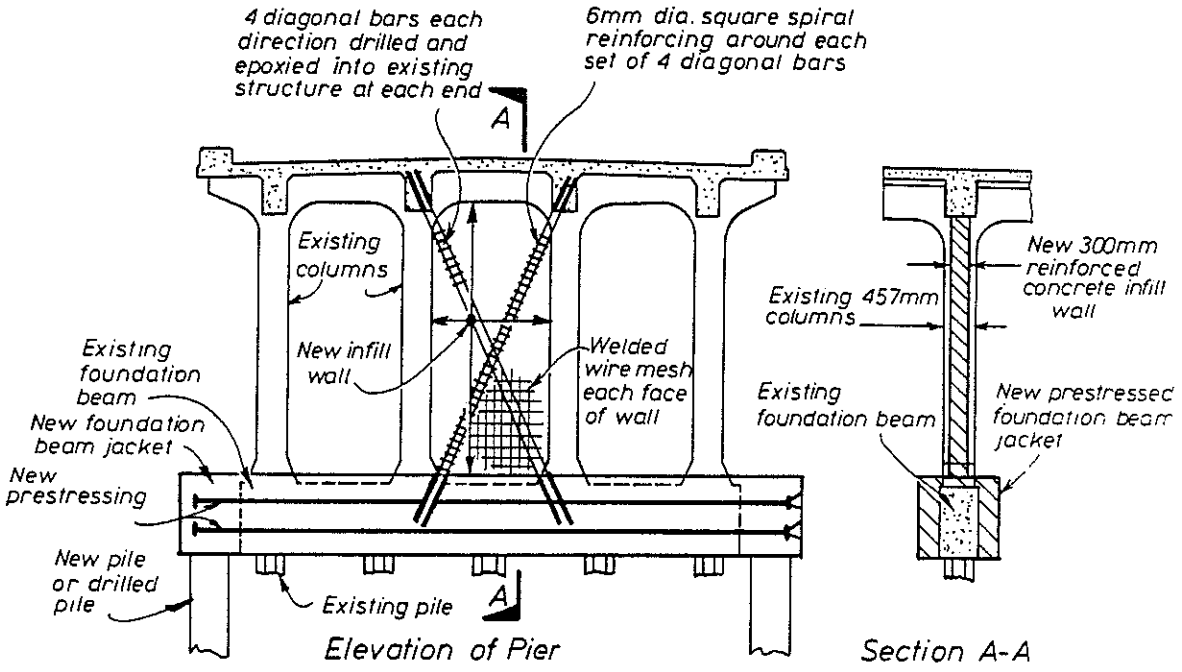

Figure 4.8 Possible seismic strengthening using a reinforced-concrete infill wall and foundation strengthening.

The infill-wall retrofit, which greatly increases the strength and stiffness of the existing bridge, is most appropriate if control of damage is an important retrofit goal, rather than just the prevention of collapse. The retrofit would allow the bridge to respond elastically to large earthquakes.

4.6.3 Added Braces and Energy-dissipation Devices

A third possible retrofit solution would be the addition of supplemental steel braces with energy-dissipation devices, as shown in Figure 4.9. Depending on the chosen properties of the energy-dissipation devices, the foundation of the bridge may not need strengthening. If properly designed, such a retrofit could prevent serious

damage to the bridge because less earthquake energy would need to be dissipated in the plastic-hinge regions of the concrete columns. The use of energy-dissipation devices seems particularly appropriate for structures with plain-round reinforcing (such as the subject bridge), because the energy-dissipation capacity in the as-built structure alone is relatively small as shown by the pinched hysteretic response resulting from bond slip.

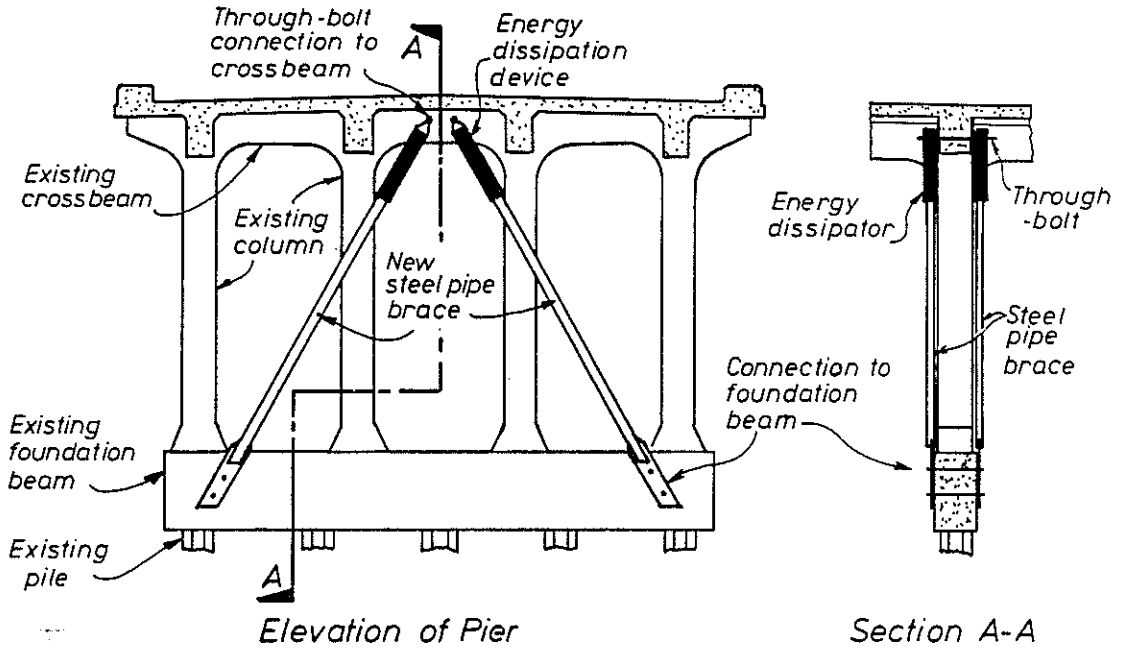

Figure 4.9 Possible seismic retrofitting using added steel braces with energy-dissipation devices.

5. INELASTIC EARTHQUAKE TIME-HISTORY ANALYSES

In Chapter 4 of this report, the seismic performance of the 1936-designed New Zealand bridge was predicted to be good, because of the substantial lateral strength and displacement capacity of the structure. In this chapter a series of computer analyses are described which were used to verify that prediction. The analyses also help quantify (a) the benefit of retrofitting bar anchorages, and (b) the effect of the pinched hysteretic response which is characteristic of structures with plain-round reinforcement. In all, twenty-four inelastic dynamic time-history analyses were run.

5.1 Modelling of Structure Behaviour

The inelastic time-history analysis program *Ruaumoko* (Carr 1995) was used to model the earthquake response characteristics of the 1936-designed bridge. Three different structures were modelled:

1. the bridge in its unretrofitted condition,
2. the bridge after retrofitting with anchorage end plates at the top of the column bars, as described in Section 2.4 of this report, and
3. an ideal structure with the same capacity as the anchorage-retrofit bridge but assumed to have deformed column bars with good bond characteristics.

5.1.1 General Assumptions

As with the previous assessment and experimental studies of the subject bridge (Chapman 1991), discussed in Chapters 2, 3, and 4 of this report, only the transverse-direction response of the bridge was considered. A lumped-mass, single-degree-of-freedom model was used, calibrated to the target values of the structural parameters shown in Table 5.1. The target parameters also included a matching of the hysteresis loop shapes and envelopes from the experimental results shown in Figures 2.7, 3.8, and 4.3. The Wayne Stewart hysteresis model (Carr 1995) was used.

The dynamic, inelastic time-history analyses use the Newmark constant average acceleration method, and P-Δ effects are modelled by modifying the member stiffness, given the static dead load (Carr 1995). Initial-stiffness Raleigh damping is used at a damping ratio of 2% of critical. Earthquake input is in the horizontal direction only. The *Ruaumoko* input data are shown in Table 5.2.

5.1.2 Modelled Hysteresis Loops

The modelled hysteresis loops obtained for the subject bridge are shown in Figure 5.1. The loops were carefully matched to the experimental results and calculated and measured capacities. Figure 5.1(a) shows the pinched hysteresis loops used to model the unretrofitted bridge. Figure 5.1(b) shows similar pinched hysteresis loops, but with a lateral capacity 18% higher than the unretrofitted bridge and with a rate of strength degradation (with drift) 1.5 times lower.

Table 5.1 Structural modelling parameters used for time-history analyses.

Parameter	Unretrofitted Bridge	Anchorage-Retrofit Bridge	Ideal Structure
Lateral capacity/seismic weight	0.45	0.53	0.53
Hysteresis loop shape	Pinched	Pinched	Not pinched
Initial stiffness	5.9 kN/mm	5.9 kN/mm	7.8 kN/mm
Strength degradation at 4% drift (not including P-Δ)	21%	14%	14%

Table 5.2 Values used for *Ruaumoko* input and time-history analyses.

Input Parameter	Unretrofitted Bridge	Anchorage-Retrofit Bridge	Ideal Structure
Member length (shear span)	1.80 m	1.54 m	1.54 m
Moment of inertia	$720(10)^{-6}$ m^4	$450(10)^{-6}$ m^4	$600(10)^{-6}$ m^4
Bi-linear stiffness factor	0.4	0.4	0.4
Tri-linear stiffness factor	-0.030	-0.020	-0.015
Ultimate moment	185 kN-m	185 kN-m	185 kN-m
"Yield" moment	122 kN-m	122 kN-m	122 kN-m
Hysteresis model	Wayne Stewart	Wayne Stewart	Wayne Stewart
Intercept moment for pinching	40 kN-m	40 kN-m	90 kN-m
Pinching factor, α	0.6	0.6	1.0
Unloading factor	1.0	1.0	1.0
Factor, β	1.09	1.09	1.09
Strength degradation factor after 10 cycles	0.7	0.9	0.9
Damping ratio	2%	2%	2%

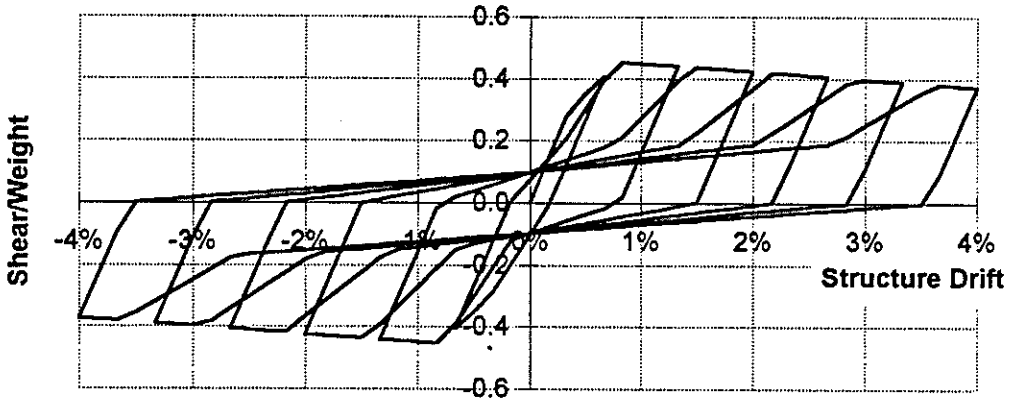

(a) Unretrofitted bridge

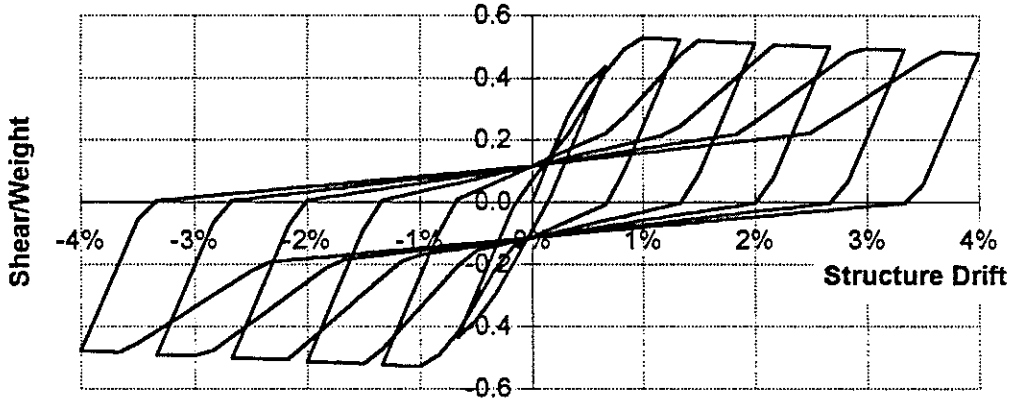

(b) Anchorage-retrofit bridge

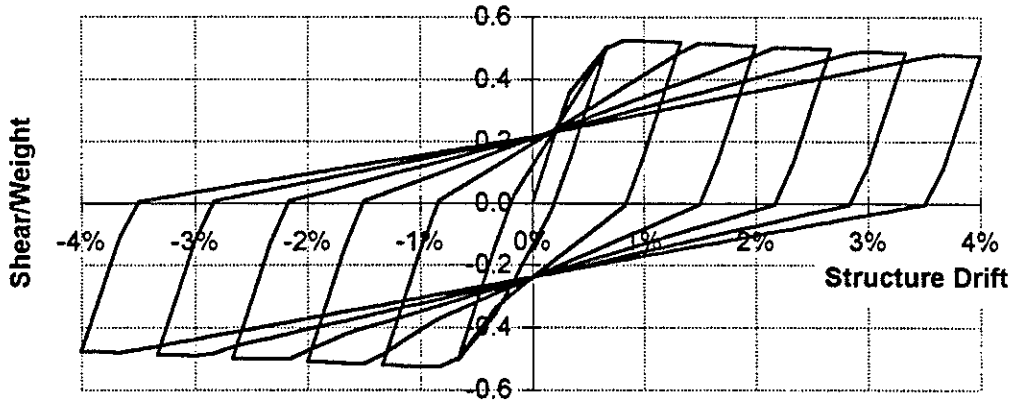

(c) Ideal structure

Figure 5.1 Hysteresis loops obtained from time-history analyses to model structural behaviour.

Figure 5.1(c) represents the hysteretic behaviour of an "ideal" structure. The ideal structure has the same lateral strength as the anchorage-retrofit bridge but with a slightly higher initial stiffness and without pinched hysteresis loops. The ideal structure could be considered to be the subject bridge as if it had deformed column bars with hooks at each end, and assuming that the column transverse reinforcement is adequate to prevent bar buckling. With deformed column bars, significant bond slip would not occur and therefore the hysteretic response of the column would not be pinched.

The initial stiffness of the ideal structure is modelled to be 1.33 times higher than that of the structures with plain-round bars. This assumption is based on the observation from the test results, discussed in Section 3.3 of this report, that the stiffness of the column specimen with plain bars degraded during the first four cycles of testing in each direction, prior to the yielding of the column bars. A column with well-bonded, deformed reinforcement would not be expected to suffer such pre-yield stiffness degradation, and therefore its initial stiffness would be somewhat higher.

Figure 5.2 shows the capacity envelopes of the three structural models, plotted on the same graph for comparison. Figure 5.2 shows clearly the higher capacity of the ideal and anchorage-retrofit structures compared to the unretrofitted, the higher rate of strength degradation of the unretrofitted bridge, and the higher initial stiffness of the ideal structure. Note that the strength degradation evident in the plots of Figures 5.1 and 5.2 does not include a degradation of strength based on number of cycles or the reduction of lateral capacity related to the P-Δ effect, both of which are considered in the *Ruaumoko* analysis. The strength degradation based on number of cycles was not found to be significant in the analysis results.

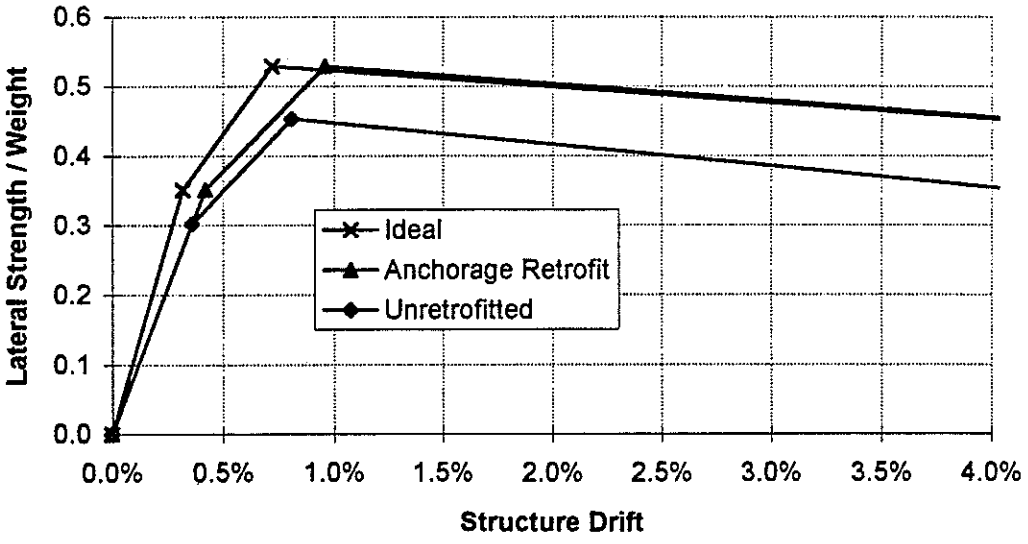

Figure 5.2 Lateral strength envelopes for hysteresis models.

5.2 Earthquake Input

Eight different earthquake records, listed in Table 5.3, were used as input to the analysis. The eight records cover a wide range of earthquake characteristics.

5.2.1 Selection of Earthquake Records

The first earthquake record used in the analysis is an artificial record called Bridgeza. This record was created to produce a response spectrum matching that used for the seismic design of bridges in New Zealand's most active seismic zone. Thus, the earthquake record represents the seismic demands which have been considered appropriate for the design of new bridges.

Table 5.3 Earthquake records used for the inelastic time-history analysis.

Record Name	Filename	Earthquake Date	Direction	Record Duration (seconds)	Peak Ground Accel (g)
Bridgeza	BRIDGEZA.EQC	Artificial	-	20.00	0.50
Pacoima Dam	PACMSW.EQB	9 Feb. 1971	S14W	20.30	1.20
El Centro	EL4ONSC.EQB	18 May 1940	N-S	20.06	0.37
Parkfield	PARKNE.EQB	27 June 1966	N65E	21.10	0.49
Taft	TAFTNW.EQB	21 July 1952	N69W	30	0.16
Bucharest	BUCHNSC.EQB	4 March 1977	N-S	16.22	0.21
Mexico D	MEXTLHDL.DQC	19 Sept. 1985	N-S	150	0.12
Mexico S	MEXSCT1T.EQC	19 Sept. 1985	E-W	150	0.17

Mexico D - obtained from Tlahuac Deportivo
Mexico S - obtained from Secretariá Comunicationes y Transportes

The next four records in Table 5.3, Pacoima, El Centro, Parkfield and Taft, were obtained from Californian earthquakes, and have commonly been used in structural analyses. The last three records, Bucharest and two from Mexico, are included to consider the performance of the bridge as if it were located on a soft-soil site.

Naeim and Anderson (1993) provide an excellent classification and evaluation of earthquake records, which was used to help select the records for this study. Table 5.4 shows additional data from Naeim and Anderson on the six earthquake records used here.

The Pacoima dam record is notable for its high peak ground acceleration, velocity, and displacement. The Parkfield record is notable for its high incremental velocity, and both the Parkfield and Pacoima records are among the records with the largest

mean input energy in the period band from 0.5 to 0.8 seconds (Naeim and Anderson 1993, Tables 5-1 and 6-5). The 1940 El Centro and the 1952 Taft records are considered notable for their reasonably long durations, but Naeim and Anderson (1993, p.156) note that *...some of the acceleration records commonly used for earthquake resistant design, such as 1940 El Centro, have very limited damage potential compared to other records contained in the database...*

The Mexico D record was initially selected for the analysis to represent soft-soil earthquake input. The analysis showed that the subject structure responded in a fully elastic manner. Two other soft-soil records were also run: Bucharest and Mexico S. The Mexico S record has the highest peak ground acceleration of any of the 1985 Mexico City records and is considered notable for its peak displacement and incremental velocity (Naeim and Anderson 1993). (As shown later, both the Mexico S and Bucharest records would have had little damaging effect on the subject bridge.)

Table 5.4 Additional data on earthquake records, taken from Naeim and Anderson (1993, Table 3-1).

No.	Year	Earthquake Name	Station Name	D	Mag	PA	PV	PD	(D)
147	1971	San Fernando	Pacoima Dam	8	6.6	1125	113.09	38.28	33.9
11	1940	El Centro	El Centro	12	7.0	338	36.45	10.88	29.3
52	1966	Parkfield CA	Cholame-Shandon Array 2	7	6.1	466	77.59	26.74	12.1
29	1952	Kern County	Taft	42	7.4	183	17.80	7.27	15.6
805	1985	Mexico D	Tlahuac Deportivo	410	8.1	115	34.26	18.53	18.7
799	1985	Mexico S	Sec.Com.yTrans.	400	8.1	168	60.38	20.57	33.1

D = epicentral distance, km
Mag = magnitude
PA = peak ground acceleration, cm/sec^2
PV = peak ground velocity, cm/sec
PD = peak ground displacement, cm
(D) = 0.05 g bracketed duration, sec
El Centro - Imperial Valley Irrigation District
Mexico S -Secretariá Comunicationes y Transportes

5.2.2 Response Spectra

The characteristics of each of the eight earthquake records are illustrated by their response spectra, shown in Figure 5.3(a)-(f). The response spectra show a tremendous variation in earthquake characteristics between the different records, and compared to the code-assumed response spectrum approximated by the Bridgeza record of Figure 5.3(a). Only the 1940 El Centro record, Figure 5.3(c), even vaguely resembles the Bridgeza record. The Pacoima spectrum, Figure 5.3(b), greatly exceeds the Bridgeza spectrum in most period bands. The Parkfield spectrum, Figure 5.3(d), greatly exceeds the Bridgeza spectrum in the period range of 0.3 to 0.8 seconds,

which is critical for the subject bridge. The Taft spectrum, Figure 5.3(e), shows that this record has much lower demands than the Bridgeza record. The soft-soil records from Bucharest and Mexico, Figures 5.3(e) and (f), show extremely high demands in the period range around 2 seconds, but much lower demands in the period range of the response of the subject structure, 0.4 to 1.0 seconds.

The spectra shown in Figure 5.3(a)-(f) are plotted on acceleration versus displacement (A-D) axes. This presentation allows the consideration of spectral displacements as well as accelerations. As shown in Figure 5.3, lines of constant period extend radially from the origin. Two lines of constant pseudo-velocity are also shown faintly on each of the plots of Figure 5.3. The shape of these lines on the plots is that of an inverse function (i.e. $y = kx^{-1}$).

The plotting of the spectra in A-D co-ordinates allows the structure's force-displacement response to be superimposed on the spectrum plot. This has been done in Figure 5.3, using the envelopes of force-displacement response for the unretrofitted bridge. Each bridge response envelope is plotted to the peak displacement reached in the analysis for that particular earthquake record.

5.3 Analysis Results

The results of the 24 computer analyses show a large variation in response depending on the earthquake input, and also point to some differences in seismic performance between the unretrofitted, anchorage-retrofit, and ideal structures.

5.3.1 Structure Drift

Table 5.5 shows the peak levels of structure drift in each direction resulting from the inelastic computer analyses. The structure drift for the subject bridge, as defined in Section 4.2.5.1, is equal to the lateral displacement of the bridge superstructure with respect to the foundation, divided by the height of 4.80 m between the centreline of the foundation beam and the centreline of the crossbeam. Figure 5.4 shows a graph of the peak structure drift values resulting from the 24 analysis runs.

The peak structure drift is a fairly good measure of the level of earthquake damage sustained by the bridge. Peak structure drift levels below about 0.7% indicate elastic or nearly elastic response.

A structure drift level of 4.0% indicates a global displacement ductility of μ=6, sometimes considered (SANZ 1995) to be the upper limit to reliable structural ductility capacity. The level of damage to the test specimen column at a structure drift of 4.0% is shown in Figure 3.2(c). For a structure with deformed column bars at a drift of 4%, the level of deterioration in the column could be greater.

Figure 5.3 Response spectra (a) and (b) for the earthquake records used as input to the *Ruaumoko* analysis.

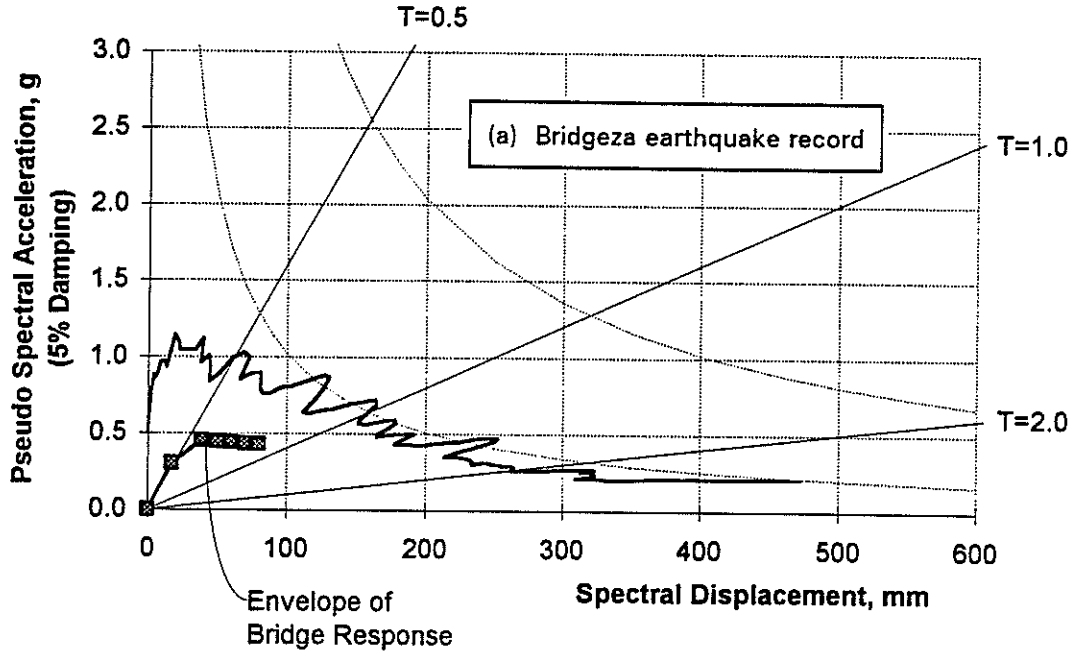

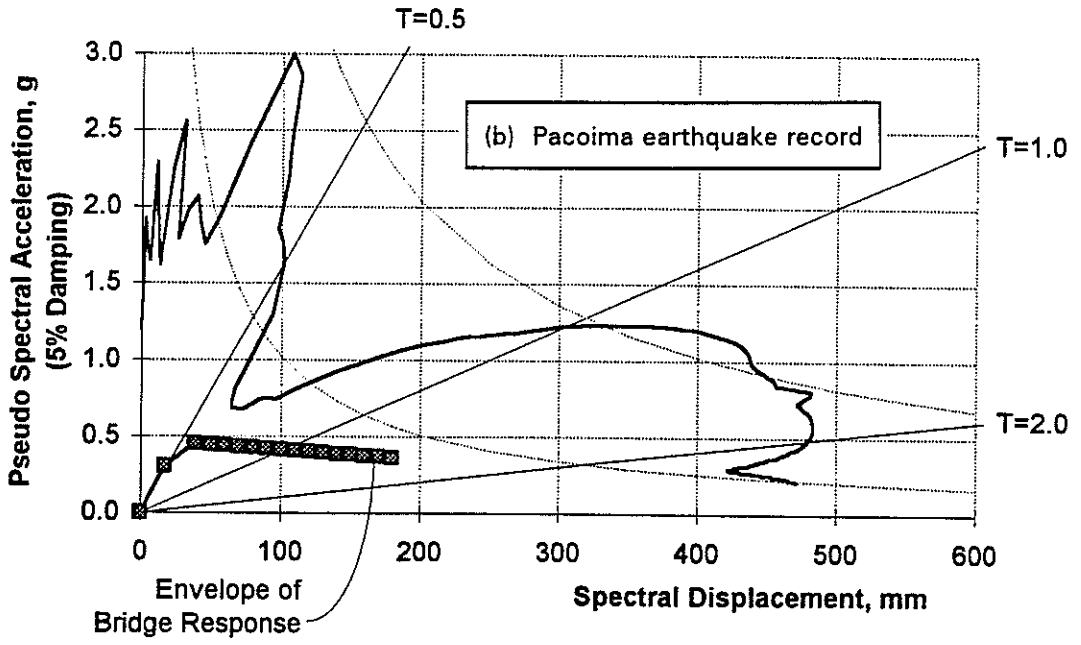

Figure 5.3 (continued) Response spectra (c) and (d) for the earthquake records used as input to the *Ruaumoko* analysis.

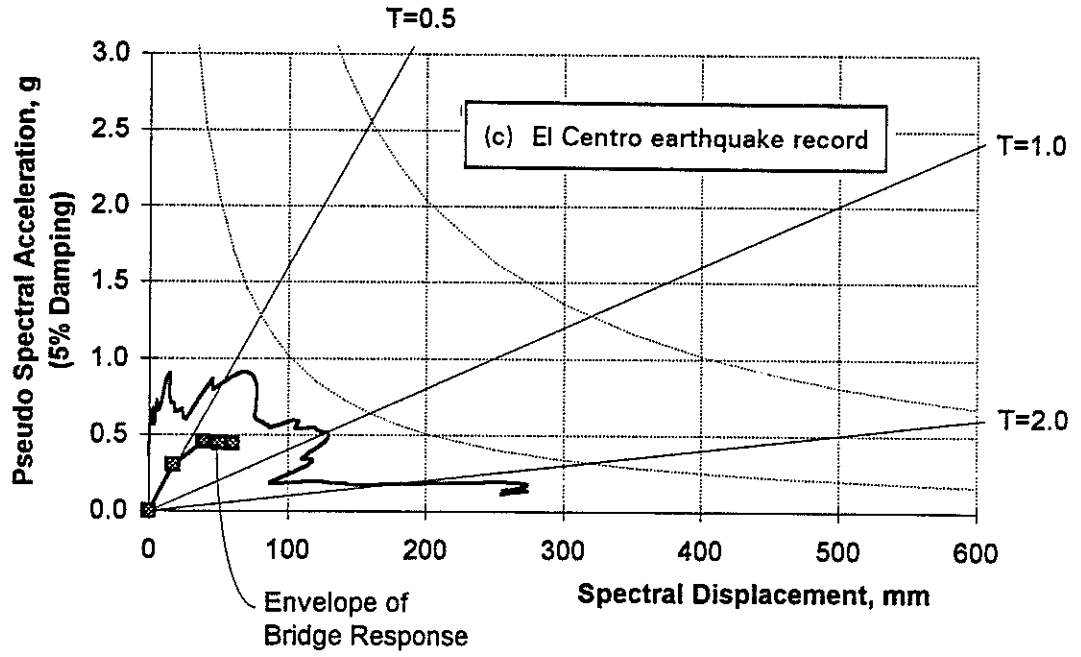

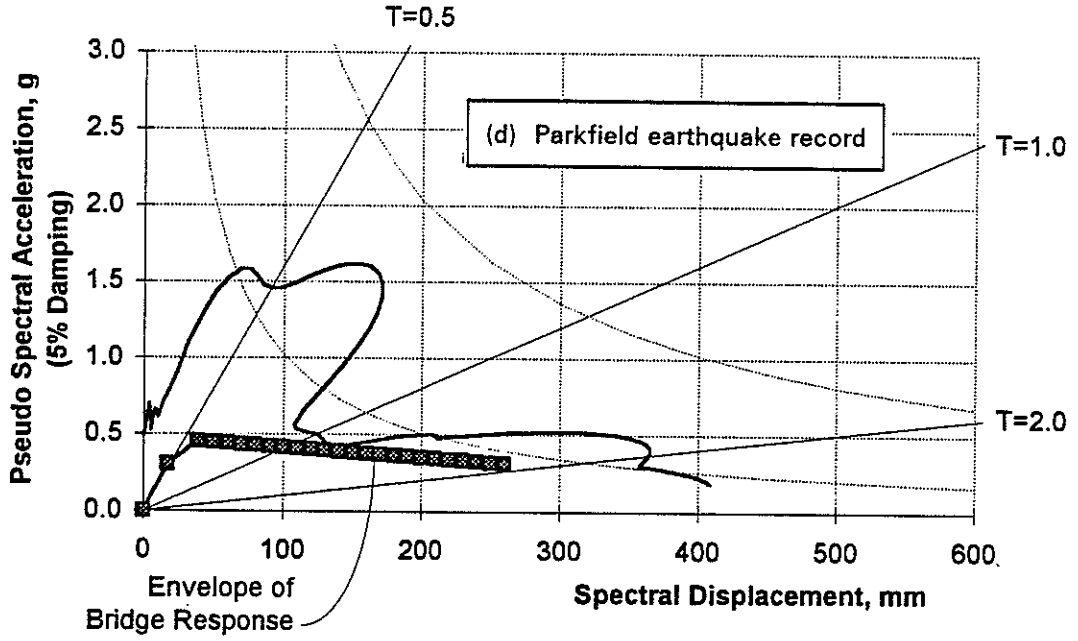

Figure 5.3 (continued) Response spectra (e) and (f) for the earthquake records used as input to the *Ruaumoko* analysis.

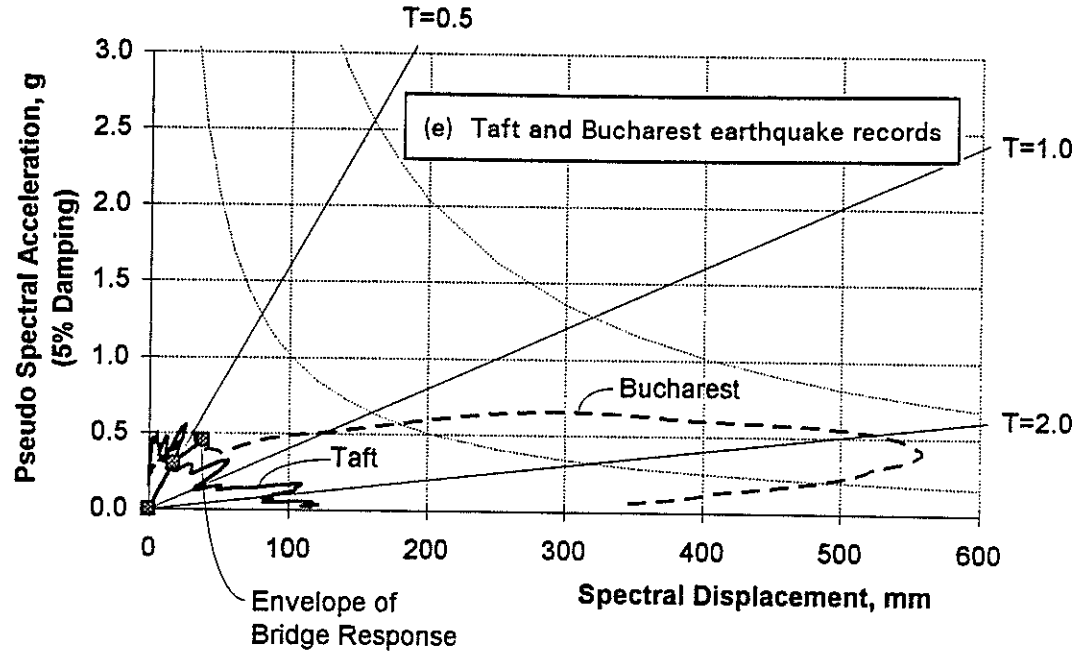

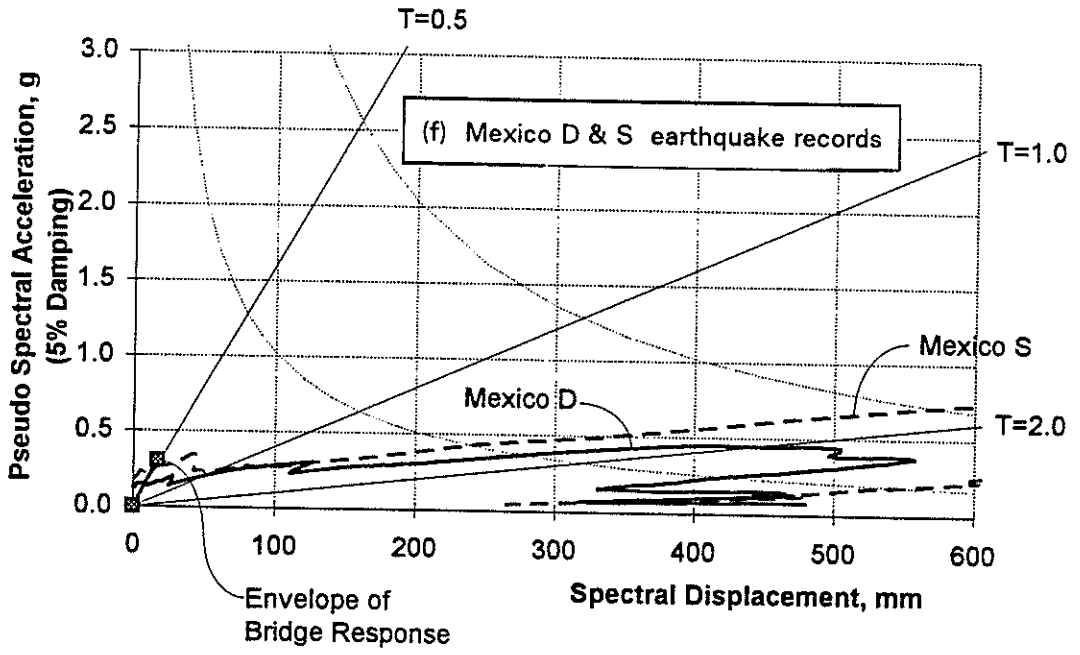

Table 5.5 Maximum structure drift results from the inelastic time-history analyses of the subject bridge.

Earthquake Record	Peak Structure Drift (Positive and Negative) %					
	Unretrofitted Bridge		Anchorage-Retrofit Bridge		Ideal Structure	
Bridgeza	1.76%	-1.45%	1.83%	-1.15%	1.48%	-0.51%
Pacoima	3.76	-1.80	3.11	-1.50	2.06	-1.55
El Centro	1.27	-0.68	1.07	-0.73	0.75	-0.43
Parkfield	5.42	-1.89	4.57	-3.25	2.37	-1.33
Taft	0.51	-0.48	0.56	-0.60	0.58	-0.32
Bucharest	0.44	-0.43	0.45	-0.43	0.23	-0.30
Mexico D	0.22	-0.17	0.22	-0.17	0.20	-0.14
Mexico S	0.26	-0.23	0.26	-0.23	0.18	-0.16

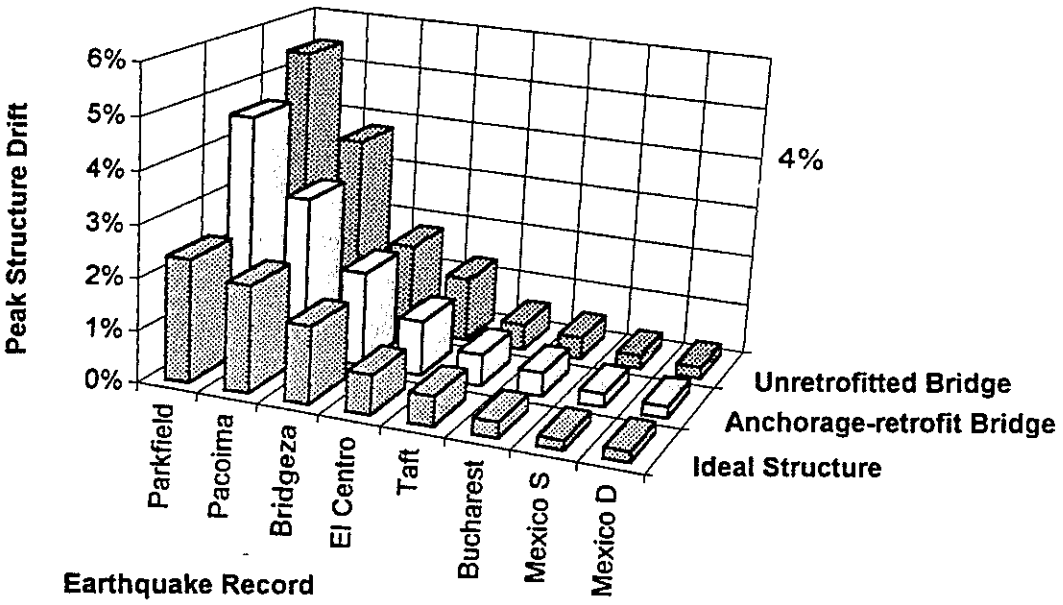

Figure 5.4 Peak structure drift results from the inelastic time-history analyses.

5.3.2 Bridge Performance Limit States

Peak drift levels for the subject bridge could be associated with performance limit states (Paulay and Priestley 1992). Table 5.6 outlines the estimated relationship of bridge performance with peak drift levels. The table is based primarily on the test results of Chapters 3 and 4. The table shows that below a drift of 0.7% (Limit State A) no bridge damage or repair is expected. Between 0.7 and 1.5% drift, cracking and some inelastic behaviour is expected but spalling of the concrete is not expected. Limit State B with concrete spalling is expected when more than 1.5% drift occurs.

Limit State C marks the traditional serviceability limit, beyond which a bridge will not remain fully functional for carrying traffic, and beyond which more serious repair or retrofit measures will be required. This limit state may depend more on the residual or permanent drift of the structure after the earthquake than on the peak drift during earthquake shaking. However, the higher the peak drift, the greater the chance that the structure will be left with an unacceptable level of residual drift.

Also, a structure with deformed reinforcement, for the same peak drift, may be more likely to have an unacceptable level of residual drift than a structure with plain-round reinforcement. This is because a structure with deformed reinforcing would undergo greater levels of inelastic strain in the column bars. Considering these points, Limit State C is estimated to be reached at a peak drift of about 2.5% for the bridge with plain bars, and to be reached at a drift of about 2% for the bridge with deformed bars.

Limit State D marks the traditional damage-control limit state, beyond which damage is not economically repairable. Based on the test results of Chapters 3 and 4, the subject bridge seems to be able to sustain very high drift levels before suffering irreparable damage. Until a drift of 6% is reached, damage consists only of cracking and spalling in the column end regions, and the reinforcing bars do not buckle. Beyond the 6% drift level, anchorage-splitting failures could occur which would be difficult to repair. Thus a peak drift level of 6% is associated with Limit State D for the subject bridge with plain-round bars. For the ideal bridge with deformed bars Limit State D is estimated to occur at a drift of about 5%, when the column bars would be likely to buckle, as discussed in Section 4.3.

Limit State E of Table 5.6 represents the traditional survival or no-collapse limit state. The test results show that the subject bridge with plain-round bars will not collapse even at the extreme drift levels, i.e. about 8%, to which the bridge was tested. For the hypothetical bridge with deformed bars, the peak drift to cause collapse cannot be estimated, because of the lack of specific test results.

Table 5.6 Estimated relationship of bridge drift level to performance limit states.

Limit State	Bridge Damage and Likely Repair	Bridge Serviceability	Peak Structure Drift Corresponding to Limit State	
			Unretrofitted or Anchorage-Retrofit Bridge	"Ideal" Structure
	No damage, no repair required	No loss of bridge service		
A			0.7%	0.7%
	Minor damage, epoxy injection of cracks required			
B			1.5%	1.5%
	Moderate damage, epoxy injection and patching of spalled concrete required			
C			2.5%	~2%
	Moderate to heavy damage. May need to jack bridge to remove permanent lean and/or add bracing retrofit to restore stiffness. Also patching and epoxy injection required.	Temporary loss of bridge service except for emergency traffic		
D			6%	~5%
	Heavy damage. Column-bar buckling or anchorage splitting. Not economically repairable.	Bridge unsafe even for emergency traffic		
E			> 8%	Unknown
	Collapse			

Note: Only transverse-direction structural response is considered.

5.3.3 Responses for Different Earthquake Records

Figure 5.4 clearly illustrates the large variation in structural response depending on the earthquake input. The force-displacement-response envelopes for the unretrofitted bridge are also shown on the spectra plots of Figure 5.3. Four of the earthquake records cause little or no damage to the bridge models, because for the two Mexico records the response is fully elastic, and for the Bucharest and Taft records the response is nearly elastic. The structure drift in some cases reaches the bi-linear region of the capacity envelopes shown in Figure 5.2, but does not reach the tri-linear region. Thus none of the four records, Taft, Bucharest, Mexico S, and Mexico D, affect the structures enough to cause them to reach their ultimate strengths. The good lateral strength of the subject structure, as noted in Section 4.4 of this report, prevents any damage from occurring if analysed using these four earthquake records.

Of more interest are the Bridgeza and El Centro earthquake results. The Bridgeza earthquake causes peak structure drifts of up to 1.8%, while the El Centro record causes drifts of up to 1.3%. These results confirm that the performance of the modelled structures under a code-implied level of earthquake shaking will be good. The Bridgeza and El Centro earthquakes impart only a limited level of ductility demand on the structures, and the maximum displacement-ductility demand for these earthquake inputs is less than 3.

The Pacoima and Parkfield earthquake records impart more extreme demands on the modelled structures. For the Pacoima record the peak structure drift is 3.8%; for the Parkfield record it is 5.4%. As previously noted, these two earthquakes have very high input energy in the period range of the structural response. For both of these records the earthquake energy is released in a few major pulses, over a duration of just a few seconds.

Naeim (1995) has found these same characteristics in the strongest records from the 1994 Northridge earthquake. Such earthquake records, with a few major pulses of ground motion which greatly exceed code-implied earthquake demands, have also been observed in the 1995 Hyogo-ken Nanbu (Kobe) earthquake, and in the 1992 Petrolia (California) earthquake. Such earthquake shaking characteristics tend to be found in locations "downstream" from the earthquake source, i.e. in the direction of the fault propagation. In this direction the earthquake waves tend to stack up on each other causing larger pulses for shorter durations. For the 1940 El Centro record, the earthquake fault propagation was directed away from the recording station (Carr pers.comm.) causing a smaller amplitude of shaking with a longer duration. Current seismic design codes tend to assume an El Centro type of earthquake response spectrum, although some engineers have proposed to account for more extreme earthquake effects using a near-field factor (SEAONC 1995).

Figure 5.5 Structure drift time-history results for the Bridgeza earthquake record.

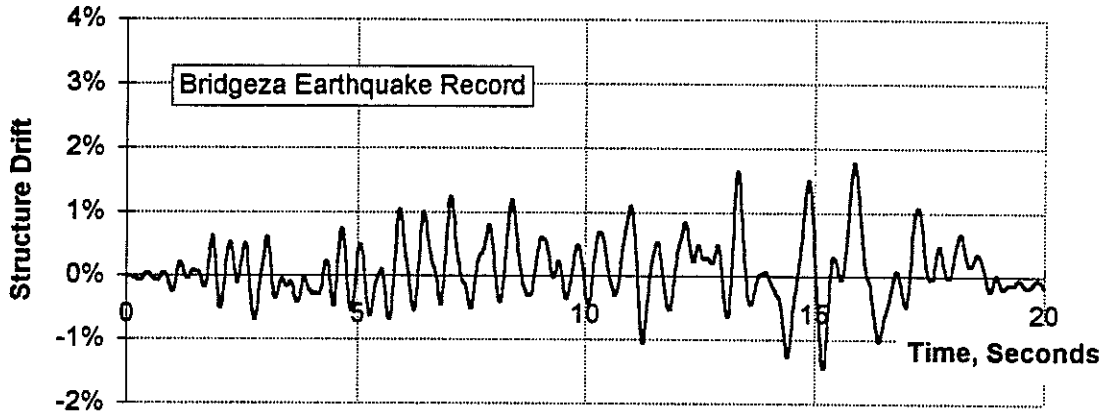

(a) Unretrofitted bridge

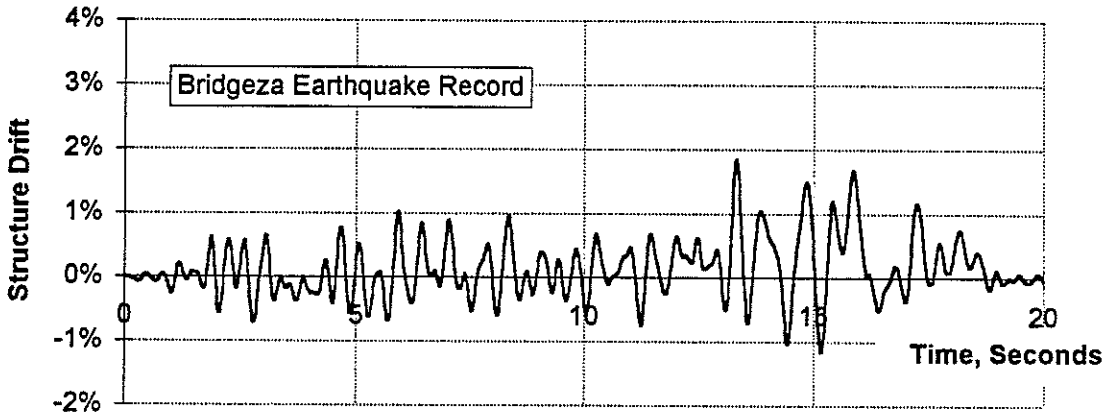

(b) Anchorage-retrofit bridge

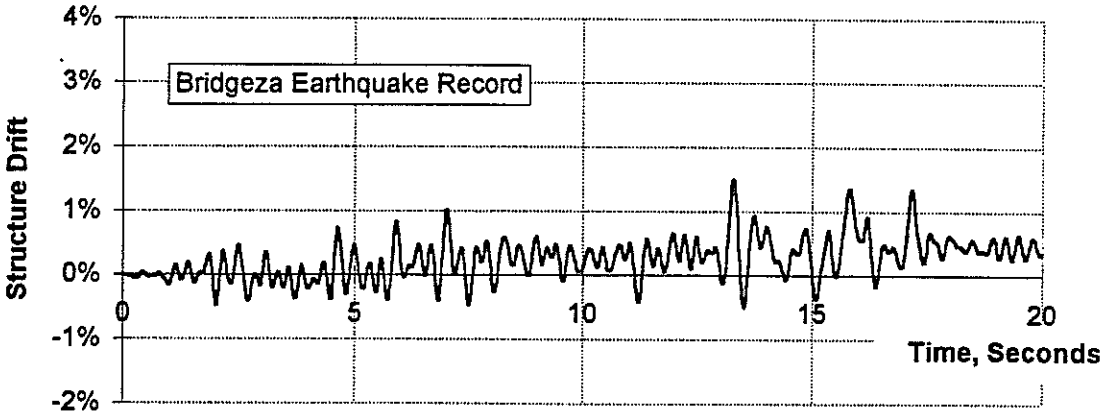

(c) Ideal structure

Figure 5.6 Lateral-force versus lateral-displacement hysteretic response for the Bridgeza earthquake record.

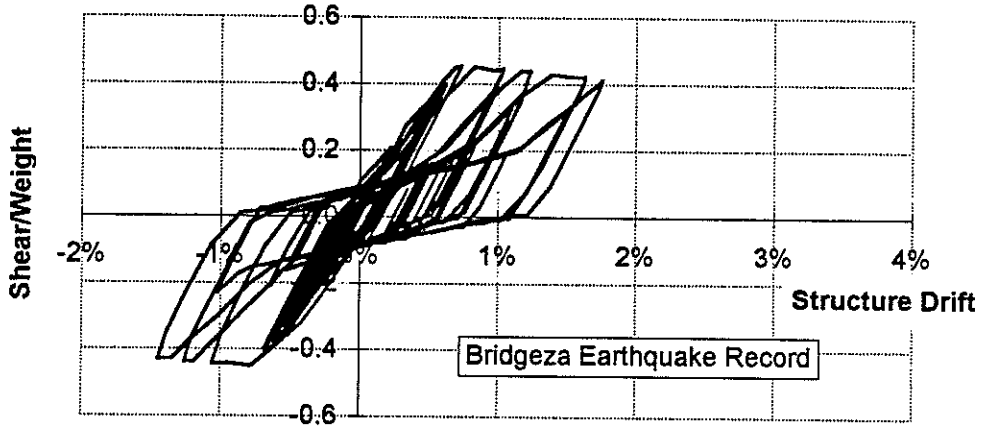

(a) Unretrofitted bridge

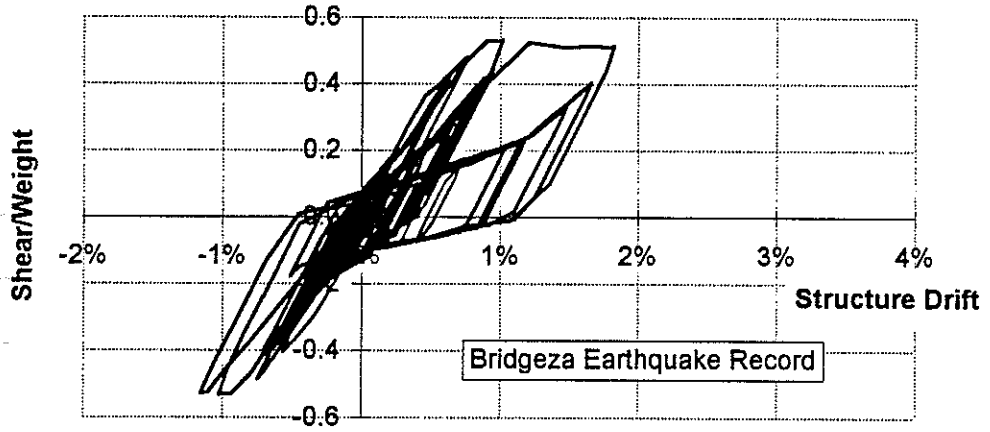

(b) Anchorage-retrofit bridge

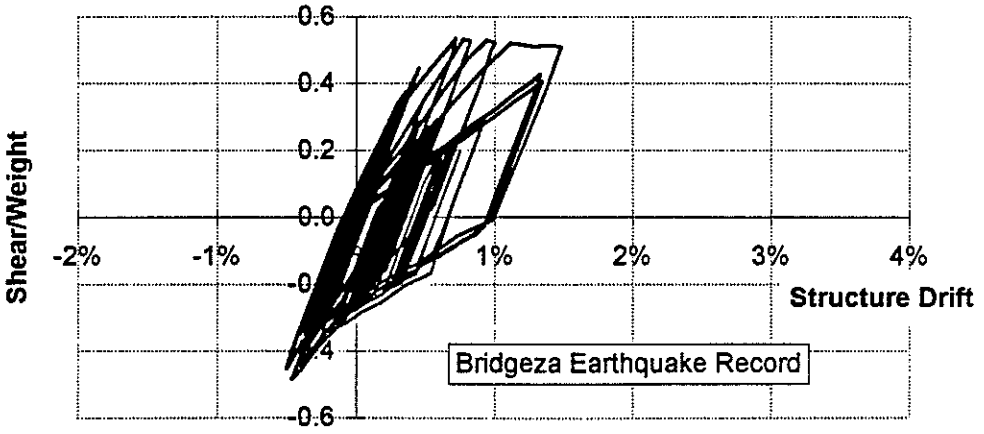

(c) Ideal structure

5.3.4 Response for Different Hysteresis Models

As well as showing a strong dependency on earthquake input, the peak displacement results of Table 5.5 and Figure 5.4 show some consistent differences in the response of the three different hysteresis models. Typically, the seismic response of the anchorage-retrofit bridge is slightly improved over that of the unretrofitted bridge, and the response of the ideal structure is further improved over that of the other two models.

For the Taft, Bucharest, and Mexico earthquake records there is, understandably, little difference in the peak displacement response between the three structural models. As previously noted, the behaviour for these earthquake inputs is elastic or nearly elastic, and therefore of little interest.

5.3.4.1 Bridgeza and El Centro earthquakes

For the two earthquake records which produce moderate displacement demands, Bridgeza and El Centro, some differences between the three structures are evident. For the El Centro earthquake, the peak drift of the anchorage-retrofit bridge is 16% less than for the unretrofitted bridge. For the Bridgeza earthquake the peak drift for these two structures is about the same, but the maximum drift in the negative direction is reduced by about 20% for the anchorage-retrofit bridge (see Table 5.5 and Figures 5.6a and 5.6b). Comparing the ideal structure with the anchorage-retrofit bridge, the peak response for the El Centro and Bridgeza earthquakes is reduced by about 20% to 30% for the ideal structure.

For the Bridgeza earthquake the structure drift time-history results are shown in Figure 5.5, and the lateral-force versus displacement-hysteresis responses are shown in Figure 5.6. These figures again show (a) only a slight reduction in response for the anchorage-retrofit bridge over the unretrofitted, and (b) a more significant reduction in response for the ideal structure over the anchorage-retrofit bridge.

Interestingly, although a peak drift is the least for the ideal structure, the *residual* drift is the greatest. The residual drift is shown at the end of the time-history of Figure 5.5(c) to be about 0.4%. This level of residual lean in the bridge may be noticeable but would not compromise the ability of the structure to resist future earthquakes or its design loads. For the unretrofitted and anchorage-retrofit bridges the residual drift is nearly zero.

5.3.4.2 Pacoima and Parkfield earthquakes

For the two earthquake records which produce large displacement demands, Pacoima and Parkfield, the differences between the three structural models are more pronounced. Comparing the anchorage-retrofit bridge to the unretrofitted, the results show a reduction of peak displacement by about 16%. Comparing the ideal structure with the anchorage-retrofit bridge, a reduction in peak displacements of about 40% is evident.

For the Pacoima earthquake, structure drift time history results are shown in Figure 5.7 and lateral-force versus lateral-displacement hysteresis response plots are shown in Figure 5.8. The figures show the significant difference in structural response between the three models.

Figure 5.8(a) shows that the unretrofitted bridge is subjected to most of its inelastic displacement demands in one pulse which pushes the structure to a drift of 3.4%. Figure 5.7(a) shows that this is the first major pulse of the Pacoima record, occurring about 3 seconds into the earthquake time history. A similar type of response occurs for the unretrofitted bridge in reaction to the Parkfield earthquake. Naeim (1995) has noted that for such types of earthquake records damping is of little benefit, and the earthquake's energy must be dissipated as hysteretic energy by the structure.

The increased strength of the anchorage-retrofit and ideal structures allows them to dissipate the earthquake energy of the first strong earthquake pulse with less lateral displacement, as shown in Figures 5.8(b) and 5.8(c). The fatter hysteresis loops of the ideal structure allow the structure to dissipate the input energy of the subsequent earthquake pulses with less displacement than that suffered by the anchorage-retrofit bridge.

For the unretrofitted bridge, not only is the peak level of drift considerable, so is the residual drift. As shown in Figure 5.7(a), at the end of the Pacoima earthquake, the structure is left-leaning at a drift of about 0.9%. For the anchorage-retrofit and ideal structures, the residual drift is about 0.3%.

5.4 Final Assessment

The analyses results show that the seismic performance of the bridge depends greatly on the earthquake input. Because of its substantial lateral strength, the bridge is able to respond essentially elastically for a number of earthquake records. Earthquake records with demands similar to those assumed by design codes, e.g. the Bridgeza and El Centro records, produce only moderate displacement demands on the structures. More severe earthquake records with extreme ground-motion pulses, such as Pacoima and Parkfield, produce higher displacement demands but do not cause bridge collapse. The performance of each of the three structures is summarised below for both the *code-implied* and *severe* earthquakes.

5.4.1 Performance for Code-implied Earthquake Levels

All of the structures perform very well for code-implied earthquake levels, and the difference in response between the three structures is not dramatic. Considering the limit states listed in Table 5.6, it is estimated that the structures could survive such earthquakes with only moderate damage that could easily be repaired. The bridges may also be able to survive such earthquakes without loss of service or traffic disruption.

Figure 5.7 Structure drift time-history results for the Pacoima earthquake record.

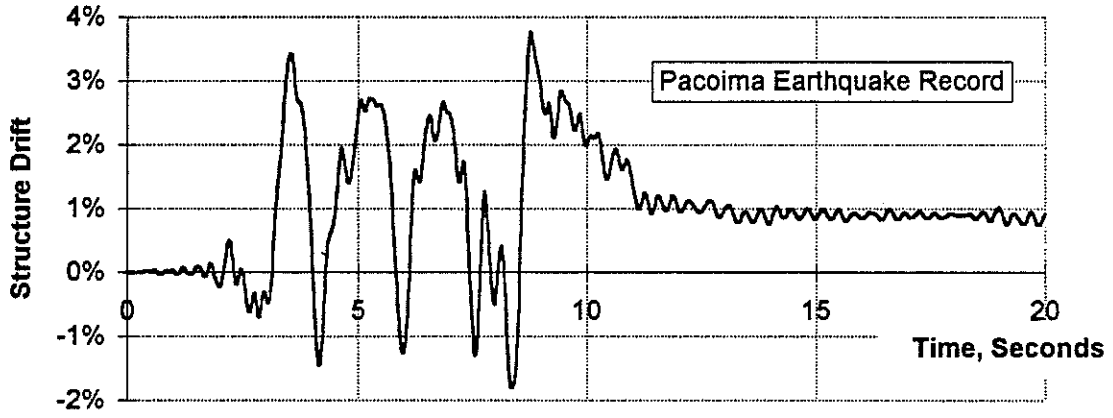

(a) Unretrofitted bridge

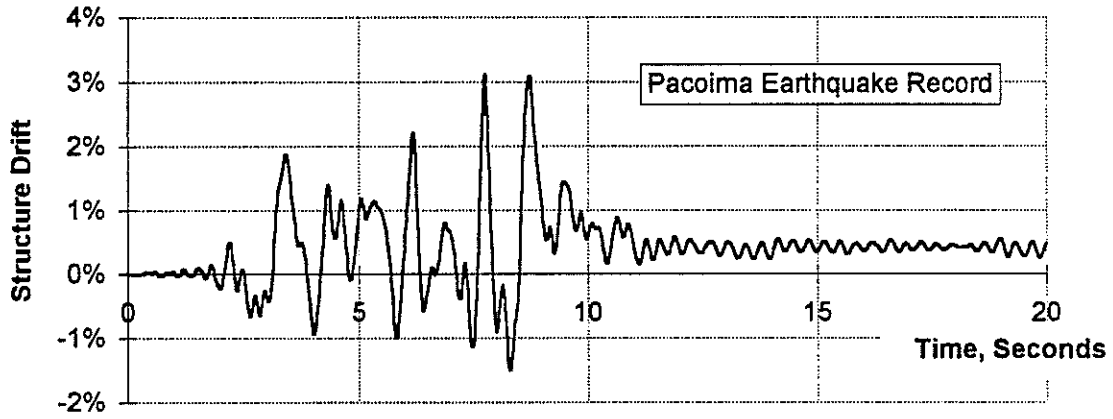

(b) Anchorage-retrofit bridge

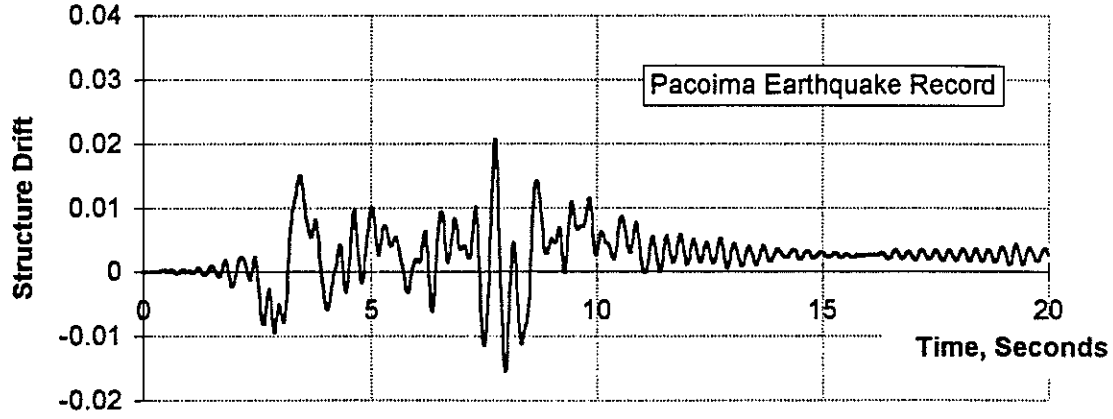

(c) Ideal structure

Figure 5.8 Lateral-force versus lateral-displacement hysteretic response for the Pacoima earthquake record.

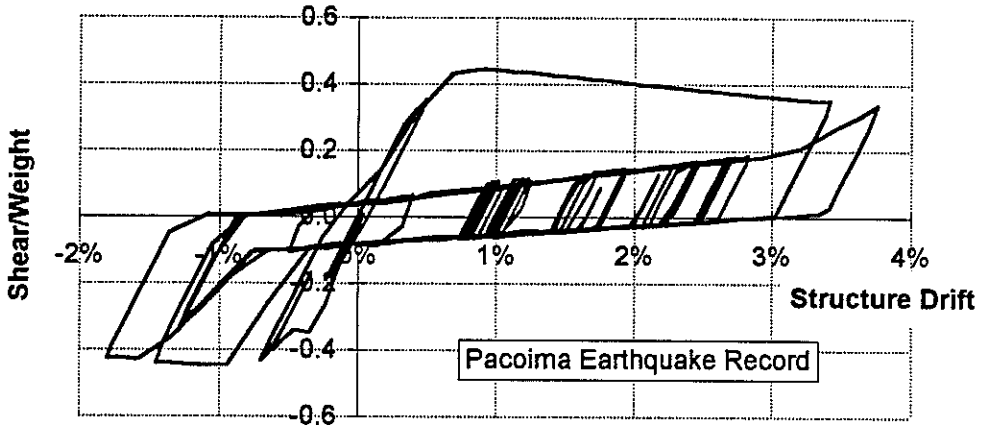

(a) Unretrofitted bridge

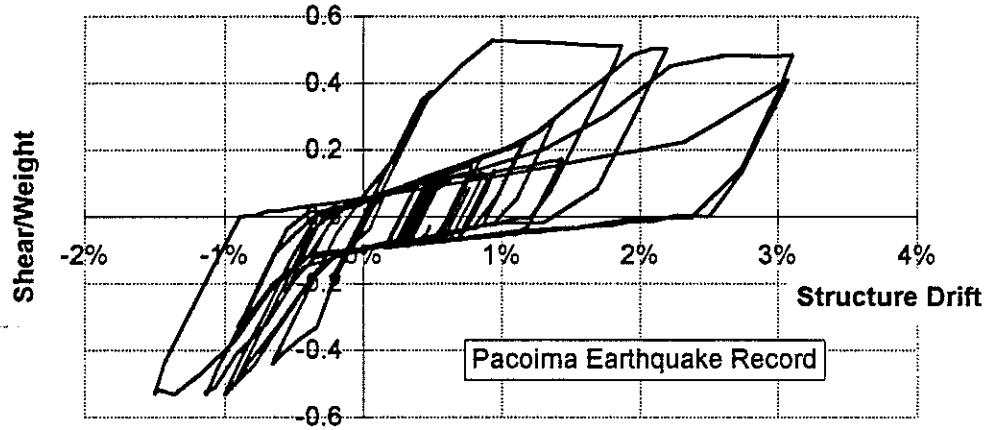

(b) Anchorage-retrofit bridge

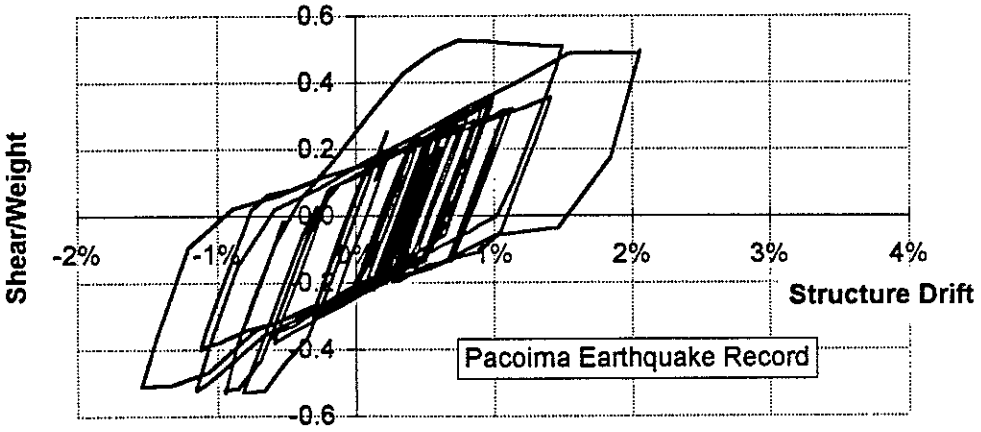

(c) Ideal structure

The retrofitting of the column-bar end anchorages can result in a slight decrease in displacement response compared to the unretrofitted bridge. However, the small improvement in bridge performance for this level of earthquake would not justify the cost of the retrofit.

The reduced response for the ideal structure compared to the anchorage-retrofit bridge indicates the better hysteretic energy-dissipating capacity of structures with deformed reinforcing. For the code-implied earthquake level, however, the reduction in response is not dramatic. Also this benefit may be offset by the fact that, for the same drift level, greater structural deterioration and residual drift can occur for structures with deformed reinforcing bars.

5.4.2 Performance for Severe Earthquake Levels

For severe earthquake inputs, the differences in structural performance for the three models become magnified. For the unretrofitted and anchorage-retrofit bridge, moderate to heavy damage would be suffered and the structure is likely to be left with a noticeable residual drift and a degraded stiffness. Despite the extreme displacement response, the bridge would not collapse and might still be repairable, perhaps by using an added bracing retrofit, as shown in Figure 4.9. The new braces could restore the degraded bridge stiffness and also be used, with jacking equipment, to straighten any residual lean in the structure.

The anchorage-retrofit structure shows a consistently reduced response compared to the unretrofitted structure. However, the moderate level of improvement, and the low probability of such extreme earthquake shaking, mean that such a retrofit would be difficult to justify.

For the severe earthquake input the ideal structure shows a substantial reduction in seismic response. This shows a clear benefit in the use of deformed column bars instead of plain bars. For severe earthquake shaking, as represented by the Parkfield and Pacoima records, the structure with deformed reinforcing would suffer less damage than the comparable bridge with plain-round reinforcing.

6. CONCLUSIONS & RECOMMENDATIONS

6.1 Conclusions

The studies of the 1936-designed New Zealand bridge have lead to several conclusions regarding the seismic assessment of existing reinforced-concrete structures:

- *Bond resistance of plain reinforcing bars*
  Compared with deformed reinforcement, plain-round reinforcement offers much poorer bond resistance and undergoes a more rapid degradation of bond under cyclic earthquake actions. The New Zealand concrete code NZS 3101:1982 (SANZ 1982) specifies that the embedment length of plain-round reinforcement should be twice that required of deformed reinforcement. This factor of two may not be sufficient to account for the poor bond of plain-round reinforcement, particularly at higher ductility levels. The 1995 revision to NZS 3101 prohibits the use of plain-round bars for main longitudinal reinforcement.

- *Stiffness degradation and hysteretic response*
  Structures with plain-round reinforcement suffer stiffness degradation under earthquake actions, and a pinching of lateral-force versus lateral-displacement hysteretic response resulting from the bond slip of the reinforcing. The stiffness degradation and pinched hysteresis loop shape could compromise the earthquake performance of structures with plain-round reinforcing bars, particularly for severe earthquake shaking characterised by a few very strong pulses.

- *Strength, displacement capacity, and seismic performance*
  Despite the pinched hysteretic response, the subject bridge has high lateral strength and displacement capacity which result in excellent seismic performance and allow the structure to survive severe earthquake shaking without collapse.

- *Bar-anchorage retrofit*
  If the bridge is retrofitted by welding anchorage end-plates to the tops of the column longitudinal bars, the peak lateral strength of the bridge increases and the degree of strength degradation reduces. As verified by the inelastic analyses, the anchorage retrofit would improve the seismic performance of the bridge. However, the amount of improvement probably does not justify the expense of such a retrofit.

- *Diagonal bars*
  The supplementary diagonal reinforcing bars at the top and bottom end-flares of the bridge column contribute significantly to both flexural and shear strength of the critical section of the column. A seismic evaluation which neglected the contribution of these bars would under-estimate the earthquake-resisting capacity of the structure.

- *Concrete confinement*
  For columns with low axial load, the NZS 3101:1982 concrete code (SANZ 1982) is conservative in its requirements for concrete confinement. For the subject bridge this code over-estimates the required amount of transverse steel by a factor of 3. The revised NZS 3101:1995 code (SANZ 1995) has more accurate requirements, and it is recommended as a basis for seismic assessment criteria.

- *Column-tie spacing*
  For columns with low axial load, good shear capacity, and large-diameter longitudinal reinforcing, the column-tie spacing requirements of the 1982 and 1995 NZS 3101 concrete codes (SANZ 1982 and 1995) may be conservative. A more accurate requirement has been proposed by the author, and it is recommended for the seismic evaluation of such columns, except where the requirements of shear reinforcement result in a smaller spacing.

- *Seismic evaluation assumptions*
  A preliminary seismic assessment of the subject bridge based on current design codes and practice concluded that *...the pier-columns are unlikely to tolerate cyclic displacements much exceeding yield* .... The laboratory testing and detailed analyses carried out for the present study have shown this conclusion to be incorrect. This shows that assumptions used for the evaluation of existing structures often need to be more accurate than those used for the design of new structures.

- *Confinement retrofit*
  The subject bridge as shown by the tests and the detailed evaluation is not vulnerable to earthquake damage that is related to insufficient transverse reinforcing or shear capacity. Thus implementing a confinement-retrofit of the bridge columns, such as adding new column ties or an external column jacket, would have no benefit and is unwarranted. Originally a confinement-retrofit of the column to foundation-beam specimen had been proposed, but because of the above findings the idea was discarded.

- *Research of structures with plain reinforcing bars*
  Concrete structures with plain-round longitudinal bars may require less transverse reinforcement than similar structures with deformed longitudinal bars. Research is needed on (a) bar buckling and (b) mechanisms of shear resistance for such structures. More in-depth studies of bond-slip behaviour are recommended.

- *Earthquake input*
  Inelastic time-history analyses of the subject bridge show that bridge response depends greatly on the earthquake input. Some earthquakes have a much higher potential to damage bridges than the earthquake levels that have been assumed in bridge design codes.

6.2 Recommendations

The research findings raise several important questions which should be investigated further. Additional research on the seismic performance of concrete bridges with plain-round reinforcement is recommended. Specific topics of study should include:

- Determining the required amount of transverse reinforcement to confine concrete and prevent longitudinal-bar buckling in the plastic-hinge regions of structural members.
- Determining the dominant mechanisms of shear resistance and the required shear reinforcement.
- Analysing and modeling the effect of bond slip on structural response.
- Evaluating additional sample bridges with different structural characteristics.

Because structures with plain-round reinforcement are much more prevalent in New Zealand than in California, or in other areas where seismic structural research is carried out, New Zealand cannot rely entirely on overseas research on this topic.

The response of bridges under earthquakes with strong pulses should also be studied further. As shown in this report, records show that some earthquakes have a much higher potential to cause damage than the earthquake levels that have typically been assumed in the bridge design and retrofitting.

7. REFERENCES

Carr, A.J. 1995. *RUAUMOKO Inelastic Frame Analysis Program.* Department of Civil Engineering Computer Program Library, University of Canterbury, Christchurch, New Zealand.

Chapman, H.E. 1991. Retrofitting - New Zealand. Pp. 505-527 in *Proceedings of the International Workshop on Seismic Design and Retrofitting of Reinforced Concrete Bridges*, GM Calvi and MJN Priestley (Editors), Bormio, Italy.

Dekker, D.R., Park, R. 1992. The repair and strengthening of reinforced concrete bridge piers. *Civil Engineering Research Report 92-1.* University of Canterbury, Christchurch, New Zealand.

Kordina, K., Hegger, J., Teutsch, M. 1989. Shear strength of prestressed concrete beams with unbonded tendons. *ACI Structural Journal 86(2):* 143-149. American Concrete Institute, Detroit, Michigan.

Maffei, J. 1996. *The seismic evaluation and retrofitting of bridges.* Thesis in partial fulfilment of the requirements for PhD degree. Department of Civil Engineering, University of Canterbury, New Zealand.

Maffei, J. 1997. Seismic evaluation and retrofit technology for bridges. *Transfund New Zealand Research Report No. 77.* 100pp. Wellington, New Zealand.

Naeim, F. 1995. On seismic design implications of the 1994 Northridge earthquake records. *Earthquake Spectra 11(1):* 91-109. Journal of the Earthquake Engineering Research Institute, Oakland, California.

Naeim, F., Anderson, J.C. Classification and evaluation of earthquake records for design. *Report Number CE 93-08,* Department of Civil Engineering, University of Southern California, Los Angeles, California.

NZBRC (New Zealand Building Regulations Committee). 1931. *Draft general earthquake building by-law.* Appendices 1 and 2 of a report to Parliament following the Hawkes Bay earthquake, June 1931.

NZPW (New Zealand Public Works Engineer's Department). 1936. Structural drawings for ["Bridge A"].

Park, R., Paulay, T. 1975. *Reinforced concrete structures.* Wiley-Interscience Publication, New York.

Park, R., Rodriguez, M. 1991. Retrofitting of reinforced concrete bridge piers for seismic performance. Pp. 43-58 in *Proceedings of the Technical Conference of the New Zealand Concrete Society,* Wairakei, New Zealand.

Park, R., Rodriguez, M., Dekker, D.R. 1993. Assessment and retrofit of a reinforced concrete bridge pier for seismic resistance. *Earthquake Spectra 9(4):* 781-801. Journal of the Earthquake Engineering Research Institute, Oakland, California.

Paulay, T., Priestley, M.J.N. 1992. *Reinforced concrete and masonry buildings design for seismic resistance*. John Wiley & Sons Inc., New York.

Priestley, M.J.N., Verma, R., Yan Xiao. 1994. Seismic shear strength of reinforced concrete columns. *Journal of Structural Engineering, ASCE, 120(8):* 2310-2329.

Rodriguez, M., Park, R. 1994. Seismic load tests of reinforced concrete columns strengthened by jacketing. *ACI Structural Journal 91(2):* 150-159.

SANZ (Standards Association of New Zealand). 1982. Code of practice for the design of concrete structures. *NZS 3101: 1982.* Standards Association of New Zealand, Wellington.

SANZ. 1992. Code of practice for general structural design and design loads for buildings. *NZS 4203: 1992.* Standards Association of New Zealand, Wellington.

SNZ (Standards New Zealand). 1995. Code of practice for the design of concrete structures. *NZS 3101: 1995.* Standards New Zealand, Wellington.

SEAONC (Structural Engineers Association of Northern California). 1995. Minutes of the Seismology Committee, San Francisco, California.

Watson, S., Zahn, F.A., Park, R. 1994. Confining reinforcement for concrete columns. *Journal of Structural Engineering, ASCE, 120(6):* 1798-1824.